Title

Secondary Brown Carbon Formation From Nighttime Oxidation of Heterocyclic Volatile Organic Compounds

Permalink

https://escholarship.org/uc/item/8wk1d4mk

Author

Chen, Kunpeng

Publication Date

2024

Peer reviewed|Thesis/dissertation

UNIVERSITY OF CALIFORNIA
RIVERSIDE

Secondary Brown Carbon Formation from Nighttime Oxidation of Heterocyclic Volatile
Organic Compounds

A Dissertation submitted in partial satisfaction
of the requirements for the degree of

Doctor of Philosophy

in

Environmental Sciences

by

Kunpeng Chen

June 2024

Dissertation Committee:
        Dr. Ying-Hsuan Lin, Chairperson
        Dr. Roya Bahreini
        Dr. Haofei Zhang

The Dissertation of Kunpeng Chen is approved:

_____

_____

_____
                                        Committee Chairperson

University of California, Riverside

Acknowledgements

The fruition of this dissertation was made possible through the invaluable support and guidance of my family, friends, and dissertation committee.

First, I would like to express my deepest gratitude to my advisor, the chair of my dissertation committee, Dr. Ying-Hsuan Lin. Dr. Lin has been an excellent guide and mentor, offering unwavering support throughout my PhD journey. She taught me all the technical details, from experimental work to academic writing, and steered me towards becoming a proficient scholar. She also played a pivotal role in providing insightful advice and assistance in developing a comprehensive career plan within academia. Her expertise, encouragement, and constructive feedback have been instrumental in shaping this dissertation.

I am also grateful to Dr. Roya Bahreini and Dr. Haofei Zhang, the esteemed members of my dissertation committee, for their very helpful suggestions and substantial contributions to my research. During my PhD journey, I engaged in numerous in-depth discussions with them, particularly within the brown carbon project meetings, and received highly beneficial and motivating feedback. I really appreciate their suggestions in professional development and writing impactful papers. Their expertise and steadfast support have significantly elevated the quality of this dissertation.

I also wish to express my sincere appreciation to Dr. King-Fai Li and Dr. David Cocker for their comments and suggestions in my oral qualifying exam, which helped shape the framework of my dissertation. Also, I would like to thank Dr. Li for his

I would also like to extend my heartfelt thanks to Hengjia Ou, Kin Fai Hao, Tianyi Ouyang, Dr. Jun Xu, Dr. Chuanye Xiong, Dr. Hanwei Zhu, Xiangyu Wang, Yuhua Situ, Dr. Chuanyang Shen, Wen Zhang, Xiaoyan Yang, Dr. Zekun Liu, and Dr. Liang Wu for their encouragement, understanding, and support during the ups and downs of this challenging endeavor. Their friendship and camaraderie have made this journey more fulfilling and enjoyable.

Finally, to my dad and mom, Mr. Gang Chen and Ms. Kai-Jian Wu, and my grandma, Ms. Jie-Fang Wu, thank you all for your support in these five years. I owe the deepest gratitude for your unwavering love, encouragement, and sacrifices throughout my academic pursuits. Your endless support and belief in me have been my source of strength and inspiration.

Copyright Acknowledgements

Dedicated to

My family

ABSTRACT OF THE DISSERTATION

Secondary Brown Carbon Formation from Nighttime Oxidation of Heterocyclic Volatile
Organic Compounds

by

Kunpeng Chen

Doctor of Philosophy, Graduate Program in Environmental Sciences
University of California, Riverside, June 2024
Dr. Ying-Hsuan Lin, Chairperson

This dissertation investigates the formation of secondary brown carbon (BrC) from nighttime oxidation of heterocyclic volatile organic compounds (VOCs) such as furans and pyrroles under diverse environmental conditions. This dissertation focuses on clarifying the effects of different environmental factors such as nitrate radical (NO_3) levels, pre-existing particles, and relative humidity (RH) on the optical properties of secondary BrC and the chemical composition of secondary organic aerosols (SOAs) derived from the heterocyclic VOCs.

NO_3 levels exhibit insignificantly influence on the overall composition of furan-derived SOA, while pre-existing particles show considerable effects on its chemical composition. The mass absorption coefficients (MAC) revealed the divergent impacts of NO_3 levels and pre-existing particles on BrC light absorption, suggesting NO_3 facilitates the generation of light-absorbing compounds whereas pre-existing particles may facilitate gas-to-particle partitioning of non-absorbing products. The effects of RH on secondary BrC formation were investigated through furan and pyrrole oxidation, revealing

substantial effects on particulate size distribution dynamics. The pyrrole oxidation products exhibit higher potential in producing ultrafine particles via nucleation. The increase of RH leads to increased mass fractions of oxygenated compounds in both SOAs, indicating the enhanced gas-phase and/or multiphase oxidation processes in humid environments. Interestingly, higher RH leads to decreased MAC, contrasting to the trend observed in the secondary BrC derived from homocyclic precursors. This divergence is owing to the formation of non-absorbing high-molecular-weight oxygenated compounds and the reduced mass fractions of molecular chromophores. Furthermore, this dissertation highlights the crucial role of carbonyl chromophores in the light absorption of secondary BrC derived from a variety of heterocyclic VOCs. In particular, N-containing carbonyl chromophores (e.g., imides and amides) derived from pyrroles are potentially important chromophores in secondary BrC. The contribution of chromophores on the overall BrC light absorption may vary significantly across wavelengths, underscoring their distinct significance at different wavelength ranges. Overall, this dissertation contributes to the fundamental insights of secondary BrC formation in the complicated atmospheric environments, especially those within the wildfire smoke. All of these findings will be helpful for improving the evaluation of BrC's radiative forcing and its impact on climate change.

Table of Contents

List of Figures

List of Tables

Chapter 4

Chapter 1. Introduction

1.1.Background

1.1.1. Light-absorbing Organic Carbon in Atmosphere Aerosols

Aerosols, the suspended particles in the atmosphere, can have direct and indirect radiative effects and modulate the climate system. The direct radiative effect means the scattering or absorption of sunlight, while the indirect radiative effect refers to the interactions between aerosols and clouds. The Intergovernmental Panel on Climate Change (IPCC) has demonstrated that aerosols and their interactions with clouds contribute to the largest uncertainty of the total radiative forcing. (1) In particular, the radiative forcing of organic carbon in aerosols was less understood. Organic carbon was considered a cooling factor that can solely contribute to negative radiative forcing (radiative forcing: −0.47 to −0.08 W m^{-2}) in the fifth assessment report from the IPCC (i.e., IPCC AR5 published in 2013). (1) However, in the sixth assessment report from IPCC (i.e., IPCC AR6 published in 2021), (2) the radiative forcing of organic carbon was adjusted (radiative forcing: −0.44 to +0.02 W m^{-2}). The adjusted value demonstrated that organic carbon may partially contribute to positive radiative forcing due to the light-absorbing component. (2)

Although this adjustment was made only recently, the role of organic carbon in light absorption by aerosols has been gradually recognized over the last few decades. In 1986, a pioneering study by Mukai and Ambe reported that humic-like substances (HULIS), a mixture of organic materials with a brown color, may play a substantial role

in the light absorption of ambient aerosols. (3) In 1999, Jacobson reported a variety of light-absorbing organic compounds (e.g., nitrated aromatics, aromatic polycarboxylic acids) in ambient aerosols. (4) In 2003, Pöschl proposed a systematic classification of carbonaceous aerosols, wherein the term "colored organic carbon" was raised to represent light-absorbing organic carbon. (5) Later in 2004, Kirchstetter et al. demonstrated that the wavelength dependency of light absorption by ambient aerosols can be greatly affected by organic carbon. (6) In 2006, Andreae and Gelencsér first defined light-absorbing organic carbon in atmospheric aerosols as "brown carbon". (7) Since then, the area of brown carbon (BrC) has evolved rapidly and emerged as a critical research topic for better understanding of the global climate change. (8−12)

1.1.2. *Radiative Effects of BrC*

Radiative forcing of BrC is estimated in terms of aerosol radiative effects, including (i) direct radiative effect, which refers to the radiative forcing corresponding to direct scattering and absorption of solar radiation by BrC, and (ii) indirect and semi-direct radiative effect, which refers to the radiative forcing related to aerosol-cloud interactions. Since BrC may account for 21% of the global mean concentration of organic compounds in the surface air, (13) accurate quantification of the radiative effects of BrC is necessary for reducing the uncertainty of climate forcing on the Earth. The pioneering work by Park et al. in 2010 estimated the direct radiative effect of BrC over East Asia as +0.05 W m^{-2}. (14) Later, several studies proposed that the direct radiative effect of BrC could globally vary from +0.10 W m^{-2} to +0.14 W m^{-2}, (13, 15, 16) while Lin et al. even estimated a

much higher value of +0.22 ~ +0.57 W m^{-2}. (17) Such discrepancies may be attributed to different modeling parameterizations of BrC light absorption.

The key to quantifying BrC's direct radiative effect is the mass absorption coefficient (MAC). Since BrC has strong light absorption in near ultraviolet (UV, 290−400 nm) and visible (400−760 nm), (18−20) MAC has a strong dependency on the wavelength of sunlight, which is empirically described by the power-law expression (eq (1.1)).

$$MAC_{BrC}(\lambda) = MAC_{BrC}(\lambda_0) \cdot \left(\frac{\lambda_0}{\lambda}\right)^{AAE} \qquad (1.1)$$

Here, λ_0 is a reference wavelength for light absorption measurements, and the power coefficient is the so-called absorption Ångström exponent (*AAE*). Previous studies usually picked up 550 nm as the reference wavelength (λ_0 = 550 nm), (11, 18) but *MAC$_{BrC}$(550)* had a large range (0.09 ~ 4.1 m^{2}g^{-1}). (13) For *AAE*, Kirchstetter et al. reported that *AAE* of wood smoke particulate matter could vary from 3.0 to 7.4, with the average at 5.0. (21) The established climate models typically adopt fixed values for *MAC$_{BrC}$(550)* and *AAE* to estimate the direct radiative effect of BrC aerosols, (13, 16, 22) but the variations in *MAC$_{BrC}$(550)* and *AAE* suggest that BrC light absorption may be greatly controlled by emission sources and atmospheric conditions.

The indirect radiative effect of BrC has been less investigated. Typically, an increase in the number of aerosols can enhance the cloud albedo (i.e., reflectivity) and increase low-level cloudiness, contributing to the Earth's surface cooling. (23, 24) However, the IPCC AR5 suggested that the heating effects caused by aerosol absorption

of solar radiation can reduce the amount of clouds. (1) Brown et al. also suggested that the light absorption of BrC could affect the atmospheric circulation and further reduce the global amount of low cloud cover. (15) These complete processes relating to cloud formation, albedo, and lifetime can have complex consequences on the Earth system.

1.1.3. *Sources and Fates of BrC*

Sources of BrC can be divided into primary sources and secondary sources. Primary sources refer to direct emissions of BrC, for example, emissions of polyaromatic hydrocarbons (PAHs) from incomplete combustion in biomass burning and fossil fuel usage. Secondary sources refer to BrC formation from secondary processing in the atmosphere, for example, the atmospheric oxidation of volatile organic compounds (VOCs) that produce light-absorbing secondary organic aerosols (SOAs). BrC directly emitted from primary sources is called "primary BrC," while BrC generated from secondary sources is called "secondary BrC."

In particular, biomass burning is recognized as the predominant source of primary BrC; (25−27) its importance was highlighted when light-absorbing organic carbon in aerosols was first observed. (3) Prescribed fires and natural wildfires are the major biomass burning sources. Fossil fuel combustion is another important source of BrC, which is directly related to anthropogenic activities. (28−30) Secondary sources of BrC are mainly attributable to the atmospheric oxidation of VOCs. Specifically, atmospheric oxidation of SOA precursors in the fire plume can contribute to BrC, which is the main focus of this dissertation, as discussed in section 1.3. The contribution of different sources may vary depending on the season. For example, in central Los Angeles, biomass

burning could contribute to more than 50% of BrC in cold seasons, while in warm seasons, fossil fuel combustion and secondary sources may contribute to 38% and 30% of BrC, respectively. (31)

Once released (i.e., emitted or generated) from its sources, atmospheric aging processes can gradually bleach BrC. (32, 33) For example, aging by atmospheric radicals (e.g., hydroxyl radicals) is known to play a key role in BrC evolution. Although a large fraction of BrC can be bleached within one day, certain fractions may persist and contribute to long-term light absorption. (34)

1.1.4. BrC Chromophores

BrC chromophores are the light-absorbing molecules in BrC aerosols, which may only occupy a small fraction of aerosol mass. (35) However, this "small fraction" is the pivot of the positive radiating forcing driven by BrC. So far, many studies have already managed to experimentally identify the molecular formula and tentative structures of a large fraction of constituents in BrC aerosols. Typical BrC chromophores include nitroaromatics, polycyclic aromatic hydrocarbons (PAHs), imidazoles, and light-absorbing oligomers. Nitroaromatics can be generated by both the photooxidation and nighttime chemistry of aromatic VOCs. (36, 37) PAHs can be directly emitted by biomass burning. (33, 38, 39) Imidazoles are generated by reactions between ammonium cation (or amines) and carbonyls in the aqueous particles. (40−43) Light-absorbing oligomers are generated from the photooxidation of biogenic monoterpenes/isoprene and anthropogenic aromatics. (41, 44, 45) A comprehensive review of BrC chemistry is provided by Laskin et al. (8)

The most ubiquitous BrC chromophore is nitroaromatics. Jacobson proposed that nitroaromatic compounds in the atmosphere could contribute to 25-30% of total light absorption in the near-UV region over Los Angeles. (4) Bluvshtein et al. and Lin et al. reported that nitroaromatics are the major contributors to BrC light absorption (>50% at above 350 nm) in wildfire smoke. (46, 47) Many kinds of nitroaromatic chromophores have been identified, such as nitrophenols, nitrocatechols, nitroguaiacols, and nitrosyringols. (33, 38, 39, 47) Particularly, 4-nitrophenol and 4-nitrocatechol, as well as their derivatives, were usually identified as the dominant products in field studies. (48, 49) Given the ubiquity and representativeness of these two compounds, previous experimental studies also employed them as model compounds to explore the kinetics of BrC evolution, including radical-driven oxidation, photobleaching, and photo-enhancement. (50−52) All of these studies highlight the key role of nitroaromatics in BrC light absorption.

1.2. Knowledge Gaps and Objectives of the Dissertation

This dissertation focuses on addressing two knowledge gaps: (i) the impact of environmental conditions on secondary BrC formation, and (ii) the role of understudied molecular chromophores in BrC light absorption. The hypotheses are that (i) changes in environmental conditions can substantially influence the optical properties and chemical composition of secondary BrC, and (ii) the understudied molecular chromophores may have substantial contributions to BrC light absorption.

Given the complicated composition of molecular chromophores in BrC, the uncertainty of BrC radiative effects is likely owing to insufficient understanding of the

6

compositional change of BrC aerosols during atmospheric processing. In particular, nighttime chemistry was recently identified as an important source of secondary BrC in wildfire smoke. (53) Among the wildfire emissions, heterocyclic VOCs are the second largest contributor to SOA precursors, (54) and may play a potentially important role in secondary BrC formation. (55) Due to the heteroatoms, heterocyclic VOCs may be more reactive compared to homocyclic VOCs such as benzene and toluene. (56) Nitro-substituted heterocyclic products such as nitrothiophene and nitropyrrole may be the key chromophores. (55) Chen et al. used time-dependent density functional theory (TD-DFT) calculations to support the light absorption of nitrate-derivatized heterocyclic products. (57) However, little has been discovered related to secondary BrC formation from the nighttime oxidation of heterocyclic VOCs, which will be the focus of my dissertation.

1.3. Research Aims of the Dissertation

This dissertation aims to clarify how different environmental conditions affect secondary BrC formation from the nighttime oxidation of heterocyclic VOCs and provide a more comprehensive characterization of molecular chromophores. This dissertation includes three research chapters and one conclusion chapter.

Chapter 2 focuses on the effects of nitrate radical level and pre-existing particles on both the light absorption properties and chemical compositions of secondary BrC from nighttime oxidation. Furan was used as the heterocyclic VOC in this study, since furans is the most abundant group of heterocyclic VOCs in wildfire plumes and furan is the representative backbone. (54) Chamber experiments were conducted to simulate SOA and secondary BrC formation under different environmental conditions. SOA composition, BrC

light absorption properties, and molecular chromophores under the studied environmental conditions were analyzed. This study aims to provide more insights about the role of nitrate radical level and pre-existing particles in secondary BrC formation.

Chapter 3 focuses on the effects of relative humidity (RH) on secondary BrC from the nighttime oxidation. Furan and pyrrole were selected to generate secondary BrC samples via nighttime oxidation in the chamber experiments. The influence of RH on size distribution dynamics, chemical composition, and the optical properties of secondary BrC was studied. This study aims to provide more in-depth insights into the physicochemical processes associated with RH and their modulation of secondary BrC formation in wildfire smoke.

Chapter 4 focuses on the role of carbonyl chromophores in secondary BrC from the nighttime oxidation. Nighttime oxidation of a variety of unsaturated VOCs (i.e., pyrrole, 1-methylpyrrole, 2-methylpyrrole, furan, and furfural) was used as the model systems for SOA and secondary BrC formation. Carbonyl chromophores in the SOA samples were thoroughly characterized by employing multiple instruments coupled with the theoretical calculations of UV-visible spectra. This study aims to estimate the light absorption contribution of carbonyl chromophores in secondary BrC.

Chapter 5 presents the concluding remarks of this dissertation and outlines the directions for future BrC research.

1.4. References

1. Stocker, T. F.; Qin, D.; Plattner, G. K.; Tignor, M.; Allen, S. K.; Boschung, J.; Nauels, A.; Xia, Y.; Bex, V.; Midgley, P. M., IPCC, 2013: Climate Change 2013: The Physical Science Basis. Contribution of Working Group I to the Fifth Assessment Report of the Intergovernmental Panel on Climate Change. Cambridge University Press, Cambridge, United Kingdom and New York, NY, USA: **2013**.

2. Forster, P., T. Storelvmo, K. Armour, W. Collins, J.-L. Dufresne, D. Frame, D.J. Lunt, T. Mauritsen, M.D. Palmer, M. Watanabe, M. Wild, H. Zhang, The Earth's Energy Budget, Climate Feedbacks, and Climate Sensitivity. *In Climate Change 2021: The Physical Science Basis. Contribution of Working Group I to the Sixth Assessment Report of the Intergovernmental Panel on Climate Change.* [Masson-Delmotte, V., P. Zhai, A. Pirani, S.L. Connors, C. Péan, S. Berger, N. Caud, Y. Chen, L. Goldfarb, M.I. Gomis, M. Huang, K. Leitzell, E. Lonnoy, J.B.R. Matthews, T.K. Maycock, T. Waterfield, O. Yelekçi, R. Yu, and B. Zhou (eds.)] Cambridge University Press, Cambridge, United Kingdom and New York, NY, USA, pp. 923–1054, **2021**.

3. Mukai, H.; Ambe, Y., Characterization of a humic acid-like brown substance in airborne particulate matter and tentative identification of its origin. *Atmos. Environ.* **1986**, 20, (5), 813-819.

4. Jacobson, M. Z., Isolating nitrated and aromatic aerosols and nitrated aromatic gases as sources of ultraviolet light absorption. *J. Geophys. Res. Atmos.* **1999**, 104, (D3), 3527-3542.

5. Pöschl, U., Aerosol particle analysis: challenges and progress. *Anal. Bioanal. Chem.* **2003**, 375, (1), 30-32.

6. Kirchstetter, T. W.; Novakov, T.; Hobbs, P. V., Evidence that the spectral dependence of light absorption by aerosols is affected by organic carbon. *J. Geophys. Res. Atmos.* **2004**, 109, (D21).

7. Andreae, M. O.; Gelencsér, A., Black carbon or brown carbon? The nature of light-absorbing carbonaceous aerosols. *Atmos. Chem. Phys.* **2006**, 6, (10), 3131-3148.

8. Laskin, A.; Laskin, J.; Nizkorodov, S. A., Chemistry of Atmospheric Brown Carbon. *Chem. Rev.* **2015**, 115, (10), 4335-4382.

9. Wu, G.-M.; Cong, Z.-Y.; Kang, S.-C.; Kawamura, K.; Fu, P.-Q.; Zhang, Y.-L.; Wan, X.; Gao, S.-P.; Liu, B., Brown carbon in the cryosphere: Current knowledge and perspective. *Adv. Clim. Change Res.* **2016**, 7, (1), 82-89.

10. Yan, J.; Wang, X.; Gong, P.; Wang, C.; Cong, Z., Review of brown carbon aerosols: Recent progress and perspectives. *Sci. Total Environ.* **2018**, 634, 1475-1485.

11. Saleh, R., From Measurements to Models: Toward Accurate Representation of Brown Carbon in Climate Calculations. *Curr. Pollut. Rep.* **2020**, 6, (2), 90-104.

12. Wang, Q.; Zhou, Y.; Ma, N.; Zhu, Y.; Zhao, X.; Zhu, S.; Tao, J.; Hong, J.; Wu, W.; Cheng, Y.; Su, H., Review of Brown Carbon Aerosols in China: Pollution Level, Optical Properties, and Emissions. *J. Geophys. Res. Atmos.* **2022**, 127, (16), e2021JD035473.

13. Jo, D. S.; Park, R. J.; Lee, S.; Kim, S. W.; Zhang, X., A global simulation of brown carbon: implications for photochemistry and direct radiative effect. *Atmos. Chem. Phys.* **2016**, 16, (5), 3413-3432.

14. Park, R. J.; Kim, M. J.; Jeong, J. I.; Youn, D.; Kim, S., A contribution of brown carbon aerosol to the aerosol light absorption and its radiative forcing in East Asia. *Atmos. Environ.* **2010**, 44, (11), 1414-1421.

15. Brown, H.; Liu, X.; Feng, Y.; Jiang, Y.; Wu, M.; Lu, Z.; Wu, C.; Murphy, S.; Pokhrel, R., Radiative effect and climate impacts of brown carbon with the Community Atmosphere Model (CAM5). *Atmos. Chem. Phys.* **2018**, 18, (24), 17745-17768.

16. Zhang, A.; Wang, Y.; Zhang, Y.; Weber, R. J.; Song, Y.; Ke, Z.; Zou, Y., Modeling the global radiative effect of brown carbon: a potentially larger heating source in the tropical free troposphere than black carbon. *Atmos. Chem. Phys.* **2020**, 20, (4), 1901-1920.

17. Lin, G.; Penner, J. E.; Flanner, M. G.; Sillman, S.; Xu, L.; Zhou, C., Radiative forcing of organic aerosol in the atmosphere and on snow: Effects of SOA and brown carbon. *J. Geophys. Res. Atmos.* **2014**, 119, (12), 7453-7476.

18. Bond, T. C.; Bergstrom, R. W., Light Absorption by Carbonaceous Particles: An Investigative Review. *Aerosol Sci. Tech.* **2006**, 40, (1), 27-67.

19. Ramanathan, V.; Ramana, M. V.; Roberts, G.; Kim, D.; Corrigan, C.; Chung, C.; Winker, D., Warming trends in Asia amplified by brown cloud solar absorption. *Nature* **2007**, 448, (7153), 575-578.

20. Alexander, D. T. L.; Crozier, P. A.; Anderson, J. R., Brown Carbon Spheres in East Asian Outflow and Their Optical Properties. *Science* **2008**, 321, (5890), 833.

21. Kirchstetter, T. W.; Thatcher, T. L., Contribution of organic carbon to wood smoke particulate matter absorption of solar radiation. *Atmos. Chem. Phys.* **2012**, 12, (14), 6067-6072.

22. Wang, X.; Heald, C. L.; Ridley, D. A.; Schwarz, J. P.; Spackman, J. R.; Perring, A. E.; Coe, H.; Liu, D.; Clarke, A. D., Exploiting simultaneous observational constraints on mass and absorption to estimate the global direct radiative forcing of black carbon and brown carbon. *Atmos. Chem. Phys.* **2014**, 14, (20), 10989-11010.

23. Twomey, S. A.; Piepgrass, M.; Wolfe, T. L., An assessment of the impact of pollution on global cloud albedo. *Tellus B* **1984**, 36B, (5), 356-366.

24. Albrecht, B. A., Aerosols, Cloud Microphysics, and Fractional Cloudiness. *Science* **1989**, 245, (4923), 1227.

25. Formenti, P.; Elbert, W.; Maenhaut, W.; Haywood, J.; Osborne, S.; Andreae, M. O., Inorganic and carbonaceous aerosols during the Southern African Regional Science Initiative (SAFARI 2000) experiment: Chemical characteristics, physical properties, and emission data for smoke from African biomass burning. *J. Geophys. Res. Atmos.* **2003**, 108, D13, 8488.

26. Lukács, H.; Gelencsér, A.; Hammer, S.; Puxbaum, H.; Pio, C.; Legrand, M.; Kasper-Giebl, A.; Handler, M.; Limbeck, A.; Simpson, D.; Preunkert, S., Seasonal trends and possible sources of brown carbon based on 2-year aerosol measurements at six sites in Europe. *J. Geophys. Res. Atmos.* **2007**, 112, D23S18.

27. Washenfelder, R. A.; Attwood, A. R.; Brock, C. A.; Guo, H.; Xu, L.; Weber, R. J.; Ng, N. L.; Allen, H. M.; Ayres, B. R.; Baumann, K.; Cohen, R. C.; Draper, D. C.; Duffey, K. C.; Edgerton, E.; Fry, J. L.; Hu, W. W.; Jimenez, J. L.; Palm, B. B.; Romer, P.; Stone, E. A.; Wooldridge, P. J.; Brown, S. S., Biomass burning dominates brown carbon absorption in the rural southeastern United States. *Geophys. Res. Lett.* **2015**, 42, (2), 653-664.

28. Olson, M. R.; Victoria Garcia, M.; Robinson, M. A.; Van Rooy, P.; Dietenberger, M. A.; Bergin, M.; Schauer, J. J., Investigation of black and brown carbon multiple-wavelength-dependent light absorption from biomass and fossil fuel combustion source emissions. *J. Geophys. Res. Atmos.* **2015**, 120, (13), 6682-6697.

29. Xie, M.; Hays, M. D.; Holder, A. L., Light-absorbing organic carbon from prescribed and laboratory biomass burning and gasoline vehicle emissions. *Sci. Rep.* **2017**, 7, (1), 7318.

30. Li, M.; Fan, X.; Zhu, M.; Zou, C.; Song, J.; Wei, S.; Jia, W.; Peng, P. a., Abundance and Light Absorption Properties of Brown Carbon Emitted from Residential Coal Combustion in China. *Environ. Sci. Technol.* **2019**, 53, (2), 595-603.

31. Soleimanian, E.; Mousavi, A.; Taghvaee, S.; Shafer, M. M.; Sioutas, C., Impact of secondary and primary particulate matter (PM) sources on the enhanced light absorption by brown carbon (BrC) particles in central Los Angeles. *Sci. Total Environ.* **2020**, 705, 135902.

32. Dasari, S.; Andersson, A.; Bikkina, S.; Holmstrand, H.; Budhavant, K.; Satheesh, S.; Asmi, E.; Kesti, J.; Backman, J.; Salam, A.; Bisht, D. S.; Tiwari, S.; Hameed, Z.; Gustafsson, Ö., Photochemical degradation affects the light absorption of water-soluble brown carbon in the South Asian outflow. *Sci. Adv.* **2019**, 5, (1), eaau8066.

33. Fleming, L. T.; Lin, P.; Roberts, J. M.; Selimovic, V.; Yokelson, R.; Laskin, J.; Laskin, A.; Nizkorodov, S. A., Molecular composition and photochemical lifetimes of brown carbon chromophores in biomass burning organic aerosol. *Atmos. Chem. Phys.* **2020**, 20, (2), 1105-1129.

34. Forrister, H.; Liu, J.; Scheuer, E.; Dibb, J.; Ziemba, L.; Thornhill, K. L.; Anderson, B.; Diskin, G.; Perring, A. E.; Schwarz, J. P.; Campuzano-Jost, P.; Day, D. A.; Palm, B.

B.; Jimenez, J. L.; Nenes, A.; Weber, R. J., Evolution of brown carbon in wildfire plumes. *Geophys. Res. Lett.* **2015**, 42, (11), 4623-4630.

35. Laskin, J.; Laskin, A.; Nizkorodov, S. A.; Roach, P.; Eckert, P.; Gilles, M. K.; Wang, B.; Lee, H. J.; Hu, Q., Molecular Selectivity of Brown Carbon Chromophores. *Environ. Sci. Technol.* **2014**, 48, (20), 12047-12055.

36. Nojima, K.; Fukaya, K.; Fukui, S.; Kanno, S., Studies on photochemistry of aromatic hydrocarbons II: The formation of nitrophenols and nitrobenzene by the photochemical reaction of benzene in the presence of nitrogen monoxide. *Chemosphere* **1975**, 4, (2), 77-82.

37. Wang, S.; Li, H., NO3·-Initiated Gas-Phase Formation of Nitrated Phenolic Compounds in Polluted Atmosphere. *Environ. Sci. Technol.* **2021**, 55, (5), 2899-2907.

38. Lin, P.; Fleming, L. T.; Nizkorodov, S. A.; Laskin, J.; Laskin, A., Comprehensive Molecular Characterization of Atmospheric Brown Carbon by High Resolution Mass Spectrometry with Electrospray and Atmospheric Pressure Photoionization. *Anal. Chem.* **2018**, 90, (21), 12493-12502.

39. Fleming, L. T.; Lin, P.; Laskin, A.; Laskin, J.; Weltman, R.; Edwards, R. D.; Arora, N. K.; Yadav, A.; Meinardi, S.; Blake, D. R.; Pillarisetti, A.; Smith, K. R.; Nizkorodov, S. A., Molecular composition of particulate matter emissions from dung and brushwood burning household cookstoves in Haryana, India. *Atmos. Chem. Phys.* **2018**, 18, (4), 2461-2480.

40. Nguyen, T. B.; Lee, P. B.; Updyke, K. M.; Bones, D. L.; Laskin, J.; Laskin, A.; Nizkorodov, S. A., Formation of nitrogen- and sulfur-containing light-absorbing compounds accelerated by evaporation of water from secondary organic aerosols. *J. Geophys. Res. Atmos.* **2012**, 117, D01207.

41. Nguyen, T. B.; Laskin, A.; Laskin, J.; Nizkorodov, S. A., Brown carbon formation from ketoaldehydes of biogenic monoterpenes. *Faraday Discuss.* **2013**, 165, (0), 473-494.

42. Kampf, C. J.; Filippi, A.; Zuth, C.; Hoffmann, T.; Opatz, T., Secondary brown carbon formation via the dicarbonyl imine pathway: nitrogen heterocycle formation and synergistic effects. *Phys. Chem. Chem. Phys.* **2016**, 18, (27), 18353-18364.

43. Aiona, P. K.; Lee, H. J.; Leslie, R.; Lin, P.; Laskin, A.; Laskin, J.; Nizkorodov, S. A., Photochemistry of Products of the Aqueous Reaction of Methylglyoxal with Ammonium Sulfate. *ACS Earth Space Chem.* **2017**, 1, (8), 522-532.

44. Lin, Y.-H.; Budisulistiorini, S. H.; Chu, K.; Siejack, R. A.; Zhang, H.; Riva, M.; Zhang, Z.; Gold, A.; Kautzman, K. E.; Surratt, J. D., Light-Absorbing Oligomer Formation in Secondary Organic Aerosol from Reactive Uptake of Isoprene Epoxydiols. *Environ. Sci. Technol.* **2014**, 48, (20), 12012-12021.

45. Li, Y.; Ji, Y.; Zhao, J.; Wang, Y.; Shi, Q.; Peng, J.; Wang, Y.; Wang, C.; Zhang, F.; Wang, Y.; Seinfeld, J. H.; Zhang, R., Unexpected Oligomerization of Small α-Dicarbonyls for Secondary Organic Aerosol and Brown Carbon Formation. *Environ. Sci. Technol.* **2021**, 55, (8), 4430-4439.

46. Bluvshtein, N.; Lin, P.; Flores, J. M.; Segev, L.; Mazar, Y.; Tas, E.; Snider, G.; Weagle, C.; Brown, S. S.; Laskin, A.; Rudich, Y., Broadband optical properties of biomass-burning aerosol and identification of brown carbon chromophores. *J. Geophys. Res. Atmos.* **2017**, 122, (10), 5441-5456.

47. Lin, P.; Bluvshtein, N.; Rudich, Y.; Nizkorodov, S. A.; Laskin, J.; Laskin, A., Molecular Chemistry of Atmospheric Brown Carbon Inferred from a Nationwide Biomass Burning Event. *Environ. Sci. Technol.* **2017**, 51, (20), 11561-11570.

48. Desyaterik, Y.; Sun, Y.; Shen, X.; Lee, T.; Wang, X.; Wang, T.; Collett Jr, J. L., Speciation of "brown" carbon in cloud water impacted by agricultural biomass burning in eastern China. *J. Geophys. Res. Atmos.* **2013**, 118, (13), 7389-7399.

49. Li, M.; Wang, X.; Lu, C.; Li, R.; Zhang, J.; Dong, S.; Yang, L.; Xue, L.; Chen, J.; Wang, W., Nitrated phenols and the phenolic precursors in the atmosphere in urban Jinan, China. *Sci. Total Environ.* **2020**, 714, 136760.

50. Zhao, R.; Lee, A. K. Y.; Huang, L.; Li, X.; Yang, F.; Abbatt, J. P. D., Photochemical processing of aqueous atmospheric brown carbon. *Atmos. Chem. Phys.* **2015**, 15, (11), 6087-6100.

51. Hems, R. F.; Abbatt, J. P. D., Aqueous Phase Photo-oxidation of Brown Carbon Nitrophenols: Reaction Kinetics, Mechanism, and Evolution of Light Absorption. *ACS Earth Space Chem.* **2018**, 2, (3), 225-234.

52. Braman, T.; Dolvin, L.; Thrasher, C.; Yu, H.; Walhout, E. Q.; O'Brien, R. E., Fresh versus Photo-recalcitrant Secondary Organic Aerosol: Effects of Organic Mixtures on Aqueous Photodegradation of 4-Nitrophenol. *Environ. Sci. Technol. Lett.* **2020**, 7, (4), 248-253.

53. Li, C.; He, Q.; Hettiyadura, A. P. S.; Käfer, U.; Shmul, G.; Meidan, D.; Zimmermann, R.; Brown, S. S.; George, C.; Laskin, A.; Rudich, Y., Formation of Secondary Brown Carbon in Biomass Burning Aerosol Proxies through NO$_3$ Radical Reactions. *Environ. Sci. Technol.* **2020**, 54, (3), 1395-1405.

54. Palm, B. B.; Peng, Q.; Fredrickson, C. D.; Lee, B. H.; Garofalo, L. A.; Pothier, M. A.; Kreidenweis, S. M.; Farmer, D. K.; Pokhrel, R. P.; Shen, Y.; Murphy, S. M.; Permar, W.; Hu, L.; Campos, T. L.; Hall, S. R.; Ullmann, K.; Zhang, X.; Flocke, F.; Fischer, E. V.; Thornton, J. A., Quantification of organic aerosol and brown carbon evolution in fresh wildfire plumes. *PNAS* **2020**, 117, (47), 29469.

55. Jiang, H.; Frie, A. L.; Lavi, A.; Chen, J. Y.; Zhang, H.; Bahreini, R.; Lin, Y.-H., Brown Carbon Formation from Nighttime Chemistry of Unsaturated Heterocyclic Volatile Organic Compounds. *Environ. Sci. Technol. Lett.* **2019**, 6, (3), 184-190.

56. Gupta, R. R.; Kumar, M.; Gupta, V., Five-Membered Heterocycles with One Heteroatom. *In Heterocyclic Chemistry: Volume II: Five-Membered Heterocycles*, Gupta, R. R.; Kumar, M.; Gupta, V., Eds. Springer Berlin Heidelberg: Berlin, Heidelberg, **1999**; pp 3-179.

57. Chen, J. Y.; Rodriguez, E.; Jiang, H.; Chen, K.; Frie, A.; Zhang, H.; Bahreini, R.; Lin, Y.-H., Time-Dependent Density Functional Theory Investigation of the UV–Vis Spectra of Organonitrogen Chromophores in Brown Carbon. *ACS Earth Space Chem.* **2020**, 4, (2), 311-320.

Chapter 2. Effects of Nitrate Radical Levels and Pre-Existing Particles on Secondary Brown Carbon Formation from Nighttime Oxidation of Furan

2.0. Abstract

Furans are predominant heterocyclic volatile organic compounds (VOCs) in the atmosphere from both primary and secondary sources, such as direct emissions from wildfires and atmospheric oxidation of dienes. Formation of secondary organic aerosols (SOAs) from the oxidation of furans has been reported. Previous research has shown that furan SOA generated from nighttime oxidation contributes to brown carbon (BrC) formation; however, how nighttime oxidant levels (represented by nitrate radical (NO_3) levels) and pre-existing particles influence the SOA chemical composition and BrC optical properties is not well constrained. In this study, we conducted chamber experiments to systematically investigate the role of these two environmental factors in furan-derived secondary BrC formation during the nighttime. Our results suggest that the bulk compositions of SOA measured as ion fragment families by an aerosol mass spectrometer (mAMS) are unaffected by changes in NO_3 levels, but can be influenced by the presence of pre-existing ammonium sulfate particles. Based on the mass absorption coefficient (MAC) profiles of SOA produced under different experimental conditions, the BrC light absorption was enhanced by higher NO_3 levels and reduced by the presence of pre-existing ammonium sulfate seed particles, suggesting that NO_3-initiated oxidation of furan can promote the formation of light-absorbing products while pre-existing particles may facilitate the partitioning of non-absorbing organics in the aerosol phase. Furthermore, molecular-level compositional analysis reveals a similar pattern of

chromophores under various studied environmental conditions, in which highly oxygenated monomers (e.g., $C_4H_4O_6$ and $C_4H_3NO_7$), dimers, and oligomers can all contribute to BrC chromophores. Taken together, the NO_3 levels and pre-existing particles can influence secondary BrC formation by altering SOA compositions, which is critical for assessing BrC optical properties in a complex environment.

2.1. Introduction

Heterocyclic volatile organic compounds (VOCs) are a class of ubiquitous but understudied precursors of secondary organic aerosols (SOAs) that have a substantial impact on air quality and the solar radiative budget of the Earth. Heterocyclic VOCs emitted from biomass burning (1−3) are expected to become increasingly important due to the combustion of fossil fuels (4, 5) and the increased wildfire episodes with global warming. (6−8) Because of the heteroatoms, heterocyclic VOCs with aromatic rings exhibit distinctive reactivity when compared to the homocyclic compounds (e.g., toluene, naphthalene), and thus their fates in atmospheric oxidation have gained increasing attention. In particular, furans are common heterocyclic VOCs that are released when cellulose and hemicellulose are pyrolyzed during biomass burning, (9−11) especially when burning wiregrass, (12) and are often observed in field measurements. (3, 13, 14) Furans are also secondary products of atmospheric hydroxyl radical (OH)-initiated oxidation of dienes (e.g., butadiene and isoprene). (15−17) Recent research suggested that furans may contribute to around 20-30% of SOA generated in biomass burning, (18, 19) highlighting the crucial role of furans as SOA precursors.

The gas-phase oxidation pathways of furans are widely studied and have been incorporated into mechanistic models, (20, 21) whereas the aerosol-phase compositions are less well-defined. Alvarez et al. (22) reported that OH-initiated oxidation of furans can produce a large set of unsaturated 1,4-dicarbonyls in the aerosol phase, while Joo et al. (23) suggested that nitrate radical (NO_3)-initiated oxidation of 3-methylfuran can not only generate a variety of carbonyls but also dimers and oligomers. Strollo and Ziemann (24) indicated that oligomerization is the key to SOA formation during 3-methylfuran daytime oxidation, while Jiang et al. (25) highlighted the potentially important role of multifunctional dihydroxyl organonitrate products in SOA formation in the furan-NO_x-NaCl system. However, our understanding of the chemical composition of reaction products in furan oxidations is still limited, making it difficult to evaluate the physicochemical properties of furan SOA.

The optical properties of aerosols, in particular, are critical for influencing atmospheric radiative balance, (26) but the optical properties of furans SOA have not been thoroughly investigated. Grace et al. (27) suggested that furan derivatives in aqueous aerosols could potentially contribute to the formation of brown carbon (BrC), which is defined as the light-absorbing organic matter in aerosols. Jiang et al. (28) reported that nighttime oxidation of furan can produce secondary BrC. Even though furans have been shown to be a precursor of SOA and BrC, it is unclear how environmental conditions regulate furan SOA and BrC formation. Tsigaridis and Kanakidou (29) hypothesized that oxidant levels (i.e., concentration of oxidants) and pre-existing particles are two crucial environmental factors that will influence the future SOA

burden in the atmosphere. Oxidant levels are anticipated to affect the oxidation products and, consequently, the optical properties of SOA, (30) whereas pre-existing particles may alter the amount of SOA constituents by facilitating gas-particle partitioning and heterocyclic reactions. However, the relationship between these processes and BrC formation has not been thoroughly investigated. Since furans can contribute to 5-37% of the emitted VOCs in biomass burning smoke, (3, 10) it is essential to constrain the role of oxidant levels and pre-existing particles in the formation of BrC from the oxidation of furans under various environmental conditions.

In this study, chamber experiments were carried out to determine the effects of oxidant levels and the presence of pre-existing particles on the formation of SOA and BrC by the nighttime oxidation of furan, the representative structural backbone and most abundant component of furans. The oxidant levels here refer to NO_3 concentrations (hereafter denoted as "NO_3 levels"), which are controlled by the concentration ratios of nitrogen dioxide to ozone ($[NO_2]/[O_3]$), whereas the pre-existing particles in this study are ammonium sulfate particles. The compositional variation of SOA under various environmental conditions was investigated. Light-absorption properties of SOA and chromophores were characterized to determine the effects of NO_3 levels and pre-existing particles on secondary BrC formation.

2.2. Methods

2.2.1. Experimental setup

All the experiments were conducted in a 10 m^3 Teflon FEP chamber under dark conditions. Details of the experimental setup and procedures were introduced in our previous studies. (31, 32) In brief, 1500 ppb O_3 and 150 ppb or 450 ppb NO_2 (i.e., initial $[NO_2]/[O_3] = 0.1$ or 0.3, denoted as "low NO_3" and "high NO_3" experiments hereafter) were first injected into the chamber to produce NO_3 radicals within 1 hour of reaction, followed by the injection of ~200 ppb furan. The stabilized NO_3 radical concentration before furan injection was estimated to be ~8.0 ppb and ~22.0 ppb under the "low NO_3" and "high NO_3" experiments, respectively. (31) For experiments with pre-existing particles (denoted as "seeded experiments" hereafter), a constant output atomizer (TSI 3076) with 10 mM ammonium sulfate (($NH_4)_2SO_4$, Acros Organics, 99%, extra pure) solution and a silica-gel diffusion dryer were used to generate ~50 μg m^{-3} seed particles (central diameter ~50 nm) in the chamber before furan injection, simulating the background particles in wildfire plumes. (33, 34) All the experiments were performed at room temperature (20-25 °C) and low relative humidity (RH< 20%). It should be noted that when compared to real-world plumes, the chamber conditions may introduce some artifacts, such as much higher NO_3 radical concentrations than those reported by field measurements in the biomass burning plume, (35) negligible NO concentrations that may affect gas-phase organic peroxy radical (RO_2) chemistry, and wall loss of volatile products from NO_3-initiated reactions of furan. These artifacts may potentially influence the characterization of chemical composition in the experimental results. (36)

19

Nevertheless, these controlled chamber conditions are intended to systematically investigate the role of NO₃ levels and pre-existing particles in the formation of furan-derived secondary BrC.

2.2.2. Compositional characterization

A combination of online and offline approaches was employed to characterize the chemical composition of furan SOA. Real-time bulk composition of aerosol particles and *in situ* molecular formula of aerosol constituents were measured online by the mini-Aerosol Mass Spectrometer coupled with a compact time-of-flight mass spectrometer (mAMS, Aerodyne Research Inc.) (37) and the iodide-adduct time-of-flight chemical ion mass spectrometry coupled with the Filter Inlet for Gases and AEROsols system (FIGAERO-ToF-CIMS, Aerodyne Research Inc.), (38) respectively. Offline techniques, including attenuated total reflectance Fourier-transform infrared spectroscopy (ATR-FTIR, Thermo Nicolet 6700), gas chromatography-electron ionization mass spectrometry (GC/EI-MS, Agilent Technologies 6890N GC System and 5975 inert XL Mass Selective Detector), liquid chromatography coupled with a diode array detector, an electrospray ionization source and a quadruple-time-of-flight mass spectrometer (LC-DAD-ESI-Q-ToFMS, Agilent Technologies 1260 Infinity II and 6545 Q-ToF LC/MS), and an ion mobility spectrometry time-of-flight mass spectrometer (IMS-TOF, Tofwerk Inc.), were used to further characterize the functional group information and molecular compositions of SOA samples. Details of the instrumental setup have been introduced in previous studies. (31, 32, 39−41)

2.2.3. Optical and particulate size measurements

In situ measurements of particulate absorption coefficients at 375 nm ($\beta_{abs,375}$) were performed by a photoacoustic extinctiometer (PAX, Droplet Measurement Technology) at 1 Hz, (42) while the ultraviolet and visible absorbance (UV−vis) at 290-700 nm of SOA samples were measured offline by a UV−vis spectrophotometer (Beckman DU-640). All SOA samples were extracted with acetonitrile (ACN), a suitable solvent for secondary BrC analyses given the solubility and stability of chromophores. (32) A Scanning Electrical Mobility Spectrometer (SEMS, Brechtel Manufacturing Inc.) was used to determine the number concentration and size distribution of SOA from 10 - 800 nm with 140 bins. Online MAC at 375 nm was calculated by eq (2.1), where C_{SOA} is the mass concentration of SOA in the chamber. The offline MAC profile was calculated by eq (2.2), where $A(\lambda)$ is the absorbance along with wavelength (λ), b is the light path (i.e., 1 cm), and C_m is the mass concentration of SOA constituents in the ACN solution.

$$MAC_{online}(375) = \frac{\beta_{abs,375}}{C_{SOA}} \qquad (2.1)$$

$$MAC_{offline}(\lambda) = \ ln10 \ \times \frac{A(\lambda)}{b \times C_m} \qquad (2.2)$$

Absorption Ångström exponents (AAE) within 290-400 nm and 400-600 nm (AAE$_{290/400}$ and *AAE$_{400/600}$*) representing the wavelength dependence of light absorption in the UV and visible ranges, respectively, were calculated by the power-law dependence of offline MAC on the wavelengths (eq (2.3)).

$$AAE_{\lambda_1/\lambda_2} = \frac{-ln\left(\frac{MAC_{offline}(\lambda_1)}{MAC_{offline}(\lambda_2)}\right)}{ln\left(\frac{\lambda_1}{\lambda_2}\right)} \qquad (2.3)$$

Particulate effective density and organic aerosol fraction of furan SOA under different environmental conditions are summarized in **Table S2.1** for estimating C_{SOA} and C_m. Details of the instrumental setup and calculations of parameters were illustrated in our previous studies. (31, 32)

2.2.4. Computational details of UV−vis spectra simulations

Time-dependent density functional theory (TD-DFT) was employed to confirm the light absorptivity of oxidation products with high double bond equivalence (DBE) identified by FIGAERO-ToF-CIMS. All the computations were performed using the Gaussian 16 program (revision C. 01). (43) Geometrical optimizations, excitation wavelengths, and oscillator strengths were computed by the B3LYP functional (44, 45) implemented with the 6-311++G(d,p) basis set, (46) which is suggested by previous studies. (47, 48) The integral equation formalism extension of the polarizable continuum model (IEFPCM) (49) was used to simulate the ACN environment. All the theoretical UV−vis spectra were generated by the GaussView 6 program. The Cartesian coordinates for all the geometrical structures are summarized in **Table S2.2**.

2.3. Results and Discussions

2.3.1. The role of NO$_3$-initiated oxidation

In order to investigate secondary BrC formation from furan, it is essential to determine whether NO$_3$-initiated reactions play a predominant role in furan SOA formation during the nighttime, given that O$_3$ concentration is significantly higher than NO$_2$ concentration in biomass burning plumes, where O$_3$ and NO$_3$ are likely to compete for furan oxidation. (35, 50, 51) The reaction rate constant of "furan + NO$_3$" ($k_{furan+NO_3}$) in the gas phase is 6 orders of magnitude greater than that of "furan + O$_3$" ($k_{furan+O_3}$), (52−54) indicating that NO$_3$-initiated reactions should account for the majority of oxidation products; the dominance of NO$_3$-initiated oxidation can be further verified by the method described by Draper et al. (55) (i.e., $[NO_2]/[furan] > k_{furan+O_3}/k_{O_3+NO_2}$). Here, iodide-adduct CIMS was used to measure the gas-phase oxidation products. The O$_3$-only experiments (~1500 ppb O$_3$ as the oxidant) were implemented as a NO$_x$-free benchmark for comparison. **Figure 2.1** shows the comparison of gas-phase products under low NO$_3$ and O$_3$-only conditions, where the *m/z* 200-250 range reveals nearly identical oxidation products under both conditions, whereas the *m/z* 250-310 range reveals products that are completely dissimilar. In the presence of NO$_2$, despite the concentration of NO$_2$ being much lower than that of O$_3$, only nitrogen-containing products were detected in the *m/z* 250−310 range, indicating that NO$_3$-initiated oxidation significantly altered the reaction pathways. Moreover, as the NO$_3$ levels increased, the mass spectra of gas-phase products remained relatively unchanged but the intensity-weighted average values of the oxygen-to-carbon and nitrogen-to-carbon ratios

(i.e., <O/C> and <N/C>) increased (**Figure S2.2**), implying that NO_3 levels may have minimal effects on changing the molecular composition of oxygenated products but lead to a greater amount of oxidation products.
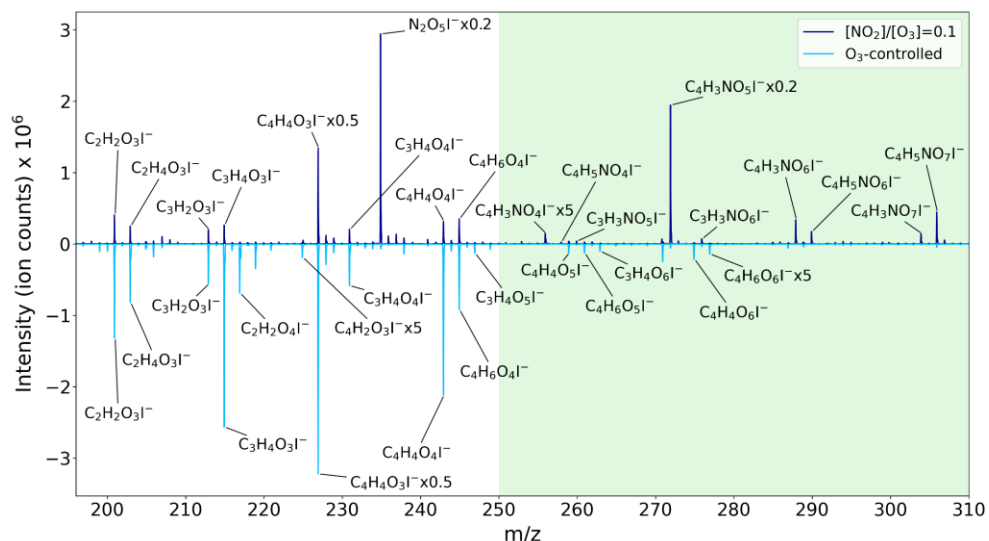
Figure 2.1. Comparison of gas-phase products from nighttime oxidation of furan between the low-NO_3 and O_3-only experiments. The green area highlights the compositional difference under the two environmental conditions.

Gas-phase products can contribute to SOA formation via new particle formation or gas-particle partitioning on aerosols, where heterogeneous and multiphase chemistry (e.g., reactive uptake of gaseous oxidants onto aerosols) can promote further reactions and thus generate a wider array of secondary products. However, since the mechanistic understanding of NO_3-initiated oxidation of furan is still lacking, process-level insights into SOA formation in this case are very limited. Berndt et al. (56) and Zhang et al. (57) reported the formation mechanisms of 3H-furan-2-one and dicarbonyls (e.g., *cis-*

butenedial) initiated by NO_3 addition on the furan ring, whereas Jiang et al. (21) recently proposed a mechanistic scheme of NO_3-initiated reactions with furan. Nonetheless, little understanding of oxidation products has been experimentally supported thus far. In this study, **Figure 2.1** may suggest the generation of 2-peroxyl-5-nitrate-furan ($C_4H_5NO_6$), 5-nitrate-furan-2-one ($C_4H_3NO_5$, the highest peak in the upper panel) and formyl nitrate methyl formylate ($C_3H_3NO_6$) in the mechanisms proposed by Jiang et al. (21) In addition, nitrate-furan ($C_4H_3NO_4$) was detected here, which is consistent with our previous findings. (28) Furthermore, our data could support field observations. For example, Palm et al. (14) proposed that furan oxidation may contribute to $C_4H_4O_4$ and $C_3H_4O_4$ observed in the biomass burning plume, which can be supported by **Figure 2.1**.

While the characterization of gas-phase products reveals the remarkable alteration of oxidation pathways in the presence of NO_2, SEMS measurements highlight the effect of NO_3-initiated reactions on SOA formation kinetics. As soon as furan was injected into the chamber where NO_2 and O_3 had been reacting for 1 h, SOA was formed immediately (**Figure 2.2A, C**). In the O_3-only experiments, no particles were generated within ~30 min after furan injection (**Figure 2.2E**). As seed particles were added, instant generation of SOA occurred after furan injection (**Figure 2.2B, D**), whereas no rapid formation of SOA was observed in O_3-only, seeded experiments (**Figure 2.2F**). These results demonstrate the advantage of NO_3-initiated reactions in rapidly producing low volatile products and thus accelerating SOA formation, and consequently, NO_3-initiated oxidation should account for the majority of furan SOA in nighttime biomass burning plumes.
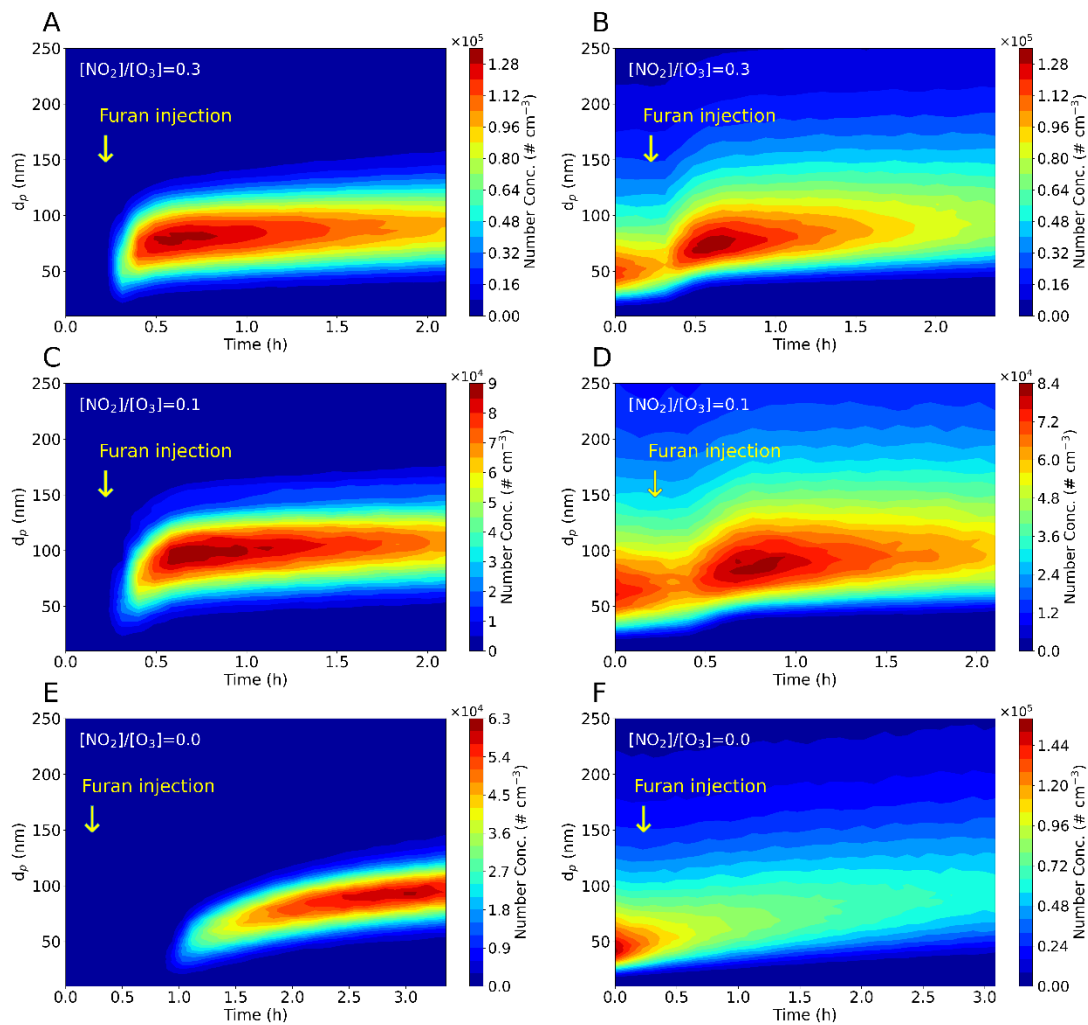
Figure 2.2. Size and number distribution of furan SOA along with the experimental time. Experimental conditions: (A) $[NO_2]/[O_3] = 0.3$, non-seeded, (B) $[NO_2]/[O_3] = 0.3$, seeded, (C) $[NO_2]/[O_3] = 0.1$, non-seeded, (D) $[NO_2]/[O_3] = 0.1$, seeded, (E) O_3-only, non-seeded, (F) O_3-only, seeded.

2.3.2. SOA constituents under various environmental conditions

Figure 2.3 depicts the characterization of SOA in bulk composition and at the molecular level measured by mAMS and FIGAERO-ToF-CIMS, respectively. In this study, pie charts were used to visualize the average relative abundance of $C_xH_y^+$, $C_xH_yO^+$, $C_xH_yO_{>1}^+$, $C_xH_yN^+$, and $C_xH_yNO^+$ fractions during the experiments. To show the change in relative abundance of fraction signals during the experiments, the average value of each fraction was calculated at (1) 20-30 minutes and (2) 95-115 minutes after the injection of furan. These time intervals were selected to represent the early and late stages of the experiment, and the corresponding averages are named as "early averages" and "late averages" (**Figure S2.1**). The comparison of these two timeframes allows differentiation between mechanisms of particle formation; the "early average" represents the nucleation of atmospheric particles, whereas the "late average" represents the condensation of oxidation products on already formed SOA. **Figure S2.1** reveals that the two mechanisms may result in overall similar chemical compositions, meaning that the SOA generated from the nucleation in the non-seeded experiments may have on average a comparable composition to those formed from the condensation process. The condensation process is expected to be more atmospherically relevant due to the abundance of pre-existing particles in the biomass burning plume. The relative abundance of investigated fragments ($C_xH_y^+$, $C_xH_yO^+$, $C_xH_yO_{>1}^+$, $C_xH_yN^+$ and $C_xH_yNO^+$) is roughly consistent among all of the experimental conditions, where $C_xH_yO^+$ and $C_xH_yO_{>1}^+$ fragments contribute to ~60-70% and $C_xH_yN^+$ plus $C_xH_yNO^+$ contribute to ~8-13%,

27

suggesting the dominance of $C_xH_yO_z$-containing products and a considerable amount of nitrogen-containing products in furan SOA.

In addition, the ratio of NO^+/NO_2^+ in all experiments was higher than what is expected from inorganic nitrates (1.30-1.42) (58, 59) (**Table S2.3**), confirming that some of the measured nitrate by the mAMS was organic in nature. However, the ratio did not show significant changes with oxidation time, suggesting that the contribution of the organic portion of nitrate to total nitrate did not change with the extent of oxidation. More importantly, higher NO_3 conditions did not result in significantly higher NO^+/NO_2^+ ratios for non-seeded experiments, suggesting again that the fraction of organonitrates/nitro-organic species in total nitrate was independent of the NO_3 concentration. In contrast, seeded, high NO_3 experiments displayed higher ratios of NO^+/NO_2^+ compared to seeded, low NO_3 experiments, indicating that higher NO_3 levels had resulted in a higher fraction of organonitrate/nitro-organics in the aerosols instead of inorganic nitrate. Regardless of NO_3 levels, the presence of seed decreased the contribution of organonitrate/nitro organics since significantly lower NO^+/NO_2^+ were observed in seeded experiments compared to non-seeded ones.

The molecular compositions of SOA constituents shown in **Figure 2.3** highlight the C_4 and C_8 products, which represent the monomer and dimer products of furan oxidation. In the non-seeded experiments, $C_4H_2O_4$ is the highest peak (**Figure 2.3A, B**), but in the seeded experiments, the intensity of $C_4H_4O_3$ is comparable to $C_4H_2O_4$ (**Figure 2.3C**) or even exceeds $C_4H_2O_4$ (**Figure 2.3D**). Since $C_4H_4O_3$ is also detected in the gas phase (**Figure 2.1, S2.2**), the $C_4H_4O_3$ found in the aerosol phase should be attributed to

gas-particle partitioning facilitated by pre-existing particles. However, $C_4H_2O_4$ is not observed in the gas-phase mass spectra, suggesting that rapid gas-particle partitioning and/or condensed-phase reactions on aerosols may contribute to this product. Notably, $C_4H_2O_5$, a more oxidized formula compared to $C_4H_2O_4$, is only detected in seeded experiments, implying that pre-existing particles may facilitate the generation of further oxidation products. Incremental addition of oxygen in other C_4 monomer series (i.e., $C_4H_4O_3$, $C_4H_4O_4$ and $C_4H_4O_5$; $C_4H_6O_4$ and $C_4H_6O_5$) is also observed in all the panels of **Figure 2.3**, indicating common pathways of $C_xH_yO_z$ product formation in furan SOA under all the environmental conditions. In addition, a series of dimers were identified in furan SOA (**Figure 2.3**). $C_8H_4O_3$ is most likely phthalic anhydride, which has been confirmed previously as a chromophore in secondary furan BrC, (32) while $C_8H_3NO_5$ could be its nitro-substituted product. Furthermore, IMS-TOF characterization of SOA constituents show significant differences in isomer distribution of oxygenated products led by the pre-existing particles while similar isomer distribution under the "high NO_3" and "low NO_3" conditions (**Figure S2.3**), revealing that pre-existing particles can alter the reaction pathways and hence modify SOA constituents.
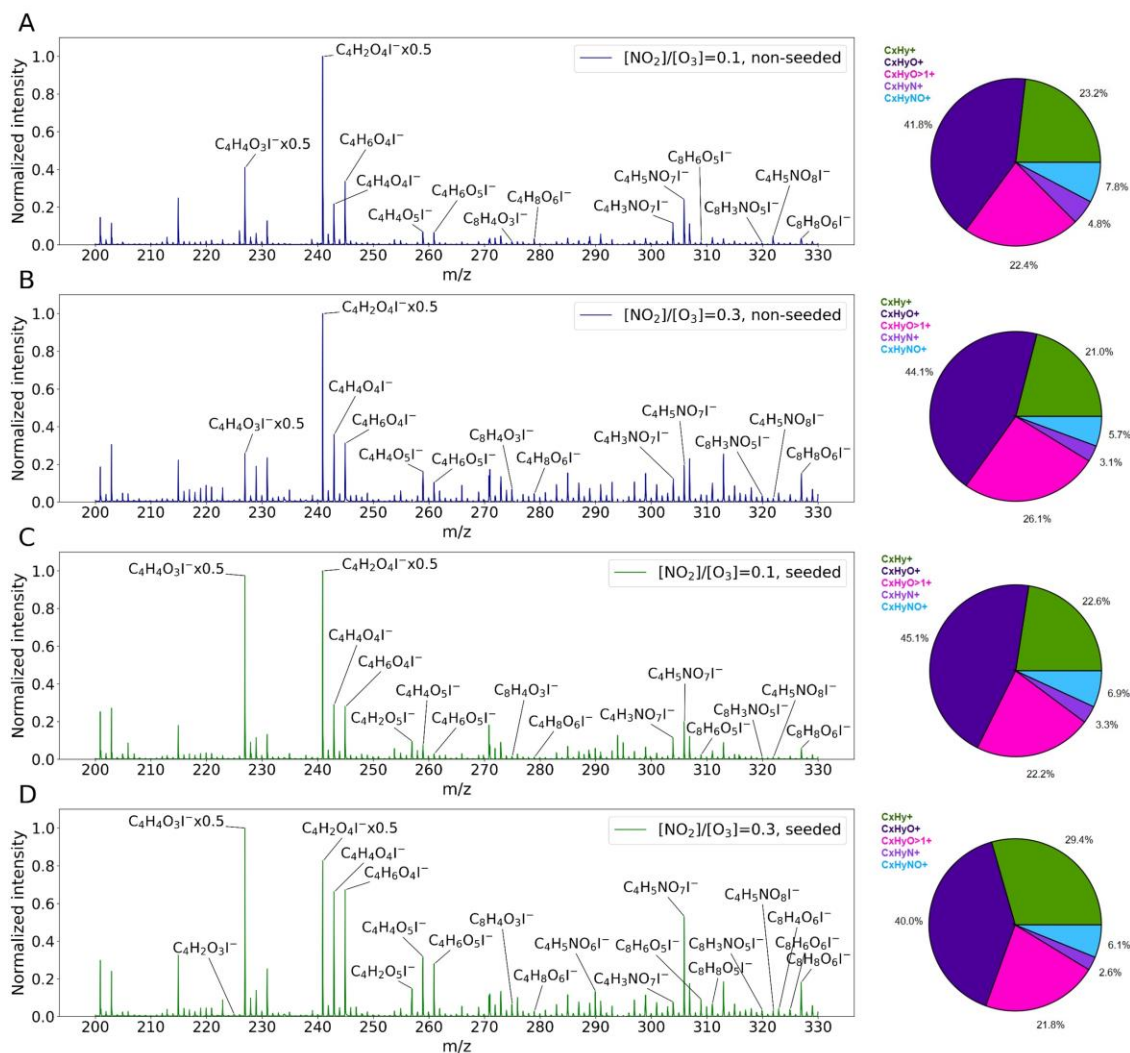
Figure 2.3. Molecular compositions of SOA measured by FIGAERO-ToF-CIMS and bulk compositions of SOA measured as ion fragment families by mAMS under various experimental conditions. (A) $[NO_2]/[O_3] = 0.1$, non-seeded; (B) $[NO_2]/[O_3] = 0.3$, non-seeded; (C) $[NO_2]/[O_3] = 0.1$, seeded; (D) $[NO_2]/[O_3] = 0.3$, seeded. Pie charts show the relative abundance of the investigated fragments: $C_xH_y^+$, $C_xH_yO^+$, $C_xH_yO_{>1}^+$, $C_xH_yN^+$ and $C_xH_yNO^+$.

Fingerprints of functional groups characterized by the ATR-FTIR can also provide further evidence to reveal the divergence of SOA constituents under various environmental conditions. **Figure 2.4** highlights three wavenumber regions that illustrate

the compositional difference. The orange area shades the wavenumber 1600−1800 cm^{-1}, which corresponds to the stretching modes of carbonyl groups (>C=O). Two peaks are seen at 1643 cm^{-1} and 1730 cm^{-1}, respectively; the first can also be attributed to the stretching of aliphatic C=C double bonds, but the latter is attributable only to >C=O stretching. (60) Without pre-existing particles, the presence of NO$_2$ flattens the peak at 1643 cm^{-1} but raises the peak at 1730 cm^{-1} (**Figure 2.4A**), which may be attributed to the higher consumption of aliphatic C=C double bonds along with the enhanced generation of carbonyl products during NO$_3$-initiated oxidation. This could be due to the fact that the NO$_3$-initiated oxidation of furan is much faster than the O$_3$-initiated oxidation, (52−54) and the "addition-elimination mechanism," in which carbonyls are produced along with the loss of NO$_2$ from the NO$_3$ groups added to furan, is the most energetically favorable pathway in the NO$_3$-initiated oxidation of furan. (57) However, the presence of pre-existing particles inhibits the peak at 1730 cm^{-1} (**Figure 2.4B**), implying further reactions of carbonyl products on the seed particles. The blue-shaded area (1300−1500 cm^{-1}) represents a mixture of functional group signals, with the O$_3$-only experiment producing three sharp peaks in the absence of seeds, while both NO$_3$ conditions produce only one peak at 1360 cm^{-1} (**Figure 2.4A**). This occurrence suggests that the presence of NO$_2$ together with O$_3$ can significantly modify the SOA compositions, but SOA compositions are insensitive to the changes in NO$_3$ levels. In contrast, only broad peaks were observed in seeded experiments (**Figure 2.4B**), highlighting the role of pre-existing particles in modifying the SOA constituents. The green-shaded area has a strong peak at 1095 cm^{-1} (i.e., C-O-C stretching (61)) in the seeded experiments, which may be attributed to the

31

gas-particle partitioning of more volatile oxidation products that preserve the furan backbone facilitated by pre-existing particles.

In addition, the formation of organosulfur products was observed in the presence of pre-existing particles (**Figure S2.4**), which indicates the unique condensed-phase chemistry supported by the sulfate-containing pre-existing particles (i.e., $(NH_4)_2SO_4$). Overall, the compositional profiles of furan-derived SOA may be resistant to the changes in NO_3 levels, but they can vary in the presence of pre-existing particles.
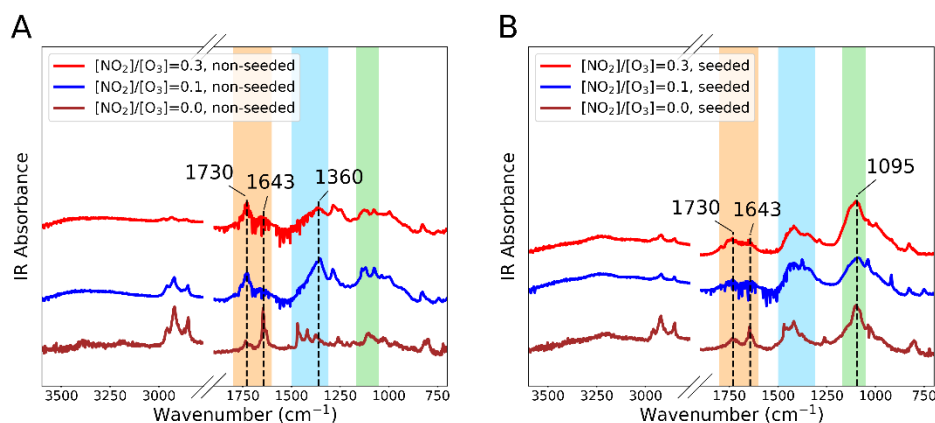
Figure 2.4. ATR-FTIR spectra corresponding to the ACN-extracted aerosol samples from nighttime oxidation of furan under different environmental conditions.

2.3.3. Light-absorption properties of furan BrC

The wavelength dependent MACs are depicted in **Figure 2.5**. The SOA mass concentration and online MAC at 375 nm (MAC_{375}) are provided in **Table 2.1**, followed by the $AAE_{290/400}$ and $AAE_{400/600}$. **Figure 2.5** shows the elevated MACs related to the

increased NO_3 levels. Given the consistent SOA mass concentrations under the various NO_3 levels studied (**Table 2.1**), our findings indicate that higher levels of NO_3-initiated oxidation can result in the production of more BrC constituents absorbing in the near UV range. Furthermore, the presence of pre-existing particles led to higher the SOA mass concentrations (**Table 2.1**) and lower MAC profiles (**Figure 2.5**). Because pre-existing particles can facilitate gas-particle partitioning and promote SOA formation by enhancing aerosol-phase reactions, it appears that the seed promoted the addition of non-absorbing products more compared to BrC chromophores. Our results may also suggest that semi-volatile products that would not condense without the seed are not as light-absorbing compared to the low-volatile products that condense under both conditions. To rule out potential interference caused by solvent effects during extractions, (32) online MAC_{375} measurements were also compared. The results show the consistency of MAC_{375} under the studied NO_3 levels but a reduction by half of MAC_{375} in the presence of pre-existing particles (**Table 2.1**). In addition, the results of $AAE_{290/400}$ and $AAE_{400/600}$ may indicate that MAC profiles have a weaker wavelength dependence of in the presence of pre-existing particles.
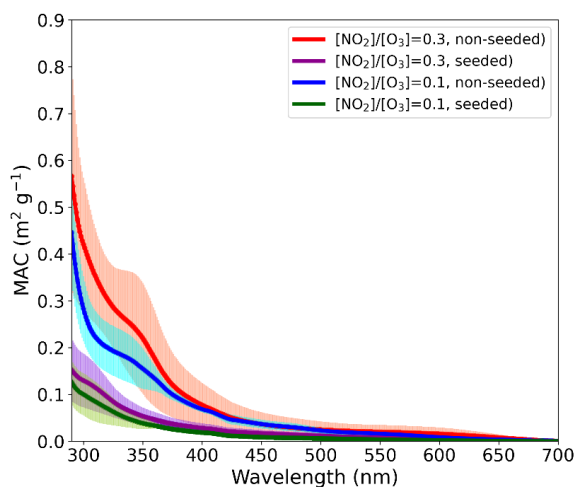
Figure 2.5. MAC profiles of furan BrC under the investigated conditions. The spectral curves are estimated by the average of three replica samples and the shared areas are estimated by the corresponding standard deviations of MAC at each wavelength.

Table 2.1. Summary of C_{SOA}, online MAC_{375}, $AAE_{290/400}$ and $AAE_{400/600}$ under different environmental conditions. Results are expressed as mean $\pm$ 1 standard deviation (SD) from triplicate experiments. The data shown in the non-seeded experiments were from our previous study. (32)

$[NO_2]/[O_3]$	Pre-existing particles	C_{SOA} (μg m^{-3})	MAC_{375} (m^2 g^{-1})	$AAE_{290/400}$	$AAE_{400/600}$
0.1	No	17.73 ± 1.68	0.09 ± 0.03	5.82 ± 0.55	5.28 ± 0.85
	Yes	42.46 ± 1.80	0.04 ± 0.01	3.26 ± 1.36	3.98 ± 0.65
0.3	No	17.74 ± 1.65	0.08 ± 0.01	5.98 ± 1.03	4.14 ± 0.30
	Yes	40.86 ± 5.15	0.04 ± 0.01	4.11 ± 0.88	3.93 ± 0.84
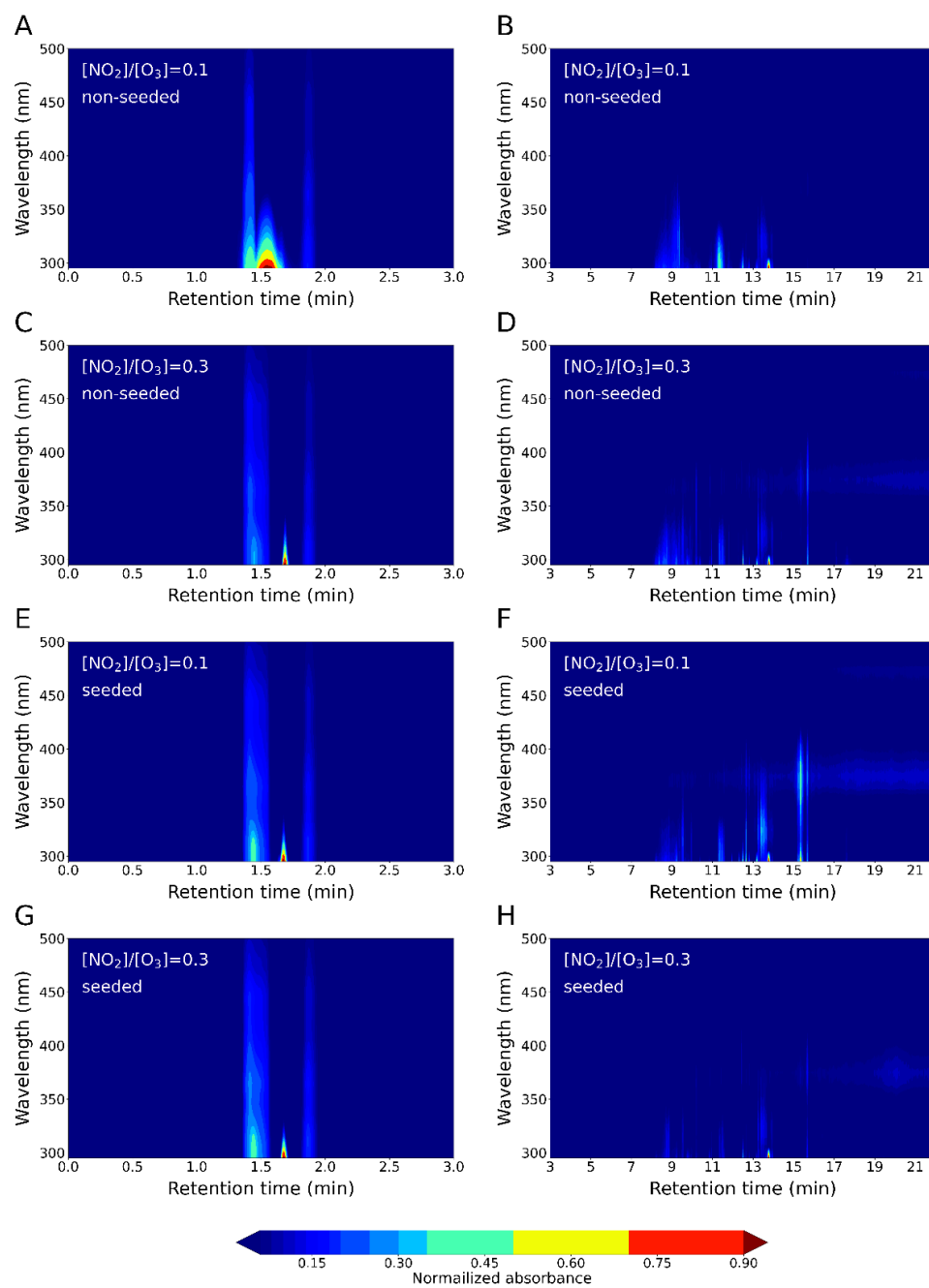
Figure 2.6. LC-DAD heatmap of furan BrC chromophores under various environmental conditions.

Moreover, **Figure 2.6** shows the LC-DAD chromatograms (absorption wavelength versus the chromatographic retention time), where each heatmap displays the relative light absorption intensity of chromophores under the corresponding experimental conditions. All the chromophores are distributed in the UV range, agreeing with the MAC profiles (**Figure 2.5**), in which the major absorption is below 400 nm. The distribution of chromophores exhibits a similar pattern in the LC-DAD chromatogram for all the experimental conditions, where the strongest light absorption hotspot emerges within the retention time between 1.5−2.0 min, while several weaker absorption hotspots are spread over 7.0−17.0 min. Moreover, the strongest hotspot has the highest absorption at ~300 nm, while those weaker hotspots are spread within the range of 300−400 nm, corresponding to the protruding shoulder at ~350 nm in the MAC profiles (**Figure 2.5**).

2.3.4. Molecular compositions of chromophores in furan BrC

Understanding the chromophore composition is fundamental to the process-level evaluation of secondary BrC formation. Since the strongest absorption hotspot in **Figure 2.6** is at around 1.7 min and 290 nm, the DAD chromatogram at 290 nm is extracted (**Figure 2.7A**) and the mass spectrum of the identified peak is analyzed (**Figure 2.7B**). The predominant peak in the mass spectrum is assigned to the deprotonated anion (i.e., [M-H]$^-$) of $C_4H_4O_6$, whose extracted ion chromatogram (EIC) also shows a distinct peak at 1.7 min (**Figure 2.7C**). $C_4H_4O_6$ is a highly oxidized product and could be generated from further oxidation of $C_4H_4O_3$, $C_4H_4O_4$ and $C_4H_4O_5$ that were identified in the FIGAERO-CIMS data (**Figure 2.3**). The measured UV−vis spectrum from LC-DAD

shows a similar sketch to the MAC profiles (**Figure 2.5**), indicating that $C_4H_4O_6$ is one of the major chromophores in furan BrC from nighttime oxidation (**Figure 2.6**).

As discussed above, the hotspots over 7.0−17.0 min from LC-DAD can contribute to the protruding shoulder in the MAC profiles (**Figure 2.5**). Compositional analysis reveals that these hotspots may be attributable to higher molecular weight oxidation products (i.e., dimers and oligomers) with high double bond equivalents (DBE). For example, **Figure S2.5A−C** shows three dimers, $C_8H_6O_4$ (DBE = 6), $C_8H_6O_6$ (DBE = 6) and $C_8H_4O_6$ (DBE = 7), which may correlate to the hotspots at 9 min and 11.2 min, respectively. The oligomers $C_{14}H_{22}O_5$ (DBE = 4), $C_{15}H_{21}NO_5$ (DBE = 5) and $C_{10}H_{13}NO_5$ (DBE = 4) shown in **Figure S2.5D−F** may correspond to the hotspots at 11.2 min and 13.5 min, respectively. Notably, because each hotspot shown in the heatmap may account for multiple chromophores (e.g., **Figure S2.5B−E**), it is challenging to quantify their contributions here without authentic standards. Nevertheless, dimers and oligomers appear to play an important role in BrC light absorption in furan SOA.

Due to the smaller proportion of nitrogen-containing products in furan SOA compositions, the solvent selectivity or artifacts during LC analysis that may further impede the detection of chromophores that are sensitive to solvent attacks (e.g., hydrolysis or methanolysis of anhydrides by LC mobile phases). (32) In addition, not all the SOA components can be efficiently ionized by the ESI source. (62, 63) As a result, identified chromophores in this subset by LC-DAD-ESI-Q-ToFMS are limited. However, several unsaturated nitrogen-containing products were identified by an independent solvent-free approach using FIGAERO-ToF-CIMS; thus, we performed TD-DFT

calculations to determine whether these products could be potential chromophores. For instance, $C_4H_3NO_7$ (DBE = 3), is a functionalized monomer which may have two light-absorbing isomers: 2-hydroxy-3-nitro-maleic acid and 2-hydroxy-3-nitro-fumaric acid (**Figure 2.8A**). $C_8H_3NO_5$ (DBE = 7) is likely nitrophthalic anhydrides that are susceptible to solvent attacks (**Figure 2.8B**). Given the strong absorptivity of these products, nitrogen-containing chromophores may still contribute significantly to BrC light absorption even though their mass fraction is small.
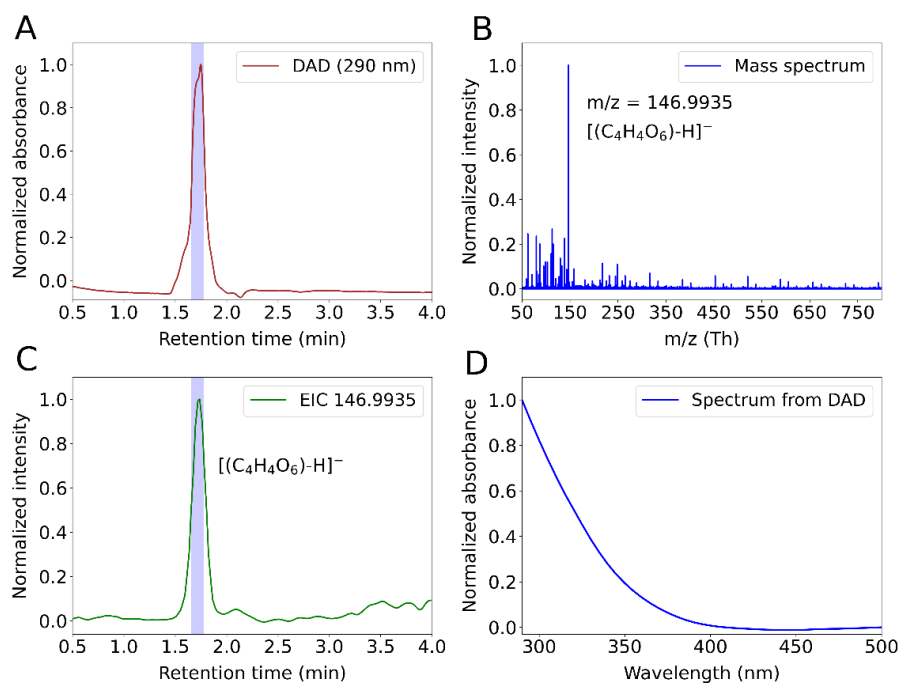
Figure 2.7. Identification of $C_4H_4O_6$ as a BrC chromophore. (A) DAD extracted wavelength chromatogram at 290 nm, (B) extracted mass spectrum of the shaded area in the DAD chromatogram, (C) EIC of the deprotonated $C_4H_4O_6$, and (D) UV−vis spectrum from the shaded area in the DAD chromatogram.
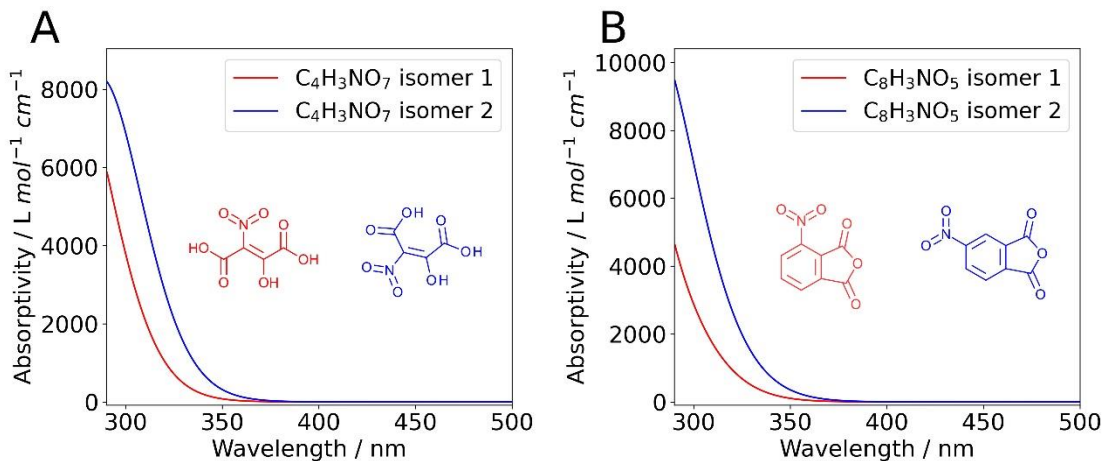
Figure 2.8. Theoretical UV−vis spectra of nitrogen-containing chromophores: (A) $C_4H_3NO_7$ and (B) $C_8H_3NO_5$.

2.4. Atmospheric implications

This study investigated the secondary BrC formation from nighttime oxidation of furan by varying the NO_3 levels and pre-existing particles. Our analysis revealed the key role of NO_3-initiated oxidation in furan oxidation under the in-plume environment and highlighted the effects of oxidant levels and pre-existing particles on chemical compositions and optical properties. Increased NO_3 levels can enhance the MAC profiles, but the overall bulk compositions in furan SOA measured as ion fragment families by mAMS are insensitive to this change. Since rapid SOA formation has been observed in biomass burning plumes exposed to NO_2 and O_3 during the nighttime but has not been well represented in modeling studies, (64) our work contributes to a better understanding of the role of nighttime oxidant levels in furan SOA formation and BrC light absorption. Our results also indicate that the pre-existing particles can increase the SOA mass concentrations but, in the meantime, decrease the MAC profiles under dry conditions

(RH< 20%). MAC reduction due to pre-existing particles under dry conditions may be an important process for evaluating BrC radiative forcing in climate models, as pre-existing particles have been demonstrated as a crucial factor that controls SOA formation in a changing climate. (65)

Our study is pertinent to biomass burning plumes with low RH (e.g., the Williams Fire plume (66)) or plumes of higher RH expanded into the low RH atmospheres, such as those in the western United States (67, 68) and Africa during dry seasons. (69, 70) The molecular compositions reported here can contribute to a more comprehensive molecular understanding of furan oxidation. We show that under different environmental conditions, highly oxidized monomers, dimers, and oligomers can contribute to BrC chromophores. Multiple anhydride species, including maleic anhydride (or furandione), phthalic anhydride, and nitrophthalic anhydrides, can be potentially important chromophores in furan BrC under dry conditions. (32) Notably, atmospheric convection can vertically transport BrC into the upper troposphere, (71) where the average relative humidity is approximately 27% and less than 10% for subtropical regions. (72) Anhydride chromophores are likely to have a longer lifetime in the upper troposphere. Even under wet conditions where anhydrides could be hydrolyzed, the resulting products may still be chromophores. For example, phthalic acid (or 1,2-benzenedicarboxylic acid), the hydrolysis product of phthalic anhydride, has been reported as one of the most prevalent BrC chromophores in ambient observations. (73, 74) Nitrophthalic acid, the hydrolysis product of nitrophthalic anhydrides, was also identified as a chromophore in the aerosols produced by the combustion of biomass. (75) Since both of these hydrolysis

products are organic markers of SOA, (76−79) the hydrolysis of anhydrides can be used to track the formation and evolution of secondary BrC. Overall, our findings highlight the influence of NO_3 levels and pre-existing particles on the chemical composition and optical properties of nighttime furan SOA, whereas bulk and molecular characterizations of SOA constituents and chromophores are necessary for better experimental constraint and a more complete process-level understanding of their formation.

2.5. Supplemental Information

Table S2.1. Summary of particulate effective density (ρ_{eff}) and organic aerosol fraction (MF_{OA}) under different environmental conditions. Results are expressed as mean $\pm$ 1 standard deviation (SD) from triplicate experiments. The data shown in the non-seeded experiments were from our previous study. (32)

[NO$_2$]/[O$_3$]	Pre-existing particles	ρ_{eff} (g cm^{-3})	MF_{OA} (%)
0.1	No	1.40 ± 0.04	94.33 ± 1.25
	Yes	1.44 ± 0.10	50.00 ± 2.00
0.3	No	1.37 ± 0.12	94.33 ± 1.25
	Yes	1.58 ± 0.11	48.33 ± 2.49

Table S2.2. Cartesian coordinates for the geometrical structures in the TD-DFT calculations.

$C_4H_3NO_7$ isomer 1

C	-1.84059600	-0.68744300	0.01099200
C	-0.53770800	0.01431000	-0.00120000
C	0.62693900	-0.73429800	-0.00571300
C	2.04326600	-0.17893700	-0.10601300
O	-2.96568200	-0.00873600	0.01470300
O	2.57850500	-0.00780300	1.09568500
O	-1.85866300	-1.91966800	0.01955500
O	2.58502300	-0.04957600	-1.17028800
O	0.61952100	-2.03166900	0.00849100
N	-0.44411200	1.44432800	-0.00574900
O	-1.49817900	2.10585900	-0.01174200
O	0.66063900	1.97129600	-0.00326600
H	-2.75280600	0.95596800	0.00463400
H	3.49917300	0.29327800	1.00422800
H	-0.35829600	-2.31896700	0.01788200

$C_4H_3NO_7$ isomer 2

C	-0.47271977	-0.06114189	0.49871577
C	0.62693900	-0.73429800	-0.00571300
C	2.04326600	-0.17893700	-0.10601300
O	-2.86544670	-0.10271093	0.90977736
O	2.37089846	0.50158606	0.98457907
O	-1.89545777	-1.83857240	-0.05099428
O	2.75617619	-0.46086884	-1.03077766
O	0.53888617	-1.92169695	-0.52123091
O	-1.28756257	1.84239989	1.50358034

O	0.83350251	1.72881400	1.09510096
H	3.29561354	0.79730272	0.92056818
H	-0.44204654	-2.19285567	-0.46647326
H	-2.15218308	1.42693133	1.46593418
N	-1.80019806	-0.71276925	0.44121609
C	-0.28973150	1.24356506	1.06261953

$C_8H_3NO_5$ isomer 1

C	0.10643200	-0.10618300	0.00003700
C	1.23560200	0.74932000	0.00000300
C	1.11094400	2.13079700	-0.00001100
C	-0.19023200	2.67356600	0.00001000
C	-1.31177500	1.85066200	0.00004200
C	-1.16819600	0.43998900	0.00005600
C	0.59655200	-1.52500200	0.00004700
C	2.46726100	-0.08121500	-0.00001200
H	1.99102300	2.78439800	-0.00003700
H	-0.31615700	3.76432400	0.00000000
H	-2.32250300	2.28596700	0.00005600
N	-2.39222100	-0.39496400	0.00009000
O	-3.46870100	0.18144100	-0.00008500
O	-2.26332700	-1.60680400	-0.00017700
O	0.10391000	-2.60791000	0.00007700
O	3.64108600	0.12315300	-0.00004000
O	2.02624000	-1.44757200	0.00001600

$C_8H_3NO_5$ isomer 2

| C | -0.62918300 | 0.55265800 | -0.00000200 |
| C | -1.03320600 | -0.81325800 | -0.00000800 |

C	-0.11943800	-1.84248700	-0.00001400
C	1.25502900	-1.49904600	-0.00001300
C	1.64208900	-0.15846400	-0.00000500
C	0.70251700	0.90699400	-0.00000100
C	-1.84407400	1.40637900	0.00000600
C	-2.52809300	-0.85472400	-0.00000200
H	-0.42426700	-2.89514900	-0.00001900
H	2.01317800	-2.29726500	-0.00001800
O	-2.07626000	2.57496500	0.00001500
O	-3.35473300	-1.71367100	-0.00000100
O	-2.96695100	0.50582800	0.00000600
N	3.08434000	0.17582100	0.00000400
O	3.39998400	1.35538800	-0.00004800
O	3.88656800	-0.74489900	0.00005700
H	1.03799200	1.95246900	0.00000600

Table S2.3. Summary of NO^+/NO_2^+ values under different environmental conditions. Results are expressed as mean $\pm$ 1 SD from triplicate experiments.

$[NO_2]/[O_3]$	Pre-existing particles	NO^+/NO_2^+	
		Early	Late
0.1	No	2.42 ± 0.13	2.41 ± 0.16
	Yes	2.16 ± 0.07	2.19 ± 0.04
0.3	No	2.58 ± 0.10	2.42 ± 0.26
	Yes	2.33 ± 0.04	2.34 ± 0.05
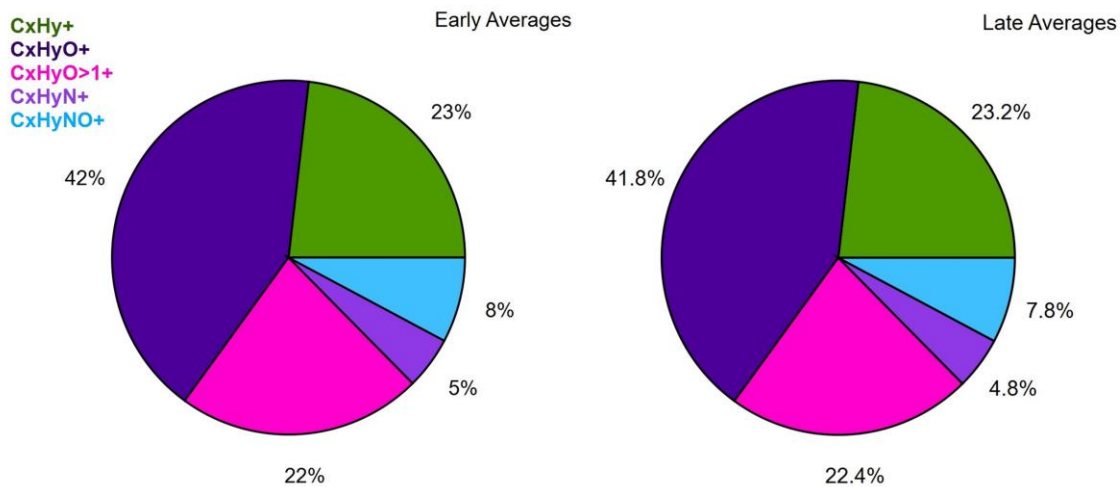
Figure S2.1. Example pie charts for comparing the early averages and the late averages of the fragment abundance measured by the mAMS. The experimental condition is low NO_3 without seeds.
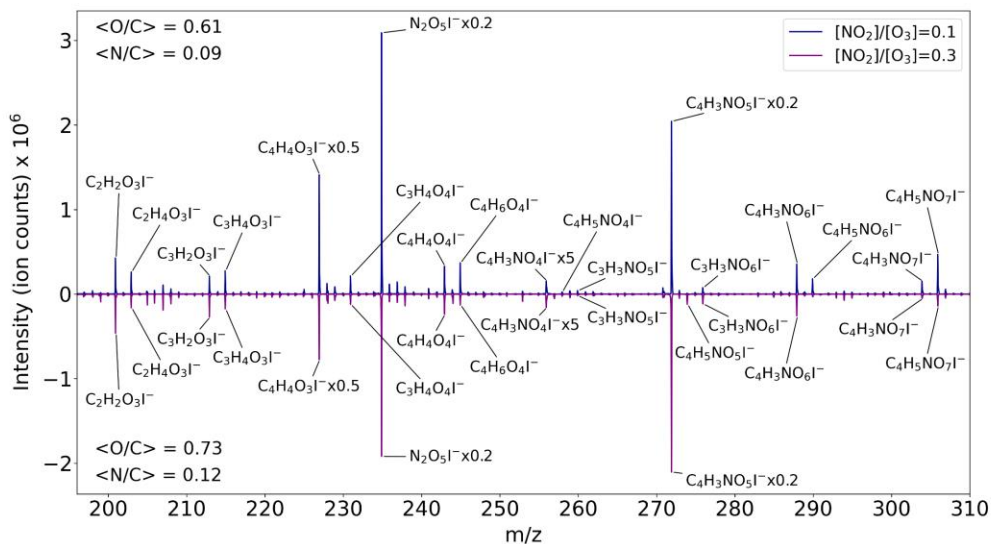
Figure S2.2. Comparison of gas-phase products from nighttime oxidation of furan between the "low NO$_3$" and "high NO$_3$" experiments (i.e., initial [NO$_2$]/[O$_3$] = 0.1 and 0.3). <O/C> and <N/C> represent the intensity-weighted average values of O/C and N/C based on the identified products.
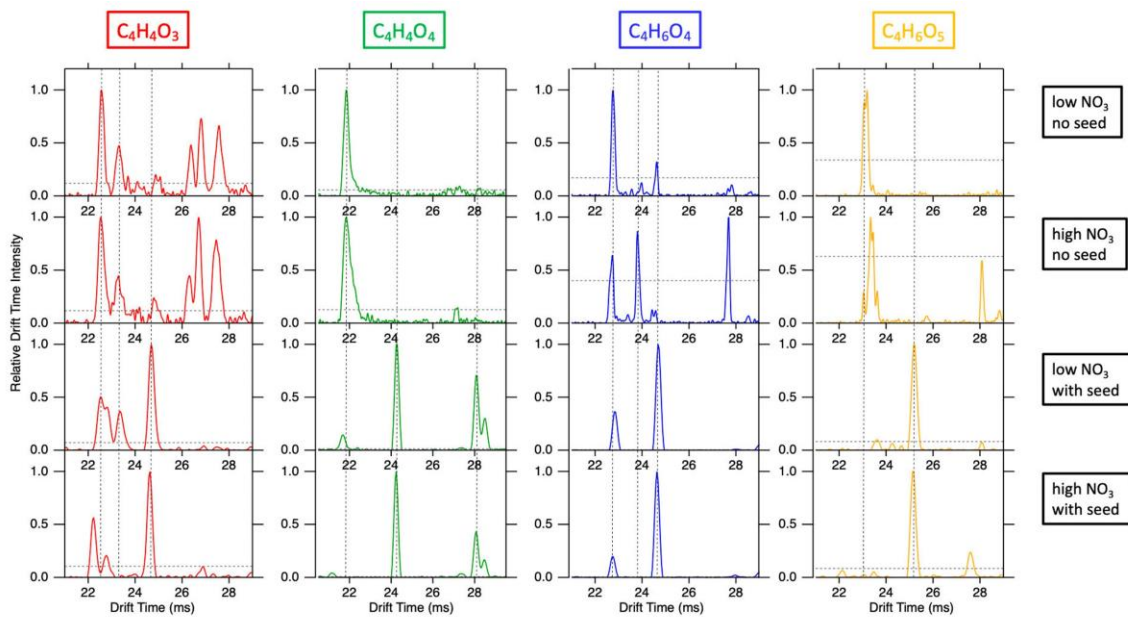
Figure S2.3. IMS-TOF characterization of isomer distribution of oxygenated products in furan SOA under different experimental conditions.
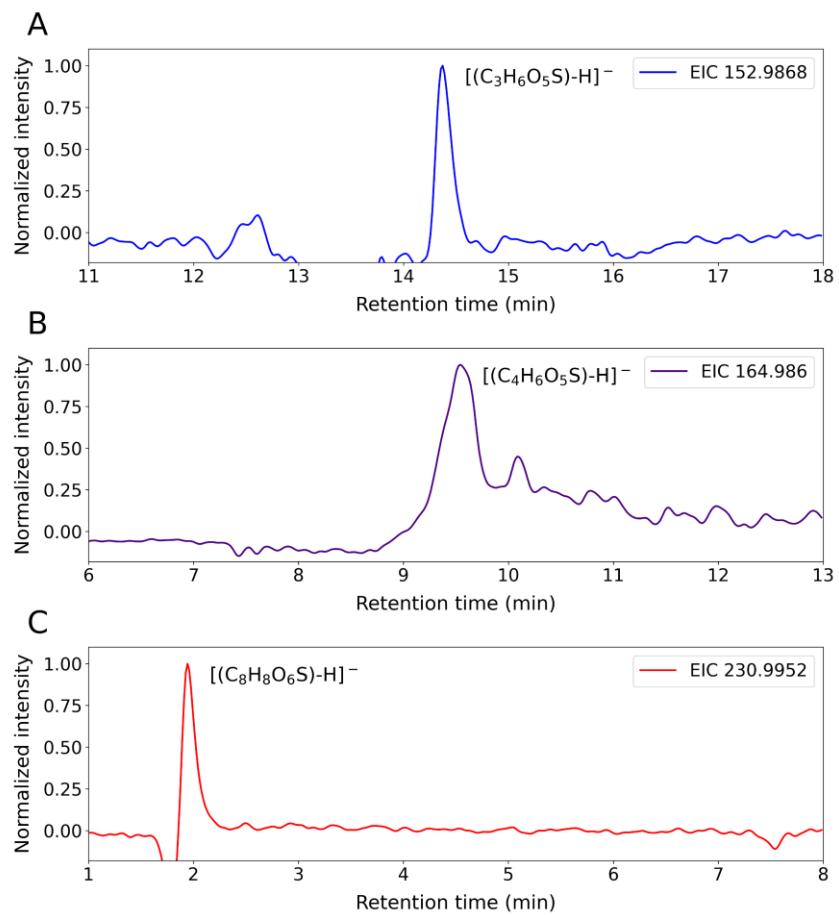
Figure S2.4. Extracted ion chromatograms (EIC) of organosulfur products.
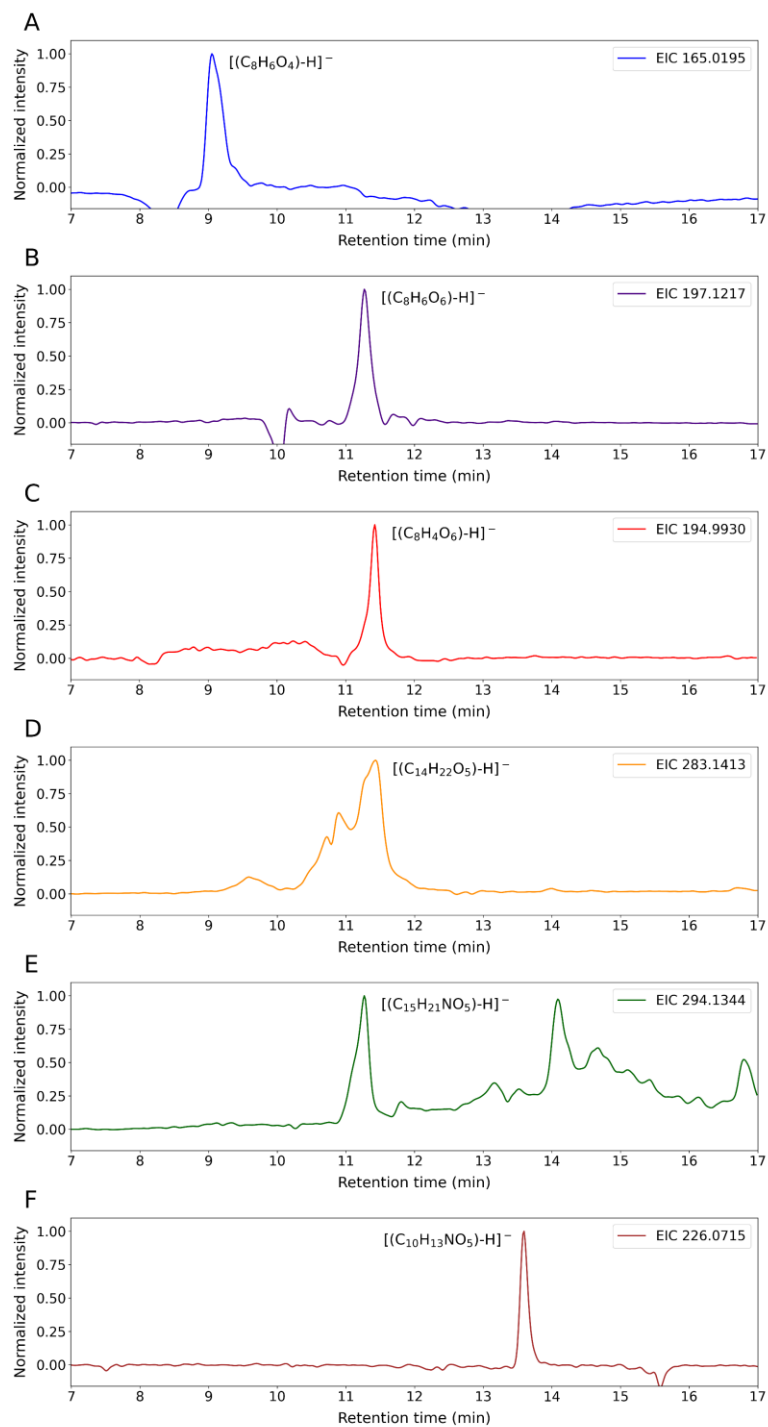
Figure S2.5. EICs of tentatively light-absorbing dimers and oligomers in furan BrC.

2.6. References

1. Ma, Y.; Hays, M. D., Thermal extraction–two-dimensional gas chromatography–mass spectrometry with heart-cutting for nitrogen heterocyclics in biomass burning aerosols. *J. Chromatogr. A* **2008**, 1200, (2), 228-234.

2. Akagi, S. K.; Yokelson, R. J.; Burling, I. R.; Meinardi, S.; Simpson, I.; Blake, D. R.; McMeeking, G. R.; Sullivan, A.; Lee, T.; Kreidenweis, S.; Urbanski, S.; Reardon, J.; Griffith, D. W. T.; Johnson, T. J.; Weise, D. R., Measurements of reactive trace gases and variable O_3 formation rates in some South Carolina biomass burning plumes. *Atmos. Chem. Phys.* **2013**, 13, (3), 1141-1165.

3. Hatch, L. E.; Luo, W.; Pankow, J. F.; Yokelson, R. J.; Stockwell, C. E.; Barsanti, K. C., Identification and quantification of gaseous organic compounds emitted from biomass burning using two-dimensional gas chromatography–time-of-flight mass spectrometry. *Atmos. Chem. Phys.* **2015**, 15, (4), 1865-1899.

4. Stefanova, M.; Marinov, S. P.; Mastral, A. M.; Callén, M. S.; Garcí, T., Emission of oxygen, sulphur and nitrogen containing heterocyclic polyaromatic compounds from lignite combustion. *Fuel Process. Technol.* **2002**, 77-78, 89-94.

5. Liang, F.; Lu, M.; Birch, M. E.; Keener, T. C.; Liu, Z., Determination of polycyclic aromatic sulfur heterocycles in diesel particulate matter and diesel fuel by gas chromatography with atomic emission detection. *J. Chromatogr. A* **2006**, 1114, (1), 145-153.

6. Westerling, A. L.; Hidalgo, H. G.; Cayan, D. R.; Swetnam, T. W., Warming and Earlier Spring Increase Western U.S. Forest Wildfire Activity. *Science* **2006**, 313, (5789), 940-943.

7. Shi, G.; Yan, H.; Zhang, W.; Dodson, J.; Heijnis, H.; Burrows, M., Rapid warming has resulted in more wildfires in northeastern Australia. *Sci. Total Environ.* **2021**, 771, 144888.

8. Baker, S. J., Fossil evidence that increased wildfire activity occurs in tandem with periods of global warming in Earth's past. *Earth Sci. Rev.* **2022**, 224, 103871.

9. Mettler, M. S.; Mushrif, S. H.; Paulsen, A. D.; Javadekar, A. D.; Vlachos, D. G.; Dauenhauer, P. J., Revealing pyrolysis chemistry for biofuels production: Conversion of cellulose to furans and small oxygenates. *Energy Environ. Sci.* **2012**, 5, (1), 5414-5424.

10. Koss, A. R.; Sekimoto, K.; Gilman, J. B.; Selimovic, V.; Coggon, M. M.; Zarzana, K. J.; Yuan, B.; Lerner, B. M.; Brown, S. S.; Jimenez, J. L.; Krechmer, J.; Roberts, J. M.; Warneke, C.; Yokelson, R. J.; de Gouw, J., Non-methane organic gas emissions from biomass burning: identification, quantification, and emission factors from PTR-ToF during the FIREX 2016 laboratory experiment. *Atmos. Chem. Phys.* **2018**, 18, (5), 3299-3319.

11. Sekimoto, K.; Koss, A. R.; Gilman, J. B.; Selimovic, V.; Coggon, M. M.; Zarzana, K. J.; Yuan, B.; Lerner, B. M.; Brown, S. S.; Warneke, C.; Yokelson, R. J.; Roberts, J. M.; de Gouw, J., High- and low-temperature pyrolysis profiles describe volatile organic compound emissions from western US wildfire fuels. *Atmos. Chem. Phys.* **2018**, 18, (13), 9263-9281.

12. Ahern, A. T.; Robinson, E. S.; Tkacik, D. S.; Saleh, R.; Hatch, L. E.; Barsanti, K. C.; Stockwell, C. E.; Yokelson, R. J.; Presto, A. A.; Robinson, A. L.; Sullivan, R. C.; Donahue, N. M., Production of Secondary Organic Aerosol During Aging of Biomass Burning Smoke from Fresh Fuels and Its Relationship to VOC Precursors. *J. Geophys. Res. Atmos.* **2019**, 124, (6), 3583-3606.

13. Gilman, J. B.; Lerner, B. M.; Kuster, W. C.; Goldan, P. D.; Warneke, C.; Veres, P. R.; Roberts, J. M.; de Gouw, J. A.; Burling, I. R.; Yokelson, R. J., Biomass burning emissions and potential air quality impacts of volatile organic compounds and other trace gases from fuels common in the US. *Atmos. Chem. Phys.* **2015**, 15, (24), 13915-13938.

14. Palm, B. B.; Peng, Q.; Fredrickson, C. D.; Lee, B. H.; Garofalo, L. A.; Pothier, M. A.; Kreidenweis, S. M.; Farmer, D. K.; Pokhrel, R. P.; Shen, Y.; Murphy, S. M.; Permar, W.; Hu, L.; Campos, T. L.; Hall, S. R.; Ullmann, K.; Zhang, X.; Flocke, F.; Fischer, E. V.; Thornton, J. A., Quantification of organic aerosol and brown carbon evolution in fresh wildfire plumes. *PNAS* **2020**, 117, (47), 29469.

15. Atkinson, R.; Aschmann, S. M.; Tuazon, E. C.; Arey, J.; Zielinska, B., Formation of 3-methylfuran from the gas-phase reaction of OH radicals with isoprene and the rate constant for its reaction with the OH radical. *Int. J. Chem. Kinet.* **1989**, 21, (7), 593-604.

16. Sprengnether, M.; Demerjian, K. L.; Donahue, N. M.; Anderson, J. G., Product analysis of the OH oxidation of isoprene and 1,3-butadiene in the presence of NO. *J. Geophys. Res. Atmos.* **2002**, 107, (D15), ACH 8-1-ACH 8-13.

17. Francisco-Márquez, M.; Alvarez-Idaboy, J. R.; Galano, A.; Vivier-Bunge, A., A Possible Mechanism for Furan Formation in the Tropospheric Oxidation of Dienes. *Environ. Sci. Technol.* **2005**, 39, (22), 8797-8802.

18. Stefenelli, G.; Jiang, J.; Bertrand, A.; Bruns, E. A.; Pieber, S. M.; Baltensperger, U.; Marchand, N.; Aksoyoglu, S.; Prévôt, A. S. H.; Slowik, J. G.; El Haddad, I., Secondary organic aerosol formation from smoldering and flaming combustion of biomass: a box model parametrization based on volatility basis set. *Atmos. Chem. Phys.* **2019**, 19, (17), 11461-11484.

19. Akherati, A.; He, Y.; Coggon, M. M.; Koss, A. R.; Hodshire, A. L.; Sekimoto, K.; Warneke, C.; de Gouw, J.; Yee, L.; Seinfeld, J. H.; Onasch, T. B.; Herndon, S. C.; Knighton, W. B.; Cappa, C. D.; Kleeman, M. J.; Lim, C. Y.; Kroll, J. H.; Pierce, J. R.; Jathar, S. H., Oxygenated Aromatic Compounds are Important Precursors of Secondary Organic Aerosol in Biomass-Burning Emissions. *Environ. Sci. Technol.* **2020**, 54, (14), 8568-8579.

20. Coggon, M. M.; Lim, C. Y.; Koss, A. R.; Sekimoto, K.; Yuan, B.; Gilman, J. B.; Hagan, D. H.; Selimovic, V.; Zarzana, K. J.; Brown, S. S.; Roberts, J. M.; Müller, M.; Yokelson, R.; Wisthaler, A.; Krechmer, J. E.; Jimenez, J. L.; Cappa, C.; Kroll, J. H.; de Gouw, J.; Warneke, C., OH chemistry of non-methane organic gases (NMOGs) emitted from laboratory and ambient biomass burning smoke: evaluating the influence of furans and oxygenated aromatics on ozone and secondary NMOG formation. *Atmos. Chem. Phys.* **2019**, 19, (23), 14875-14899.

21. Jiang, J.; Carter, W. P. L.; Cocker, D. R.; Barsanti, K. C., Development and Evaluation of a Detailed Mechanism for Gas-Phase Atmospheric Reactions of Furans. *ACS Earth Space Chem.* **2020**, 4, (8), 1254-1268.

22. Gómez Alvarez, E.; Borrás, E.; Viidanoja, J.; Hjorth, J., Unsaturated dicarbonyl products from the OH-initiated photo-oxidation of furan, 2-methylfuran and 3-methylfuran. *Atmos. Environ.* **2009**, 43, (9), 1603-1612.

23. Joo, T.; Rivera-Rios, J. C.; Takeuchi, M.; Alvarado, M. J.; Ng, N. L., Secondary Organic Aerosol Formation from Reaction of 3-Methylfuran with Nitrate Radicals. *ACS Earth and Space Chem.* **2019**, 3, (6), 922-934.

24. Strollo, C. M.; Ziemann, P. J., Products and mechanism of secondary organic aerosol formation from the reaction of 3-methylfuran with OH radicals in the presence of NO_x. *Atmos. Environ.* **2013**, 77, 534-543.

25. Jiang, X.; Tsona, N. T.; Jia, L.; Liu, S.; Zhang, H.; Xu, Y.; Du, L., Secondary organic aerosol formation from photooxidation of furan: effects of NO_x and humidity. *Atmos. Chem. Phys.* **2019**, 19, (21), 13591-13609.

26. Cao, J., The Importance of Aerosols in the Earth System: Science and Engineering Perspectives. *Aerosol Sci. Eng.* **2017**, 1, (1), 1-6.

27. Grace, D. N.; Sharp, J. R.; Holappa, R. E.; Lugos, E. N.; Sebold, M. B.; Griffith, D. R.; Hendrickson, H. P.; Galloway, M. M., Heterocyclic Product Formation in Aqueous Brown Carbon Systems. *ACS Earth Space Chem.* **2019**, 3, (11), 2472-2481.

28. Jiang, H.; Frie, A. L.; Lavi, A.; Chen, J. Y.; Zhang, H.; Bahreini, R.; Lin, Y.-H., Brown Carbon Formation from Nighttime Chemistry of Unsaturated Heterocyclic Volatile Organic Compounds. *Environ. Sci. Technol. Lett.* **2019**, 6, (3), 184-190.

29. Tsigaridis, K.; Kanakidou, M., Secondary organic aerosol importance in the future atmosphere. *Atmos. Environ.* **2007**, 41, (22), 4682-4692.

30. Lambe, A. T.; Cappa, C. D.; Massoli, P.; Onasch, T. B.; Forestieri, S. D.; Martin, A. T.; Cummings, M. J.; Croasdale, D. R.; Brune, W. H.; Worsnop, D. R.; Davidovits, P., Relationship between Oxidation Level and Optical Properties of Secondary Organic Aerosol. *Environ. Sci. Technol.* **2013**, 47, (12), 6349-6357.

31. Mayorga, R.; Chen, K.; Raeofy, N.; Woods, M.; Lum, M.; Zhao, Z.; Zhang, W.; Bahreini, R.; Lin, Y.-H.; Zhang, H., Chemical Structure Regulates the Formation of Secondary Organic Aerosol and Brown Carbon in Nitrate Radical Oxidation of Pyrroles and Methylpyrroles. *Environ. Sci. Technol.* **2022**, 56, (12), 7761-7770.

32. Chen, K.; Raeofy, N.; Lum, M.; Mayorga, R.; Woods, M.; Bahreini, R.; Zhang, H.; Lin, Y.-H., Solvent effects on chemical composition and optical properties of extracted secondary brown carbon constituents. *Aerosol Sci. Tech.* **2022**, 56, (10), 917-930.

33. Strand, T.; Larkin, N.; Rorig, M.; Krull, C.; Moore, M., PM2.5 measurements in wildfire smoke plumes from fire seasons 2005–2008 in the Northwestern United States. *J. Aerosol Sci.* **2011**, 42, (3), 143-155.

34. Ding, Y.; Cruz, I.; Freedman, F.; Venkatram, A., Improving spatial resolution of PM2.5 measurements during wildfires. *Atmos. Pollut. Res.* **2021**, 12, (5), 101047.

35. Decker, Z. C. J.; Zarzana, K. J.; Coggon, M.; Min, K.-E.; Pollack, I.; Ryerson, T. B.; Peischl, J.; Edwards, P.; Dubé, W. P.; Markovic, M. Z.; Roberts, J. M.; Veres, P. R.; Graus, M.; Warneke, C.; de Gouw, J.; Hatch, L. E.; Barsanti, K. C.; Brown, S. S., Nighttime Chemical Transformation in Biomass Burning Plumes: A Box Model Analysis Initialized with Aircraft Observations. *Environ. Sci. Technol.* **2019**, 53, (5), 2529-2538.

36. Ziemann, P. J.; Atkinson, R., Kinetics, products, and mechanisms of secondary organic aerosol formation. *Chem. Soc. Rev.* **2012**, 41, (19), 6582-6605.

37. Bahreini, R.; Keywood, M. D.; Ng, N. L.; Varutbangkul, V.; Gao, S.; Flagan, R. C.; Seinfeld, J. H.; Worsnop, D. R.; Jimenez, J. L., Measurements of Secondary Organic Aerosol from Oxidation of Cycloalkenes, Terpenes, and m-Xylene Using an Aerodyne Aerosol Mass Spectrometer. *Environ. Sci. Technol.* **2005**, 39, (15), 5674-5688.

38. Lopez-Hilfiker, F. D.; Mohr, C.; Ehn, M.; Rubach, F.; Kleist, E.; Wildt, J.; Mentel, T. F.; Lutz, A.; Hallquist, M.; Worsnop, D.; Thornton, J. A., A novel method for online analysis of gas and particle composition: description and evaluation of a Filter Inlet for Gases and AEROsols (FIGAERO). *Atmos. Meas. Tech.* **2014**, 7, (4), 983-1001.

39. Zhang, X.; Zhang, H.; Xu, W.; Wu, X.; Tyndall, G. S.; Orlando, J. J.; Jayne, J. T.; Worsnop, D. R.; Canagaratna, M. R., Molecular characterization of alkyl nitrates in atmospheric aerosols by ion mobility mass spectrometry. *Atmos. Meas. Tech.* **2019**, 12, (10), 5535-5545.

40. Zhao, Z.; Yang, X.; Lee, J.; Tolentino, R.; Mayorga, R.; Zhang, W.; Zhang, H., Diverse Reactions in Highly Functionalized Organic Aerosols during Thermal Desorption. *ACS Earth Space Chem.* **2020**, 4, (2), 283-296.

41. Mayorga, R. J.; Zhao, Z.; Zhang, H., Formation of secondary organic aerosol from nitrate radical oxidation of phenolic VOCs: Implications for nitration mechanisms and brown carbon formation. *Atmos. Environ.* **2021**, 244, 117910.

42. Dingle, J. H.; Zimmerman, S.; Frie, A. L.; Min, J.; Jung, H.; Bahreini, R., Complex refractive index, single scattering albedo, and mass absorption coefficient of secondary organic aerosols generated from oxidation of biogenic and anthropogenic precursors. *Aerosol Sci. Tech.* **2019**, 53, (4), 449-463.

43. Frisch, M. J.; Trucks, G. W.; Schlegel, H. B.; Scuseria, G. E.; Robb, M. A.; Cheeseman, J. R.; Scalmani, G.; Barone, V.; Petersson, G. A.; Nakatsuji, H.; Li, X.; Caricato, M.; Marenich, A. V.; Bloino, J.; Janesko, B. G.; Gomperts, R.; Mennucci, B.; Hratchian, H. P.; Ortiz, J. V.; Izmaylov, A. F.; Sonnenberg, J. L.; Williams; Ding, F.; Lipparini, F.; Egidi, F.; Goings, J.; Peng, B.; Petrone, A.; Henderson, T.; Ranasinghe, D.; Zakrzewski, V. G.; Gao, J.; Rega, N.; Zheng, G.; Liang, W.; Hada, M.; Ehara, M.; Toyota, K.; Fukuda, R.; Hasegawa, J.; Ishida, M.; Nakajima, T.; Honda, Y.; Kitao, O.; Nakai, H.; Vreven, T.; Throssell, K.; Montgomery Jr., J. A.; Peralta, J. E.; Ogliaro, F.; Bearpark, M. J.; Heyd, J. J.; Brothers, E. N.; Kudin, K. N.; Staroverov, V. N.; Keith, T. A.; Kobayashi, R.; Normand, J.; Raghavachari, K.; Rendell, A. P.; Burant, J. C.; Iyengar, S. S.; Tomasi, J.; Cossi, M.; Millam, J. M.; Klene, M.; Adamo, C.; Cammi, R.; Ochterski, J. W.; Martin, R. L.; Morokuma, K.; Farkas, O.; Foresman, J. B.; Fox, D. J. Gaussian 16 Rev. C.01, Wallingford, CT, **2016**.

44. Becke, A. D., Density-functional exchange-energy approximation with correct asymptotic behavior. *Phys. Rev. A* **1988**, 38, (6), 3098-3100.

45. Stephens, P. J.; Devlin, F. J.; Chabalowski, C. F.; Frisch, M. J., *Ab Initio* Calculation of Vibrational Absorption and Circular Dichroism Spectra Using Density Functional Force Fields. *J. Phys. Chem.* **1994**, 98, (45), 11623-11627.

46. Ditchfield, R; Hehre, W. J.; People, J. A., Self-Consistent Molecular-Orbital Methods. IX. An Extended Gaussian-Type Basis for Molecular-Orbital Studies of Organic Molecules. *J. Chem. Phys.* **1971**, 54, (2), 724-728.

47. Jacquemin, D.; Perpète, E. A.; Scuseria, G. E.; Ciofini, I.; Adamo, C., TD-DFT Performance for the Visible Absorption Spectra of Organic Dyes: Conventional versus Long-Range Hybrids. *J. Chem. Theory Comput.* **2008**, 4, (1), 123-135.

48. Chen, J. Y.; Rodriguez, E.; Jiang, H.; Chen, K.; Frie, A.; Zhang, H.; Bahreini, R.; Lin, Y.-H., Time-Dependent Density Functional Theory Investigation of the UV–Vis Spectra of Organonitrogen Chromophores in Brown Carbon. *ACS Earth Space Chem.* **2020**, 4, (2), 311-320.

49. Mennucci, B.; Cammi, R.; Tomasi, J., Excited states and solvatochromic shifts within a nonequilibrium solvation approach: A new formulation of the integral equation formalism method at the self-consistent field, configuration interaction, and multiconfiguration self-consistent field level. *J. Chem. Phys.* **1998**, 109, (7), 2798-2807.

50. Singh, H. B.; Anderson, B. E.; Brune, W. H.; Cai, C.; Cohen, R. C.; Crawford, J. H.; Cubison, M. J.; Czech, E. P.; Emmons, L.; Fuelberg, H. E.; Huey, G.; Jacob, D. J.; Jimenez, J. L.; Kaduwela, A.; Kondo, Y.; Mao, J.; Olson, J. R.; Sachse, G. W.; Vay, S.

A.; Weinheimer, A.; Wennberg, P. O.; Wisthaler, A., Pollution influences on atmospheric composition and chemistry at high northern latitudes: Boreal and California forest fire emissions. *Atmos. Environ.* **2010**, 44, (36), 4553-4564.

51. Decker, Z. C. J.; Robinson, M. A.; Barsanti, K. C.; Bourgeois, I.; Coggon, M. M.; DiGangi, J. P.; Diskin, G. S.; Flocke, F. M.; Franchin, A.; Fredrickson, C. D.; Gkatzelis, G. I.; Hall, S. R.; Halliday, H.; Holmes, C. D.; Huey, L. G.; Lee, Y. R.; Lindaas, J.; Middlebrook, A. M.; Montzka, D. D.; Moore, R.; Neuman, J. A.; Nowak, J. B.; Palm, B. B.; Peischl, J.; Piel, F.; Rickly, P. S.; Rollins, A. W.; Ryerson, T. B.; Schwantes, R. H.; Sekimoto, K.; Thornhill, L.; Thornton, J. A.; Tyndall, G. S.; Ullmann, K.; Van Rooy, P.; Veres, P. R.; Warneke, C.; Washenfelder, R. A.; Weinheimer, A. J.; Wiggins, E.; Winstead, E.; Wisthaler, A.; Womack, C.; Brown, S. S., Nighttime and daytime dark oxidation chemistry in wildfire plumes: an observation and model analysis of FIREX-AQ aircraft data. *Atmos. Chem. Phys.* **2021**, 21, (21), 16293-16317.

52. Atkinson, R.; Aschmann, S. M.; Carter, W. P. L., Kinetics of the reactions of O_3 and OH radicals with furan and thiophene at 298 ± 2 K. *Int. J. Chem. Kinet.* **1983**, 15, (1), 51-61.

53. Atkinson, R.; Aschmann, S. M.; Winer, A. M.; Carter, W. P. L., Rate constants for the gas-phase reactions of nitrate radicals with furan, thiophene, and pyrrole at 295 ± 1 K and atmospheric pressure. *Environ. Sci. Technol.* **1985**, 19, (1), 87-90.

54. Newland, M. J.; Ren, Y.; McGillen, M. R.; Michelat, L.; Daële, V.; Mellouki, A., NO_3 chemistry of wildfire emissions: a kinetic study of the gas-phase reactions of furans with the NO_3 radical. *Atmos. Chem. Phys.* **2022**, 22, (3), 1761-1772.

55. Draper, D. C.; Farmer, D. K.; Desyaterik, Y.; Fry, J. L., A qualitative comparison of secondary organic aerosol yields and composition from ozonolysis of monoterpenes at varying concentrations of NO_2. *Atmos. Chem. Phys.* **2015**, 15, (21), 12267-12281.

56. Berndt, T.; Böge, O.; Rolle, W., Products of the Gas-Phase Reactions of NO_3 Radicals with Furan and Tetramethylfuran. *Environ. Sci. Technol.* **1997**, 31, (4), 1157-1162.

57. Zhang, W.; Wang, T.; Du, B.; Mu, L.; Feng, C., Mechanism for the gas-phase reaction between NO_3 and furan: A theoretical study. *Chem. Phys. Lett.* **2008**, 455, (4), 164-168.

58. Farmer, D. K.; Matsunaga, A.; Docherty, K. S.; Surratt, J. D.; Seinfeld, J. H.; Ziemann, P. J.; Jimenez, J. L., Response of an aerosol mass spectrometer to organonitrates and organosulfates and implications for atmospheric chemistry. *PNAS* **2010**, 107, (15), 6670.

59. Day, D. A.; Campuzano-Jost, P.; Nault, B. A.; Palm, B. B.; Hu, W.; Guo, H.; Wooldridge, P. J.; Cohen, R. C.; Docherty, K. S.; Huffman, J. A.; de Sá, S. S.; Martin, S. T.; Jimenez, J. L., A systematic re-evaluation of methods for quantification of bulk

particle-phase organic nitrates using real-time aerosol mass spectrometry. *Atmos. Meas. Tech.* **2022**, 15, (2), 459-483.

60. Cao, G.; Yan, Y.; Zou, X.; Zhu, R.; Ouyang, F., Applications of Infrared Spectroscopy in Analysis of Organic Aerosols. *Spectr. Anal. Rev.* **2018**, 06, 12-32.

61. Jang, M.; Czoschke Nadine, M.; Lee, S.; Kamens Richard, M., Heterogeneous Atmospheric Aerosol Production by Acid-Catalyzed Particle-Phase Reactions. *Science* **2002**, 298, (5594), 814-817.

62. Leito, I.; Herodes, K.; Huopolainen, M.; Virro, K.; Künnapas, A.; Kruve, A.; Tanner, R., Towards the electrospray ionization mass spectrometry ionization efficiency scale of organic compounds. *Rapid Commun. Mass Spectrom.* **2008**, 22, (3), 379-384.

63. Oss, M.; Kruve, A.; Herodes, K.; Leito, I., Electrospray Ionization Efficiency Scale of Organic Compounds. *Anal. Chem.* **2010**, 82, (7), 2865-2872.

64. Kodros, J. K.; Papanastasiou, D. K.; Paglione, M.; Masiol, M.; Squizzato, S.; Florou, K.; Skyllakou, K.; Kaltsonoudis, C.; Nenes, A.; Pandis, S. N., Rapid dark aging of biomass burning as an overlooked source of oxidized organic aerosol. *PNAS* **2020**, 117, (52), 33028.

65. Tsigaridis, K.; Kanakidou, M., The Present and Future of Secondary Organic Aerosol Direct Forcing on Climate. *Curr. Clim. Change Rep.* **2018**, 4, (2), 84-98.

66. Akagi, S. K.; Craven, J. S.; Taylor, J. W.; McMeeking, G. R.; Yokelson, R. J.; Burling, I. R.; Urbanski, S. P.; Wold, C. E.; Seinfeld, J. H.; Coe, H.; Alvarado, M. J.; Weise, D. R., Evolution of trace gases and particles emitted by a chaparral fire in California. *Atmos. Chem. Phys.* **2012**, 12, (3), 1397-1421.

67. Westerling, A. L.; Gershunov, A.; Brown, T. J.; Cayan, D. R.; Dettinger, M. D., Climate and Wildfire in the Western United States. *Bull. Amer. Meteor. Soc.* **2003**, 84, (5), 595-604.

68. Holden Zachary, A.; Swanson, A.; Luce Charles, H.; Jolly, W. M.; Maneta, M.; Oyler Jared, W.; Warren Dyer, A.; Parsons, R.; Affleck, D., Decreasing fire season precipitation increased recent western US forest wildfire activity. *PNAS* **2018**, 115, (36), E8349-E8357.

69. Jiang, Y.; Zhou, L.; Raghavendra, A., Observed changes in fire patterns and possible drivers over Central Africa. *Environ. Res. Lett.* **2020**, 15, (9), 0940b8.

70. Ramo, R.; Roteta, E.; Bistinas, I.; van Wees, D.; Bastarrika, A.; Chuvieco, E.; van der Werf Guido, R., African burned area and fire carbon emissions are strongly impacted by small fires undetected by coarse resolution satellite data. *PNAS* **2021**, 118, (9), e2011160118.

71. Zhang, Y.; Forrister, H.; Liu, J.; Dibb, J.; Anderson, B.; Schwarz, J. P.; Perring, A. E.; Jimenez, J. L.; Campuzano-Jost, P.; Wang, Y.; Nenes, A.; Weber, R. J., Top-of-

atmosphere radiative forcing affected by brown carbon in the upper troposphere. *Nat. Geosci.* **2017**, 10, (7), 486-489.

72. Lang, T.; Buehler, S. A.; Burgdorf, M.; Hans, I.; John, V. O., A new climate data record of upper-tropospheric humidity from microwave observations. *Sci. Data* **2020**, 7, (1), 218.

73. Yan, C.; Zheng, M.; Desyaterik, Y.; Sullivan, A. P.; Wu, Y.; Collett Jr, J. L., Molecular Characterization of Water-Soluble Brown Carbon Chromophores in Beijing, China. *J. Geophys. Res. Atmos.* **2020**, 125, (15), e2019JD032018.

74. Li, X.; Hu, M.; Wang, Y.; Xu, N.; Fan, H.; Zong, T.; Wu, Z.; Guo, S.; Zhu, W.; Chen, S.; Dong, H.; Zeng, L.; Yu, X.; Tang, X., Links between the optical properties and chemical compositions of brown carbon chromophores in different environments: Contributions and formation of functionalized aromatic compounds. *Sci. Total Environ.* **2021**, 786, 147418.

75. Sun, Y.; Tang, J.; Mo, Y.; Geng, X.; Zhong, G.; Yi, X.; Yan, C.; Li, J.; Zhang, G., Polycyclic Aromatic Carbon: A Key Fraction Determining the Light Absorption Properties of Methanol-Soluble Brown Carbon of Open Biomass Burning Aerosols. *Environ. Sci. Technol.* **2021**, 55, (23), 15724-15733.

76. Schauer, J. J.; Fraser, M. P.; Cass, G. R.; Simoneit, B. R. T., Source Reconciliation of Atmospheric Gas-Phase and Particle-Phase Pollutants during a Severe Photochemical Smog Episode. *Environ. Sci. Technol.* **2002**, 36, (17), 3806-3814.

77. Zheng, M.; Cass, G. R.; Schauer, J. J.; Edgerton, E. S., Source Apportionment of PM2.5 in the Southeastern United States Using Solvent-Extractable Organic Compounds as Tracers. *Environ. Sci. Technol.* **2002**, 36, (11), 2361-2371.

78. Fine, P. M.; Chakrabarti, B.; Krudysz, M.; Schauer, J. J.; Sioutas, C., Diurnal Variations of Individual Organic Compound Constituents of Ultrafine and Accumulation Mode Particulate Matter in the Los Angeles Basin. *Environ. Sci. Technol.* **2004**, 38, (5), 1296-1304.

79. Ikemori, F.; Nakayama, T.; Hasegawa, H., Characterization and possible sources of nitrated mono- and di-aromatic hydrocarbons containing hydroxyl and/or carboxyl functional groups in ambient particles in Nagoya, Japan. *Atmos. Environ.* **2019**, 211, 91-102.

Chapter 3. Relative Humidity Modulates the Physicochemical Processing of Secondary Brown Carbon Formation from Nighttime Oxidation of Furan and Pyrrole

3.0. Abstract

Light-absorbing secondary organic aerosols (SOAs), also known as secondary brown carbon (BrC), are major components of wildfire smoke that can have a significant impact on the climate system; however, how environmental factors such as relative humidity (RH) influence their formation is not fully understood, especially for heterocyclic SOA precursors. We conducted chamber experiments to investigate secondary BrC formation from the nighttime oxidation of furan and pyrrole, two primary heterocyclic SOA precursors in wildfires, in the presence of pre-existing particles at RH < 20% and ~50%. Our findings revealed that increasing RH significantly affected the size distribution dynamics of both SOAs, with pyrrole SOA showing a stronger potential to generate ultrafine particles via intensive nucleation processes. Higher RH led to increased mass fractions of oxygenated compounds in both SOAs, suggesting enhanced gas-phase and/or multiphase oxidation under humid conditions. Moreover, higher RH reduced the mass absorption coefficients of both BrC, contrasting with those from homocyclic precursors, due to the formation of non-absorbing high-molecular-weight oxygenated compounds and the decreasing mass fractions of molecular chromophores. Overall, our findings demonstrate the unique RH dependence of secondary BrC formation from heterocyclic precursors, which may critically modulate the radiative effects of wildfire smoke on climate change.

3.1. Introduction

Light-absorbing aerosols from wildfires can affect the climate system by directly heating the atmosphere and indirectly altering the aerosol-boundary-layer-monsoon interactions. (1−3) Over the last few decades, climate change has increased the intensity and frequency of wildfires, (4−6) releasing a massive amount of volatile organic compounds (VOCs) and aerosols into the atmosphere. (7−9) However, the impact of unabated wildfire emissions is highly uncertain due to the less-constrained radiative effects of wildfire smoke, which are influenced by the composition of smoke aerosols. The major component of smoke aerosols is organics (>95%), (10, 11) contributing to ~45-86% of the total aerosol light absorption. (12) A large fraction of smoke organics (~30−56%) accounts for secondary organic aerosols (SOAs), (13) in which the light-absorbing component is known as secondary brown carbon (BrC). Thus, secondary BrC plays a critical role in moderating the climate impacts of wildfire smoke.

The formation of secondary BrC can be sensitive to the smoke environments. (14, 15) In particular, relative humidity (RH) is a well-known environmental factor that may alter SOA composition and secondary BrC light absorption. Extensive research has revealed that changes in RH can influence SOA formation by altering the gas-phase chemistry, gas-to-particle partitioning of oxidation products, phase states of aerosols, reactive uptake of radicals, and heterogeneous reactions of aerosol-phase constituents. (16−27) Prior studies also reported that higher RH increased the mass absorption coefficients (MAC) of secondary BrC derived from homocyclic aromatic precursors. (28−30) The increased MAC was associated with changes in molecular chromophores as

RH increased, which may alter the wavelength dependence of MAC profiles. (30) On the other hand, higher RH decreased the MAC of secondary BrC derived from α-pinene, (31) suggesting that the effect of RH on MAC may differ depending on the type of VOCs. It is noted that a rise in RH may result in increased liquid water content in wildfire aerosols, where water-soluble organics can contribute to a large portion (e.g., ~45% at 405 nm) of BrC light absorption. (32) Despite the extensive investigations, the effect of RH on secondary BrC formation remains inconclusive.

Heterocyclic VOCs are the second largest sources of wildfire SOA precursors, and they are more reactive compared to homocyclic VOCs (e.g., phenolics) due to their hetero atoms. (33, 34) Common heterocyclic VOCs released by wildfire include furans and pyrroles, (34−37) which account for ~30% of nitrate radical (NO_3) loss via nighttime chemistry in wildfire plumes. (38) Furans have greater emission factors but may generate less-absorbing BrC from nighttime chemistry, whereas pyrroles exhibit the opposite behavior. (35, 36, 39, 40) Secondary BrC formation from the nighttime chemistry of furans and pyrroles has been widely studied under RH conditions below 20%, (14, 15, 39−41) a typical level in dry wildfire smokes (e.g., the Williams Fire smoke (42)) or dry fire areas (e.g., western United States (43, 44) and Africa in dry seasons (45, 46)). In addition, there have been frequent observations of humid wildfire smoke worldwide, particularly those at RH ~50%, in the past two decades due to climate change. (47−49) A prior study of secondary BrC from indole, which contains a pyrrole ring in its structure, highlighted that the effects of RH on the light absorption properties of secondary BrC from heterocyclic VOCs were complicated and greatly unconstrained. (50) Hence, there

was still a significant lack of process-level understanding regarding the secondary BrC formation from heterocyclic VOCs at various levels of RH.

In this study, chamber experiments were conducted to investigate the effects of RH on the secondary BrC formation from the nighttime oxidation of furan and pyrrole, the backbone compounds of furans and pyrroles. For comparison, RH was controlled at <20% and ~50% to simulate dry and humid environments, respectively, while pre-existing particles were introduced in both RH so that the chamber conditions would be closer to the ambient atmosphere. The effects of RH on particulate size distribution dynamics, SOA composition, BrC light absorption properties, and molecular chromophores were examined to better understand how RH-related physicochemical processing modulates the secondary BrC formation from furan and pyrrole and their implications in the atmosphere. These results will provide more accurate representations of wildfire-associated secondary BrC and aid in assessing their climate impacts.

3.2. Methods

3.2.1. Experimental setup

All the experiments were carried out in a 10 m^3 Teflon fluorinated ethylene propylene (FEP) film chamber at room temperature (20−25 °C) under dark conditions. The room temperature was much lower than the temperature of wildfires but comparable to the temperature of ambient atmosphere, (47, 49, 51) where furan and pyrrole released from wildfires were observed in field studies. (34, 37) Temperature and RH were monitored by a RH-USB sensor (Omega Engineering, Inc.) attached to the chamber. A

constant output atomizer (TSI 3076) was used to produce pre-existing particles using a 10 mM ammonium sulfate ($(NH_4)_2SO_4$, Acros Organics, 99%, extra pure) solution. The pre-existing particles had a mass concentration and the central diameter of ~50 μg m^{-3} and ~50 nm, respectively, to simulate the background particles in wildfire smoke. (52, 53) Given that higher RH can introduce liquid water or increase the amount of liquid water content in wildfire aerosols, (48, 54) we generated dry pre-existing particles at RH <20% and wet aqueous pre-existing particles at RH ~50%. Because our humid condition was between the efflorescence RH and deliquescence RH of ammonium sulfate, (55) dry seed particles were produced by passing through a silica-gel filled diffusion dryer, whereas wet aqueous seed particles were produced without the dryer. (56) Chamber experiments without pre-existing particles were also performed at both RH levels. These experiments serve as a benchmark for detailed discussions on the potential mechanisms involved in SOA formation.

This study used furan (TCI America, >99%) and pyrrole (TCI America, >99%) as model compounds of heterocyclic VOCs. Each experiment involved only one VOC, in which ~200 ppbv of furan or pyrrole was injected into the chamber using ~15 lpm of zero air. The concentration of VOCs was determined based on previous studies to ensure appropriate SOA mass concentrations for online and offline analyses. (14, 15, 40, 41) After 20 minutes of mixing, a mixture of NO_2 and O_3 (molar concentration ratio ~3:2) was injected into the chamber, wherein N_2O_5 was generated and then decomposed to NO_3 radicals. O_3 was generated by an O_3 generator (A2Z Ozone 3G LAB) with pure oxygen (flow rate of 0.2 lpm), while NO_2 was directly injected from a NO_2 cylinder (4789 ppm,

Airgas) with a flow rate of 0.5 lpm. Similar to prior studies of SOA formation under humid conditions, (20, 21) the NO_2-O_3 ratio ensured that NO3 primarily drove the oxidation of pyrrole and furan in our chamber. The NO_2-O_3 mixture was first reacted in a glass vessel (total flow rate of 0.7 lpm and residence time of 206 s) before the chamber injection. The concentration of N_2O_5 produced in the glassware was estimated by modeling the reactions between NO_2 and O_3, and the initial concentration ratio of N_2O_5 to furan (or pyrrole) was approximately 2:1. While it was possible that O_3 residue was also introduced into the chamber along with N_2O_5, the reaction rate constants (k) at room temperature and atmospheric pressure for "furan/pyrrole + NO_3" ($k_{furan+NO3} = 1.4 \times 10^{-12}$ cm^3 molecule^{-1} s^{-1}; $k_{pyrrole+NO3} = 4.9 \times 10^{-11}$ cm^3 molecule^{-1} s^{-1}) are ~6 orders of magnitude higher than those of "furan/pyrrole + O_3" ($k_{furan+O3} = 2.4 \times 10^{-18}$ cm^3 molecule^{-1} s^{-1}; $k_{pyrrole+O3} = 1.6 \times 10^{-17}$ cm^3 molecule^{-1} s^{-1}). (57−59) Therefore, the oxidation of pyrrole and furan in our chamber was mostly driven by NO_3-initiated oxidation.

The injection of the NO_2-O_3 mixture marked the start of experiments. The duration of each experiment was ~2.2 hours, during which the SOA mass concentration reached a plateau. Following this plateau, the generated SOA samples were collected on polytetrafluoroethylene membrane filters (PTFE, 46.2 mm, 2.0 µm, Tisch Scientific) for subsequent offline analysis. The collection flowrate was 20 lpm, and the collection time was 1.5 hours; each filter collected the aerosols from 1.8 m^3 of chamber air. The experimental procedure was similar to the those reported in prior studies of high-RH chamber experiments. (20, 21) It has been noted that the chamber wall loss of particles may be potentially different at different RHs. However, in this study, the first-order size-

dependent particulate wall loss rates were comparable at both RH levels (**Figure S3.1**). Although vapor wall loss of oxidized products can be increased by higher RH, our data showed an increased trend of mass fractions of oxygenated composition in particle phase (**Figure S3.2**). Such evidence indicates that the chamber interference at higher RH did not significantly hinder the formation of highly oxidized products in SOA. (20) Experiments of each environmental condition were repeated for three times (n=3) to confirm the reproducibility of observed phenomena and determine the uncertainties (standard deviations) of reported values.

3.2.2. Particulate Size Distribution and Compositional Analysis

The number concentration and size distribution of SOA were measured throughout the duration of the experiments by a scanning electrical mobility spectrometer (SEMS, Brechtel Manufacturing Inc.) in the diameter range of 10−800 nm with 140 bins. The bulk composition and the *in situ* molecular composition were characterized by a mini-aerosol mass spectrometer coupled with a compact time-of-flight mass spectrometer (mAMS, Aerodyne Research Inc.) (60) and an iodide-adduct time-of-flight chemical ion mass spectrometer coupled with the filter inlet for gases and aerosols system (FIGAERO-ToF-CIMS, Aerodyne Research Inc.), (61) respectively. Attenuated total reflectance Fourier-transform infrared spectrometer (ATR-FTIR, Thermo Nicolet iS50) was used to characterize the functional group fingerprints. The measured IR spectra were deconvoluted using Igor Pro 7 (WaveMetrics, Lake Oswego, OR, USA), in which the wavenumbers of identified peaks were determined. Gas chromatography-electron ionization mass spectrometry (GC/EI-MS, Agilent Technologies 6890N GC System and

5975 inert XL Mass Selective Detector) and liquid chromatography coupled with an electrospray ionization source and a quadruple-time-of-flight mass spectrometer (LC-ESI-Q-ToFMS, Agilent Technologies 1260 Infinity II and 6545 Q-ToF LC/MS) were used to analyze the molecular composition of SOA samples. Details of the instrumental setup have been published elsewhere. (40, 41) Particulate effective density, organic mass fraction in aerosols, and SOA mass concentration in the chamber were calculated based on the methods described in our previous study (**Table S3.1**). (40)

The mass fractions of molecular chromophores were semi-quantified using surrogate standards analyzed by LC-ESI-Q-TOFMS or GC/EI-MS. Molecular chromophores in furan BrC were mainly carbonyls, while in pyrrole BrC accounted for both carbonyls and nitroaromatics. (15, 41) Therefore, we used maleic acid ($C_4H_4O_4$), maleimide ($C_4H_3NO_2$), and nitropyrroles ($C_4H_4N_2O_2$, including 2-nitropyrrole and 3-nitropyrrole) as surrogate standards for estimating chromophores in furan BrC, carbonyl chromophores in pyrrole BrC, and nitroaromatic chromophores in pyrrole BrC, respectively. $C_4H_4O_4$ was quantified by LC-ESI-Q-TOFMS, while $C_4H_3NO_2$ and $C_4H_4N_2O_2$ were quantified by GC/EI-MS with their authentic chemical standards. The mass fractions of other molecular chromophores were estimated by eq (3.1).

$$MF_{chromophore} = MF_{surrogate} \frac{c_{chromophore} M_{chromophore}}{c_{surrogate} M_{surrogate}}$$

$$= MF_{surrogate} R_F \frac{A_{chromophore} M_{chromophore}}{A_{surrogate} M_{surrogate}} \qquad (3.1)$$

Here $MF_{chromophore}$ is the mass fraction of the characterized molecular chromophore in SOA samples; $MF_{surrogate}$ is the mass fraction of the surrogate standard in SOA samples; $c_{chromophore}$ and $c_{surrogate}$ are the molar concentrations of the characterized chromophores and the surrogate standard in the SOA samples (mol L^{-1}); $M_{chromophore}$ and $M_{surrogate}$ are the molar masses of the characterized chromophores and the surrogate standard in the SOA samples (g mol^{-1}); $A_{chromophore}$ and $A_{surrogate}$ are the peak areas of parent ions of the characterized chromophores and the surrogate standard in their extracted ion chromatograms (EICs) measured by LC-ESI-Q-TOFMS. While the response factor (R_F) of molecular chromophores may exhibit certain variations compared to surrogate standards, [15] semi-quantification can still offer approximate mass fractions to elucidate their changes under different RH conditions.

3.2.3. Light Absorption Properties

The ultraviolet and visible (UV−vis) absorbance of SOA samples was measured by a UV−vis spectrophotometer (Beckman DU-640) in the range of 290-700 nm, with the reference wavelength at 700 nm. All of the SOA samples were extracted with acetonitrile (ACN), an aprotic polar solvent that is suitable for analyzing carbonyl-rich secondary BrC samples. [40] It should be noted that due to solvent selectivity, ACN may not completely extract the furan SOA and pyrrole SOA constituents from filters (i.e., extraction efficiency < 100%). [15] The MAC profiles of SOA samples are calculated by eq (3.2).

$$MAC(\lambda) = ln10 \times \frac{A(\lambda) - A(700)}{b \times C_m} \tag{3.2}$$

Here, $A(\lambda)$ is the wavelength (λ)-dependent absorbance, b is the light path length (i.e., 1 cm), and C_m is the mass concentration of SOA. Since C_m was calculated by the total on-filter SOA mass (online-monitored SOA mass concentration × air volume in filter collection) over the volume of ACN solution and given the chance that some BrC components were not completely extracted with ACN, this study estimated the lower-bound limit of BrC MAC. Since SOA formation at each environmental condition was repeated three times, the average and standard deviation of MAC at each wavelength can be calculated by three replicates of SOA samples. The relative error (i.e., standard deviation over the average value) of the MAC value at each wavelength was ~15%, as estimated by 3 repeated experiments. The wavelength dependency of $MAC(\lambda)$ was also investigated by fitting the absorption Ångström exponent (AAE), as defined by eq (3.3).

$$AAE = -\frac{\ln MAC(\lambda) - \ln MAC(\lambda_0)}{\ln \lambda - \ln \lambda_0} = -\frac{\ln[MAC(\lambda)/MAC(\lambda_0)]}{\ln(\lambda/\lambda_0)} \tag{3.3}$$

Here, λ_0 represents the reference wavelength. The fitted AAE would be equal to the slope of the linear regression of $ln[MAC(\lambda)/MAC(\lambda_0)]$ versus $-ln(\lambda/\lambda_0)$ with a zero intercept. Since our previous studies reported that AAE can be different in the UV (290−400 nm) and visible (400−600 nm) ranges, (14, 39−41) we set λ_0 as 400 nm for fitting the AAE. However, since the AAE shown in our data can largely vary along with λ, we also derive the wavelength-dependent AAE in eq (3.4).

$$AAE(\lambda) = -\frac{d \ln MAC(\lambda)}{d \ln \lambda} = -\frac{\lambda}{MAC(\lambda)}\frac{d MAC(\lambda)}{d \lambda} \approx -\frac{\lambda}{MAC(\lambda)}\frac{MAC(\lambda+\Delta\lambda) - MAC(\lambda-\Delta\lambda)}{2 \Delta\lambda} \tag{3.4}$$

The stepwise wavelength ($\Delta\lambda$) was set as 3 nm. $AAE(\lambda)$ was sketched by a stepwise scan to portray a more detailed wavelength dependency of MAC, while the

fitted AAE values reflected the overall trend. These two representations of AAE can complementarily highlight the distinction of MAC profiles at different RHs.

3.2.4. Computational Methods

Time-dependent density functional theory was employed to estimate the theoretical UV−vis spectra of molecular chromophores. All the computations were conducted using the Gaussian 16 program (revision C. 01). (62) Geometrical optimization and the computation of line-center wavelengths and oscillator strengths were performed by the B3LYP functional (63, 64) with the 6-311++G(d,p) basis set, (65) as suggested in previous studies. (14, 66, 67) The ACN environment was simulated by the integral equation formalism extension of the polarizable continuum model. (68) The theoretical UV−vis spectra were generated by the GaussView 6 program. The validation of our theoretical calculations was previously discussed in detail with similar BrC chromophores. (67) Cartesian coordinates for all the molecular structures are summarized in **Table S3.2**.

3.3. Results and Discussions

3.3.1. Size Distribution Dynamics of Furan SOA and Pyrrole SOA

Size distribution dynamics, which encompasses the change in number and size distribution of particles over time, is the physical basis of SOA formation and can be interconnected with gas-phase and/or multiphase chemistry. (69) At RH <20%, the particulate size of furan SOA gradually increased over time, but at RH ~50%, the particulate size of furan SOA rapidly increased within 10 minutes when furan oxidation

started (**Figure 3.1A, B**). However, the particle size distribution dynamics of pyrrole SOA were different. If the response of pyrrole SOA to changes in RH is similar to that of furan SOA, then an even broader size distribution of pyrrole SOA should be observed at higher RH, because distinct growth in particulate size was observed at low RH (**Figure 3.1C**), which indicated the greater potential of pyrrole oxidation products to contribute to particles with larger size. However, at higher RH, our results unexpectedly showed a much narrower size distribution of pyrrole SOA (**Figure 3.1D**). The central diameter of the particles was still ~50 nm, comparable to that of the pre-existing particles, reflecting the limited particulate growth. Correspondingly, the particle number concentration at RH ~50% was significantly higher than that at RH <20% (**Figure 3.1C, D**), indicating an intensive new particle formation (NPF) at RH ~50%. The rapid decrease of number concentration in **Figure 3.1D** may be attributed to the chamber wall loss and coagulation of particles. Although the intensive NPF was observed at a specific environmental condition (i.e., RH ~50% with pre-existing particles), our findings can be tightly related to wildfire smoke because RH ~50% and pre-existing particles are frequently observed in wildfire smoke. (47−49) All of these characteristics demonstrated the differential RH responses of furan SOA and pyrrole SOA.
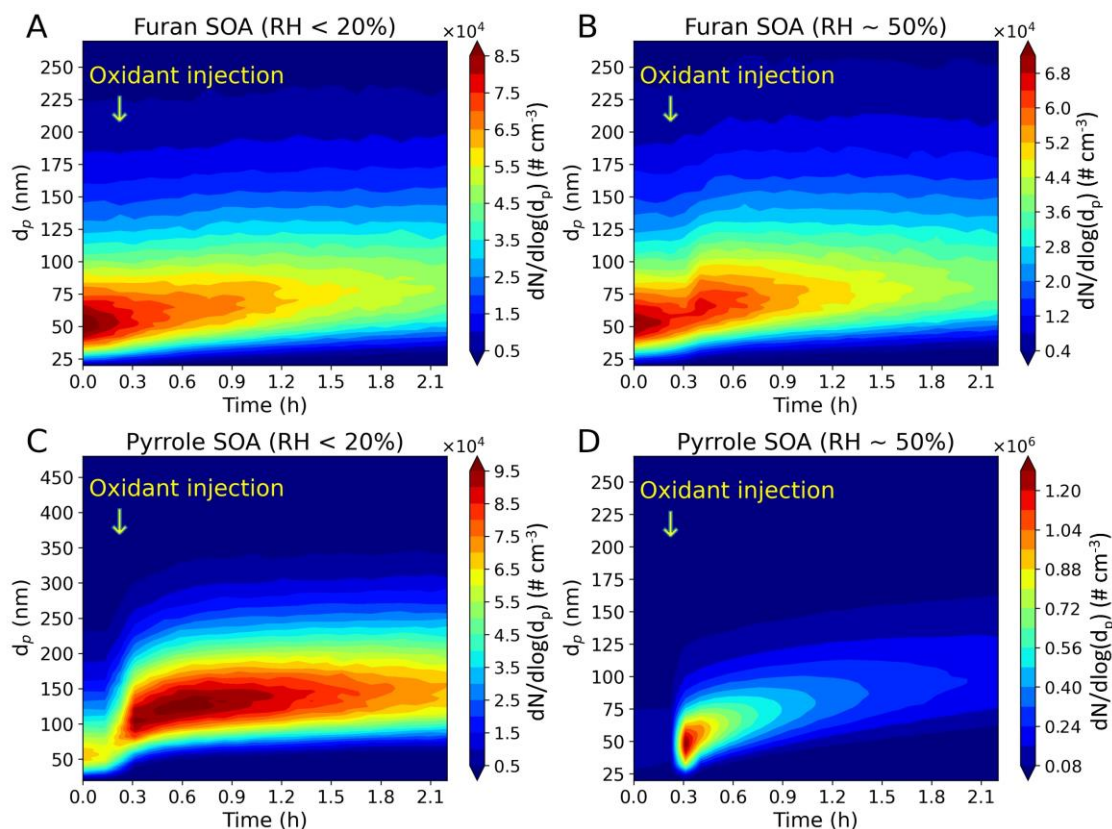
Figure 3.1. Particle size distribution dynamics of (A) furan SOA at RH <20%; (B) furan SOA at RH ~50%; (C) pyrrole SOA at RH <20%; (D) pyrrole SOA at RH ~50%.

The intensive NPF of pyrrole SOA was unexpectedly associated with the pre-existing particles, as revealed by our benchmark experiments. Without pre-existing particles, an increase in RH broadened the size distribution of both SOAs when oxidation started (**Figure S3.3**). The size distribution of pyrrole SOA at RH ~50% was much broader than that at RH <20% (**Figure S3.3C, D**), indicating that higher RH boosted particle growth accompanied by NPF so that the particulate size was larger but the particulate number concentration was lower. This phenomenon reflected that higher RH without pre-existing particles was capable of facilitating the condensation of gas-phase

products and the coagulation of ultrafine particles when pyrrole SOA was formed. These two processes would be promoted in the presence of pre-existing particles, which were expected to become the condensation sink. (70) However, intensive NPF was observed (**Figure 3.1D**), reflecting the boosted nucleation process regardless of the pre-existing particles. It is noted that the potential to form ultrafine particles via nucleation processes could be largely dependent on environmental conditions. The intensive NPF shown in **Figure 3.1D** suggests that the nighttime oxidation of pyrrole may have a stronger potential to induce nucleation in humid wildfire smoke. Although a thorough mechanistic elucidation may require further measurements of the critical nuclei composition, the unexpected NPF of pyrrole SOA can reflect that the nitrogen atom from the pyrrole backbone is the key to inducing a stronger potential for nucleation, as compared to furan SOA (**Figure 3.1B, D**). The "furan-pyrrole" comparisons highlighted the importance of VOC-specified physicochemical processing in wildfire-related SOA formation, which may influence the chemical composition.

3.3.2. Chemical Characterization of SOA Composition

To investigate the effects of RH on SOA composition, chemical characterization was conducted using multiple complementary instruments to determine the bulk and molecular compositions, as well as the molecular fingerprints. The bulk composition of SOA showed that higher RH increased the mass fraction of $C_xH_yO_{>1}^+$ fragments but decreased the mass fraction of $C_xH_y^+$ fragments in both SOAs (**Figure 3.2A, B**). However, at both RH conditions, the total mass fractions of nitrogen-containing fragments (i.e., $C_xH_yN^+$, $C_xH_yON^+$, and $C_xH_yO_{>1}N^+$) of either furan SOA or pyrrole SOA

73

were roughly consistent (**Figure 3.2A, B**). It is noted that reduced nitrogen compounds (e.g., imidazole-type compounds) may be potentially generated from particle-phase reactions between organic products and the ammonium cations in the pre-existing particles. (71−75) Here, $C_2H_2N^+$, $C_2H_3N^+$, and $C_3H_3N^+$ (typical fragments of nitrogen-containing organic compounds other than organonitrates measured by mAMS (29)) were used to quantify the mass fractions of reduced nitrogen compounds (**Table S3.3**). At higher RH, the mass fraction of $C_2H_3N^+$ was higher, but the mass fractions of $C_2H_2N^+$ and $C_3H_3N^+$ were lower. However, the total mass fraction of these fragments was roughly constant at both RH, indicating that the change in RH had a minor influence on the formation of reduced nitrogen. All these results indicated that the compositional change at higher RH mainly accounted for the generation of oxygenated products.

Moreover, our ATR-FTIR measurements showed the difference in oxygenated functional group fingerprints at different RHs, including the hydroxyl group (O−H) stretching, the carbon−oxygen double bond (C=O) stretching, and the carbon−oxygen−carbon (C−O−C) stretching (**Figure 3.2**). Functional groups were assigned to the wavenumbers based on previous IR studies of SOA composition. (76) In furan SOA, the wavenumber of the C−O peak shifted while both the number and wavenumbers of C=O peaks changed. A new O−H peak at 3391 cm^{-1} was observed, but the C−O peak at 1193 cm^{-1} disappeared at higher RH (**Figure 3.2C**). These results indicated that the change in RH may greatly alter the oxygenated constituents in furan SOA. While in pyrrole SOA, O−H and C=O peaks were similar at both RH, while at higher RH two new C−O−C peaks (1100 cm^{-1} and 1184 cm^{-1}) were identified (**Figure

74

3.2D). Since the C−O−C structure cannot be inherited from the pyrrole backbone, the new C−O−C peaks may be attributed to RH-modulated gas-phase and/or multiphase oxidation on pyrrole SOA. The observed results of functional group fingerprints from SOA formed at different RH levels reflected that higher RH could cause a shift in the distribution of wavenumbers of oxygenated functional groups suggesting a considerable change in the chemical composition of oxygenated compounds with RH.
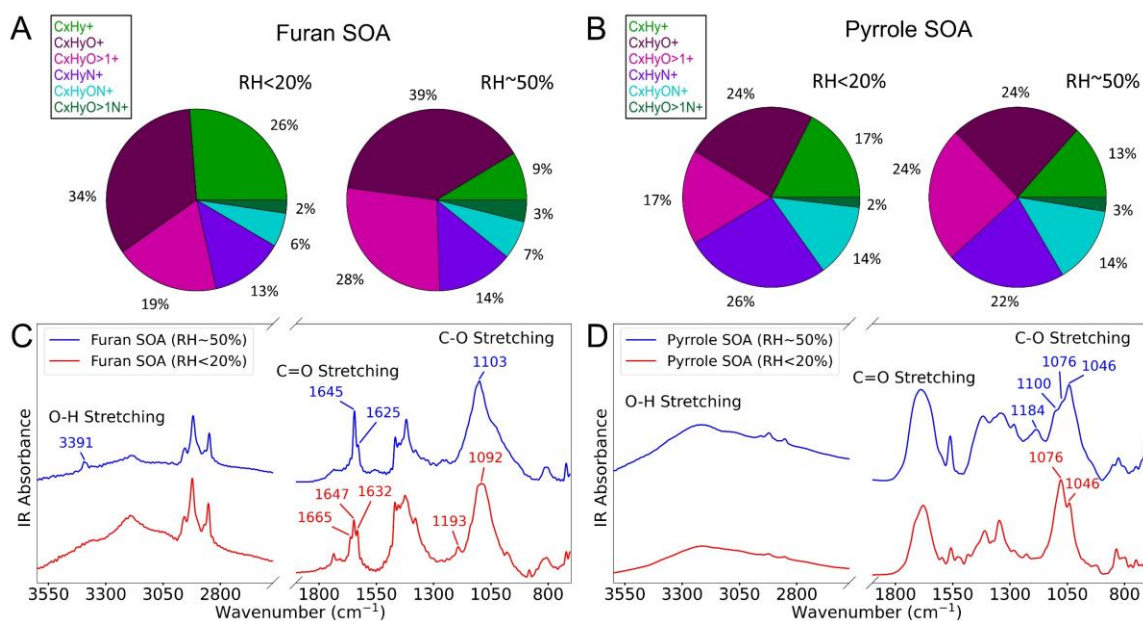
Figure 3.2. Chemical characterizations of the SOA bulk composition at RH <20% and ~50% conditions: (A) mass fractions of compositional fragments of furan SOA; (B) mass fractions of compositional fragments of pyrrole SOA; (C) functional group fingerprints of furan SOA; (D) functional group fingerprints of pyrrole SOA.

The effect of RH on the oxygenated products was further investigated through the molecular characterization of SOA samples. The average of the hydrogen-to-carbon (H/C) and the oxygen-to-carbon (O/C) ratios (i.e., <H/C> and <O/C>), weighted by

intensity from FIGAERO-ToF-CIMS measurements, of both SOA constituents increased with higher RH (**Table S3.4**). This suggests that higher RH levels can enhance the saturation and oxygenation levels of SOA constituents (**Figure 3.3**). The increasing <H/C> ratio decreased the intensity-weighted average of double bond equivalence (DBE) (i.e., <DBE>) (**Figure 3.3**). However, the nitrogen-to-carbon (N/C) ratio (i.e., <N/C>) decreased at higher RH in pyrrole SOA constituents while kept constant in furan SOA constituents (**Table S3.4**), indicating that the formation of nitrogen-containing products in pyrrole SOA characterized by FIGAERO-ToF-CIMS were more sensitive to RH change. In furan SOA, the highest peaks at both RH conditions were attributed to $C_4H_4O_3$, while the presence of its oxygenated products $C_4H_4O_4$ and $C_4H_4O_5$ was also observed (**Figure 3.3A**). It should be noted that $C_4H_4O_5$ was only observed at higher RH, which may account for the enhanced oxygenation of furan SOA constituents. In pyrrole SOA, the formation of new oxygenated products with higher H/C and O/C ratios (e.g., $C_4H_6N_2O_6$, $C_4H_5N_3O_8$) was observed (**Figure 3.3B**). The peak intensity ratios of $C_4H_5NO_3$ to $C_4H_5NO_2$ increased significantly at higher RH, contributing to the higher oxygenation level of pyrrole SOA constituents at higher RH. All of these findings not only confirmed the formation of oxygenated products at higher RH, but also demonstrated a higher saturation level of SOA constituents. The increased saturation and oxygenation levels at higher RH could be attributed to multiple processes, such as gas-phase chemistry, reactive uptake of radicals, aerosol-phase reactions, etc. (16−27) Because multiple physicochemical processes interplay during SOA formation, further research is necessary to provide a more comprehensive understanding of the influence of

each individual process involved. The compositional change due to these processes may further affect the secondary BrC light absorption properties.
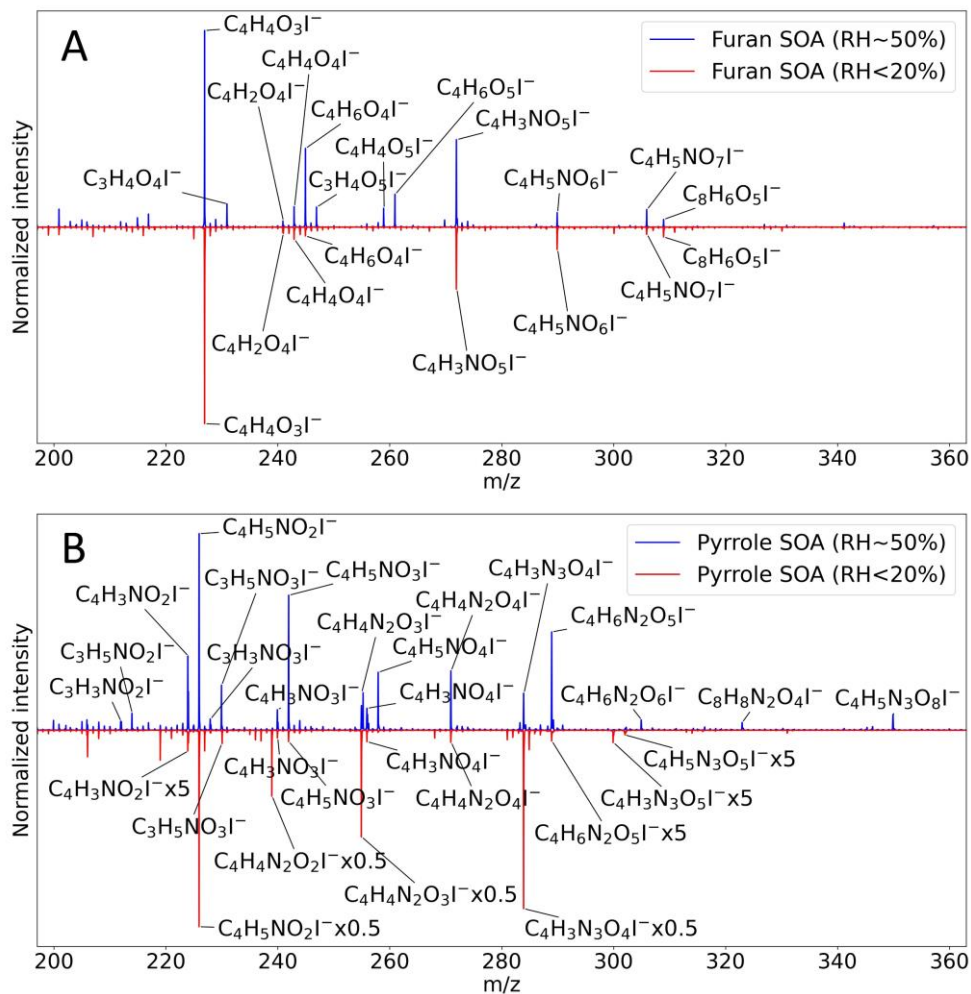
Figure 3.3. Molecular characterization of oxygenated products in (A) furan SOA and (B) pyrrole SOA at RH <20% and ~50% conditions.

3.3.3. Light Absorption Properties of Secondary BrC

The light absorption properties of secondary BrC can be affected by SOA compositional changes. Our results showed that higher RH significantly reduced the

MAC profiles for both SOAs, wherein both SOAs can fall in the moderately absorptive BrC category at RH <20% and the weakly absorptive BrC category at RH ~50% (**Figure 3.4**). (77) As compared with SOA derived from other precursors under various oxidation conditions, furan SOA was moderately absorbing at RH <20% and least absorbing at RH ~50%, while pyrrole SOA was highly absorbing at RH <20% and less absorbing at RH ~50% (**Table S3.5**). (28, 30, 50, 78) These comparisons indicated that the effects of RH on light absorption can be sensitive to SOA precursors and their explicit chemical formation pathways.

The reduction in MAC profiles at higher RH cannot be not attributed to the aqueous chemistry between ammonium cations and SOA constituents, (72, 79, 80) as these reactions may actually enhance the MAC (**Text S3.1; Figures S3.4, S3.5**). Instead, the reduced MAC observed at higher RH may be linked to enhanced formation of oxygenated products. Our results showed that non-absorbing oxygenated compounds (i.e., those with DBE = 0) were detected only at RH ~50% (**Figure S3.6**). Some of the non-absorbing compounds were the major constituents in SOA samples (**Figure S3.7**). These molecules have higher molecular weights and possess at least 8 carbons and 10 oxygens. Such high level of oxygenation only observed at higher RH suggested that higher RH may reduce MAC mostly via enhancing gas-phase and/or multiphase oxidation of SOA constituents.
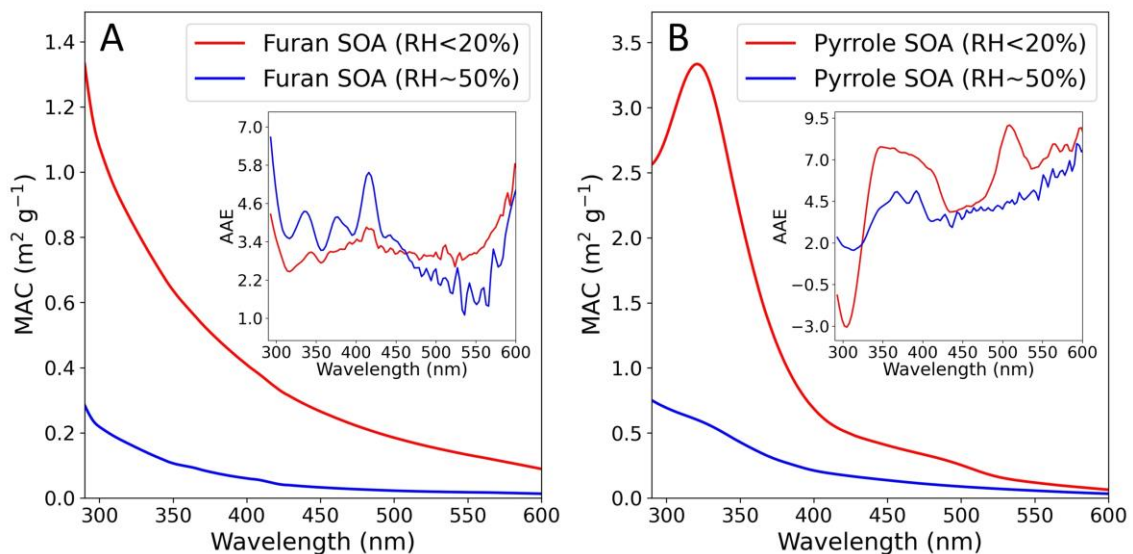
Figure 3.4. MAC profiles of (A) furan BrC and (B) pyrrole BrC at both RH <20% and ~50% conditions. The inset panels show the AAE changes along with wavelengths.

Table 3.1. Fitted AAE and R^2 in the linear regression of MAC in the UV (290−400 nm) and visible (400−600 nm) ranges.

BrC Samples	RH	AAE		R^2	
		UV	Visible	UV	Visible
Furan BrC	<20%	3.00	3.21	1.00	1.00
	~50%	3.86	3.18	1.00	0.99
Pyrrole BrC	<20%	5.74	5.79	0.95	0.99
	~50%	3.88	4.07	0.99	1.00

As illustrated by the AAE curves in the inset panels shown in **Figure 3.4**, the compositional change of BrC chromophores was also reflected in the changed shape of MAC profiles. At both RH conditions, the AAE curves of furan BrC were comparable, even though higher RH slightly increased the AAE in the UV range but slightly

decreased in the visible range (**Figure 3.4A**). The fitted AAE showed comparable values at RH <20% and ~50% in both UV and visible ranges (**Table 3.1**). However, the AAE curves of pyrrole BrC exhibited significant differences at RH <20% and ~50%; a twisting curve was shown at RH <20%, whereas a monotonously increased trend with a small bend was shown at RH ~50% (**Figure 3.4B**). The fitted AAE values were smaller at RH ~50% (**Table 3.1**), indicating that the overall wavelength dependency of MAC profiles of pyrrole BrC was diminished by higher RH levels. Taken together, the reduced MAC profiles with altered wavelength dependency point to a change in the composition of BrC chromophores.

3.3.4. Mass Fractions of BrC Chromophores in SOA

The mass fractions of molecular chromophores observed at both RH can aid in understanding the effect of RH on the MAC profiles. Semi-quantification was performed for molecular chromophores characterized in this study (**Table S3.6**). Most of the characterized chromophores listed in **Table S3.6** were also reported in our previous studies of furan- and pyrrole-derived secondary BrC. (14, 15, 39−41) While the mass fractions of some less abundant chromophores (e.g., $C_4H_3NO_3$) were similar at both RH, most of the characterized chromophores showed lower mass fractions at higher RH. In **Figure 3.5**, two newly identified compounds ($C_8H_5NO_6$ and $C_4H_2N_4O_6$) are presented as examples for detailed discussions. $C_8H_5NO_6$ was characterized as 3-nitrophthalic acid (**Figure S3.8A, C**), whereas $C_4H_2N_4O_6$ showed two peaks (**Figure 3.5B**), which corresponded to 5,6-dinitro-4*H*-1,2,4-oxadiazine-3-carbaldehyde (**Figure S3.8B, D**) and 2,3,4-trinitro-pyrrole (**Figure S3.9**). At higher RH, the mass-normalized intensity in their

extracted ion chromatograms (EICs) nearly disappeared (**Figure 3.5**). Since molecular chromophores have different contributions to the MAC profiles at different wavelengths, (15) their decreased mass fractions can reduce the MAC in specific wavelength regions. Because the spectral absorption of 3-nitrophthalic acid only covers the UV range (**Figure 3.5A**), it contributes to the reduction of MAC of furan BrC in the UV range. The reduction of MAC in the visible range may be attributed to the decreased mass fractions of other chromophores whose spectra can extend to above 400 nm (e.g., $C_4H_2O_4$). (15) The spectral absorption of 5,6-dinitro-4*H*-1,2,4-oxadiazine-3-carbaldehyde covers both UV and visible ranges (**Figure 3.5B**), with a spectral shape similar to the MAC profile of pyrrole BrC at low RH (**Figure 3.4B**). More chromophores, such as 2,3,4-trinitro-pyrrole (**Figure S3.9A**) and dinitro-pyrroles ($C_4H_3N_3O_4$), (41) can also contribute to the MAC profiles in the UV range. While it is possible that higher RH may potentially facilitate the production of new molecular chromophores with a red shift of light absorption towards longer wavelengths, (30) our findings revealed that the decrease in mass fractions of various molecular chromophores was mostly responsible for the altered wavelength dependency and lowered profiles of the MAC. The evidence together demonstrates the important role of molecular chromophores in bridging the change in environmental conditions to the light absorption properties of secondary BrC.
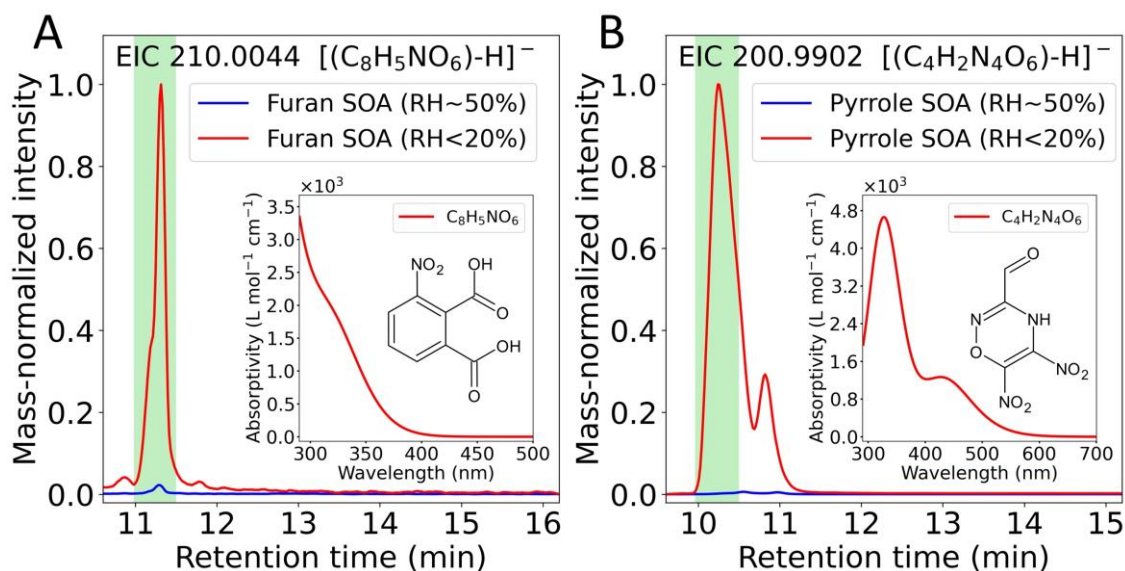
Figure 3.5. Characterization of molecular chromophores at RH <20% and ~50% conditions: (A) $C_8H_5NO_6$ in furan SOA; (B) $C_4H_2N_4O_6$ in pyrrole SOA. The mass-normalized intensity was calculated by the EIC intensity over the estimated mass of SOA samples, with the maximum value in each panel scaled to 1.0. The inset panels show the theoretical UV−vis spectra of molecular chromophores.

3.4. Atmospheric implications

This study provides evidence for the role of RH in modulating secondary BrC formation from heterocyclic VOCs, a significant group of SOA precursors in wildfire smoke, (34) through changes in size distribution dynamics, chemical composition, and light absorption properties. We also highlight the necessity of understanding explicit physicochemical pathways for evaluating the effects of RH on the climate impacts of wildfire smoke aerosols because multiple physicochemical processes can interplay during SOA formation, which can in turn alter the secondary BrC chemical composition and light absorption properties. The observations presented in this study demonstrate the intercorrelation of aerosol size distribution, chemical composition, and light absorption

properties. Specifically, the increased saturation and oxygenation levels of SOA composition at higher RH may promote the formation of non-absorbing oxygenated compounds, which can lead to decreased MAC profiles. Such process-level knowledge can aid in better understanding the effects of RH on BrC light absorption in wildfire smoke.

In contrast to secondary BrC derived from homocyclic VOCs (e.g., toluene), in which the production of nitroaromatic chromophores can be enhanced by higher RH, (28, 81, 82) our findings indicate that higher RH can lead to decreased mass fractions of nitrogen-containing chromophores (e.g., $C_8H_5NO_6$ and $C_4H_2N_4O_6$) in furan- and pyrrole-derived BrC. Such a difference highlights the critical role of SOA precursors and the molecular characteristics of chromophores in the effects of RH on secondary BrC formation. It should be noted that RH may exhibit a more complicated influence on secondary BrC light absorption (e.g., the non-monotonic RH dependency of MAC (50, 82)) or have less significant effects if the nitrogen content of secondary BrC is limited. (82) Given this complexity, understanding the explicit physicochemical processes of SOA formation would be the key to regulating secondary BrC formation. Our findings reveal that RH can greatly modulate the explicit physicochemical processing of secondary BrC formation and further alter the BrC-related radiative impacts of wildfire smoke. Therefore, this study highlights the importance of considering RH as a critical environmental factor in more accurate assessments of the climate effects of wildfire smoke aerosols.

Furthermore, this study can serve as a benchmark to help understand how the complex atmospheric environment affects the climate impacts of smoke aerosols at the

process level. Our findings reveal that dry conditions can lead to strongly absorbing secondary BrC derived from the nighttime oxidation of heterocyclic VOCs. This route may partially contribute to the strong BrC light absorption in dry wildfire smoke, as evident from recent field studies. (12, 83) More importantly, the reduced light absorption and the enhanced oxygenated mass were not only found in the NO_3-driven secondary BrC formation, but also in the aging processes of biomass-burning aerosols. (84, 85) This common characteristic suggests that the processing-level understanding reported in this study may be partially applicable to a wider range of physicochemical processes related to wildfire smoke. In addition, while previous studies have highlighted the importance of low-volatility high-molecular-weight ($\geq$400 Da) chromophores in optical properties of primary combustion BrC, (77, 86−88) this study and our prior work of furan SOA and pyrrole SOA suggest that nighttime oxidation of heterocyclic VOCs may mainly contribute to BrC chromophores with low molecular weight (<400 Da) in wildfire smoke aerosols. (14, 15, 39−41) Further research is needed to incorporate our findings into climate models to better estimate the RH influence on the radiative effects of wildfire smoke. Overall, our study demonstrates that environmental conditions such as RH in wildfire smoke can modulate secondary BrC formation and hence regulate the radiative impacts of unabated wildfires in the context of climate change.

3.5. Supplemental Information

Text S3.1. Aqueous solution experiments.

Supplementary experiments were performed to explore the effects of aqueous chemistry on BrC light absorption. We dried out the ACN-extracted SOA samples (RH <20%) and redissolved them in a 10 mM ammonium sulfate $((NH_4)_2SO_4)$ aqueous solution. The concentration of SOA aqueous solution was ~0.05 $\mu g\ \mu L^{-1}$, maintaining the light absorbance below 1.0 in the UV−vis measurements. The organic mass was assumed to be roughly consistent with the initially dissolved SOA mass, similar to previous studies. (72, 79, 80) The UV−vis spectra were measured at 0, 2, and 24 hours after the SOA samples were redissolved. If higher RH decreases the MAC profiles mainly via aqueous chemistry, the MAC profiles of the dissolved SOA should also decrease. However, our results showed increased MAC profiles in both SOAs (comparing Figures 4 and S4). A new absorption peak at ~400 nm was even observed in pyrrole BrC (**Figure S3.4B**). The aqueous chemistry promoted the formation of compounds with more nitrogen (**Figure S3.5**), which were not observed in the chamber experiments. Although the physicochemical characteristics of bulk solutions (e.g., ionic strengths) may not be identical with those in aqueous aerosols, the supplementary experiments can still support that aqueous chemistry may not lead to the decreased MAC of furan-derived and pyrrole-derived secondary BrC.

Table S3.1. Summary of particulate effective density (ρ_{eff}), organic mass fraction in aerosols (MF_{OA}), and SOA mass concentration in the chamber (C_{SOA}).

VOC	RH	ρ_{eff} (g cm^{-3})	MF_{OA}	C_{SOA} (μg m^{-3})
Furan	< 20%	1.46 ± 0.04	0.15 ± 0.03	5.41 ± 0.34
	~ 50%	1.75 ± 0.01	0.33 ± 0.04	17.28 ± 2.02
Pyrrole	< 20%	1.60 ± 0.02	0.85 ± 0.02	155.31 ± 26.45
	~ 50%	1.63 ± 0.12	0.71 ± 0.03	101.47 ± 9.42

Table S3.2. Cartesian coordinates of geometrical structures in the TD-DFT computation.

$C_8H_5NO_6$ (3-nitro-phthalic acid)

C	-1.23950200	2.04821600	0.03346700
C	-0.03776500	2.74077600	0.05294100
C	1.16037900	2.03759600	0.03848300
C	1.17474900	0.63771800	-0.00188100
C	-0.03302300	-0.08324300	-0.00285400
C	-1.21982100	0.65665700	0.01621600
H	-2.18863500	2.56523300	0.04644000
H	-0.03627200	3.82252800	0.08002800
C	2.47882800	-0.08800100	-0.08727500
O	2.59168800	-1.26136700	-0.36191500
O	3.53052000	0.70948900	0.16278900
H	4.34089000	0.18405100	0.06850100
C	-0.04854100	-1.59589900	-0.10288700
O	-0.26983300	-2.18387400	-1.13183700
O	0.20398800	-2.17520100	1.07406100
H	0.20352900	-3.13907600	0.95284900
N	-2.52828400	-0.02766000	0.04074400
O	-2.56756400	-1.17633100	0.46517900
O	-3.50553800	0.59565000	-0.35282800
H	2.10057800	2.57103000	0.04611000

$C_4H_2N_4O_6$ (5,6-dinitro-4*H*-1,2,4-oxadiazine-3-carbaldehyde)

C	-1.86103900	-0.59935700	-0.09161900
N	-1.18142100	0.52493600	-0.54599100
C	0.17529100	0.49568900	-0.33310500
C	0.75173800	-0.71672500	-0.27395300
N	-1.34419900	-1.76401800	0.00585300

O	-0.00265900	-1.80491100	-0.58580300
N	0.82717100	1.79443500	-0.03017500
O	1.40861500	2.33121500	-0.95181900
O	0.67054700	2.22955700	1.09500500
H	-1.69784500	1.39972500	-0.56376600
N	2.09319300	-0.97354600	0.19653100
O	2.43216300	-2.13824400	0.34074100
O	2.80878700	0.00889800	0.39136900
C	-3.28586000	-0.41999500	0.35213000
O	-3.81293700	0.66083100	0.27833800
H	-3.78227900	-1.32880400	0.71687000

$C_4H_2N_4O_6$ (2,3,4-trinitro-pyrrole)

C	-0.63365300	-1.99468200	0.00001200
C	-1.11756300	-0.68965900	0.00006500
C	-0.01074200	0.18566900	0.00000400
C	1.11057200	-0.61498800	-0.00010000
N	0.70769000	-1.92539200	-0.00021500
H	1.34933100	-2.71072700	-0.00035200
H	-1.16859000	-2.92925400	-0.00002000
N	-2.50329100	-0.32368600	-0.00000100
O	-2.76560300	0.87642700	-0.00021200
O	-3.33286300	-1.22596700	0.00015400
N	-0.03210300	1.65252800	-0.00002800
O	-0.04192300	2.20081100	-1.08669900
O	-0.04290400	2.20083800	1.08661100
N	2.49086800	-0.26581600	-0.00016100
O	3.30294000	-1.18766600	0.00022000
O	2.76603100	0.93037000	0.00034200

Table S3.3. Organic mass fractions of reduced nitrogen fragments in furan SOA and pyrrole SOA at RH <20% and ~50%.

VOC	RH	Organic mass fraction (%)			
		$C_2H_2N^+$	$C_2H_3N^+$	$C_3H_3N^+$	Total
Furan	< 20%	b.d.l.	0.85 ± 0.19	0.33 ± 0.08	1.18 ± 0.27
	~ 50%	b.d.l.	1.36 ± 0.50	b.d.l.	1.36 ± 0.50
Pyrrole	< 20%	1.23 ± 0.04	0.72 ± 0.03	1.30 ± 0.06	3.24 ± 0.06
	~ 50%	0.82 ± 0.03	1.00 ± 0.05	0.50 ± 0.05	2.31 ± 0.01

b.d.l.: below detection limit.

Table S3.4. Intensity-weighted average and standard deviation of H/C, O/C, N/C ratios and DBE of furan SOA and pyrrole SOA characterized by FIGAERO-ToF-CIMS at RH <20% and ~50%.

VOC	RH	<H/C>	<O/C>	<N/C>	<DBE>
Furan	<20%	1.0 ± 0.2	0.9 ± 0.3	0.1 ± 0.1	3.0 ± 0.6
	~50%	1.1 ± 0.3	1.0 ± 0.3	0.1 ± 0.1	2.7 ± 0.6
Pyrrole	<20%	1.0 ± 0.2	0.7 ± 0.2	0.5 ± 0.2	2.0 ± 0.2
	~50%	1.2 ± 0.3	0.8 ± 0.3	0.3 ± 0.1	1.9 ± 0.6

Table S3.5. MAC values at 365 nm (MAC_{365}) from this study and prior studies of secondary BrC at RH <20% and RH ~50%.

Precursors	Oxidation Type	MAC_{365} (m^2g^{-1})		Reference
		RH <20%	RH ~50%	
Furan	Nighttime oxidation	0.527	0.071	this work
Pyrrole	Nighttime oxidation	1.589	0.259	this work
Furfural	Photooxidation	0.862	0.342	Joo et al., 2024 (78)
2-Methylfuran	Photooxidation	0.121	0.077	Joo et al., 2024
3-Methylfuran	Photooxidation	0.048	0.048	Joo et al., 2024
Indole*	OH-initiated oxidation	0.959	1.644	Baboomian et al., 2023 (50)
Indole*	O_3-initiated oxidation	0.405	1.351	Baboomian et al., 2023
Indole*	NO_3-initiated oxidation	6.149	4.459	Baboomian et al., 2023
Naphthalene*	Photooxidation (low NO_x)	0.315	0.418	Klodt et al., 2023 (30)
Naphthalene*	Photooxidation (high NO_x)	0.359	0.473	Klodt et al., 2023
Trimethylbenzene*	Photooxidation	0.087	0.272	Liu et al., 2016 (28)
Toluene*	Photooxidation	0.273	0.698	Liu et al., 2016

* The data was obtained by reading the published figures with the PlotDigitizer software.

Table S3.6. Quantification of mass fraction of molecular chromophores in furan SOA and pyrrole SOA at RH <20% and ~50%.

SOA precursors	Molecular chromophores	Mass fraction (%)	
		RH <20%	RH ~50%
Furan	$C_4H_2O_4$	2.51 ± 0.06	0.85 ± 0.02
	$C_4H_4O_4$	1.44 ± 0.10	0.66 ± 0.05
	$C_4H_4O_6$	5.48 ± 2.91	0.66 ± 0.35
	$C_8H_5NO_6$	15.67 ± 3.76	0.50 ± 0.12
Pyrrole	$C_4H_3NO_2$	0.96 ± 0.02	0.56 ± 0.16
	$C_4H_3NO_3$	0.83 ± 0.11	0.78 ± 0.18
	$C_4H_3NO_4$	0.42 ± 0.02	0.58 ± 0.20
	$C_4H_4N_2O_2$	0.96 ± 0.02	0.56 ± 0.16
	$C_4H_3N_3O_4$	47.49 ± 1.21	0.12 ± 0.03
	$C_4H_2N_4O_6$	14.87 ± 1.16	0.01 ± 0.00
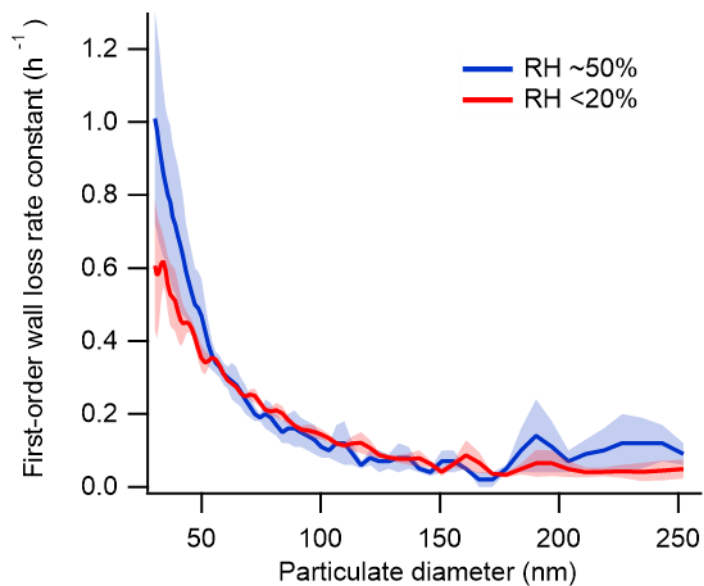
Figure S3.1. First-order wall loss rate constant along with particulate diameter at both RH. The wall loss rate constant at each particulate diameter was determined by using the first-order exponential model to fit the in-chamber decay of $(NH_4)_2SO_4$ particle number concentration within 3 hours. The red curve was reported previously. (15)
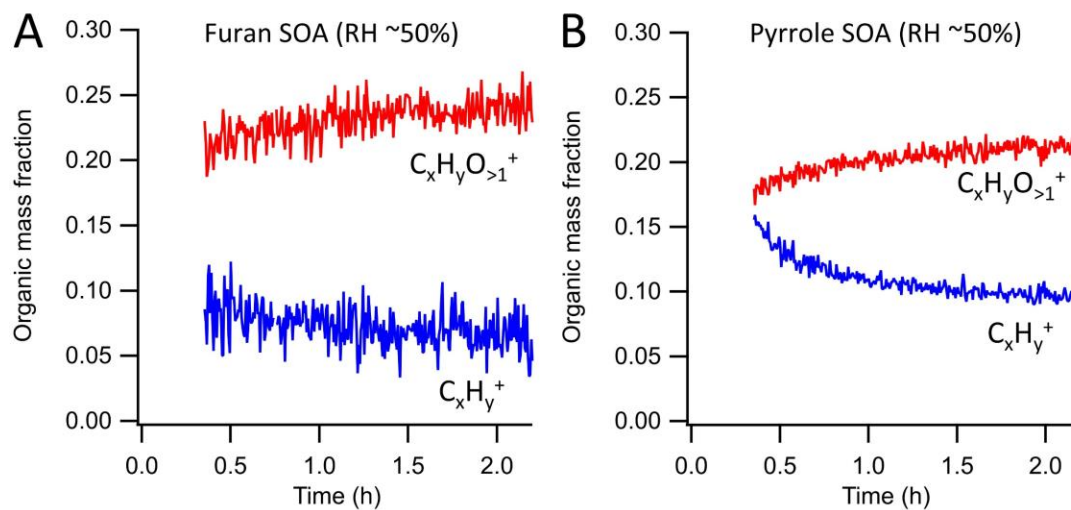
Figure S3.2. Time series of $C_xH_yO_{>1}^+$ fragments and $C_xH_y^+$ fragments from (A) furan SOA and (B) pyrrole SOA at RH ~50% after VOC injection.
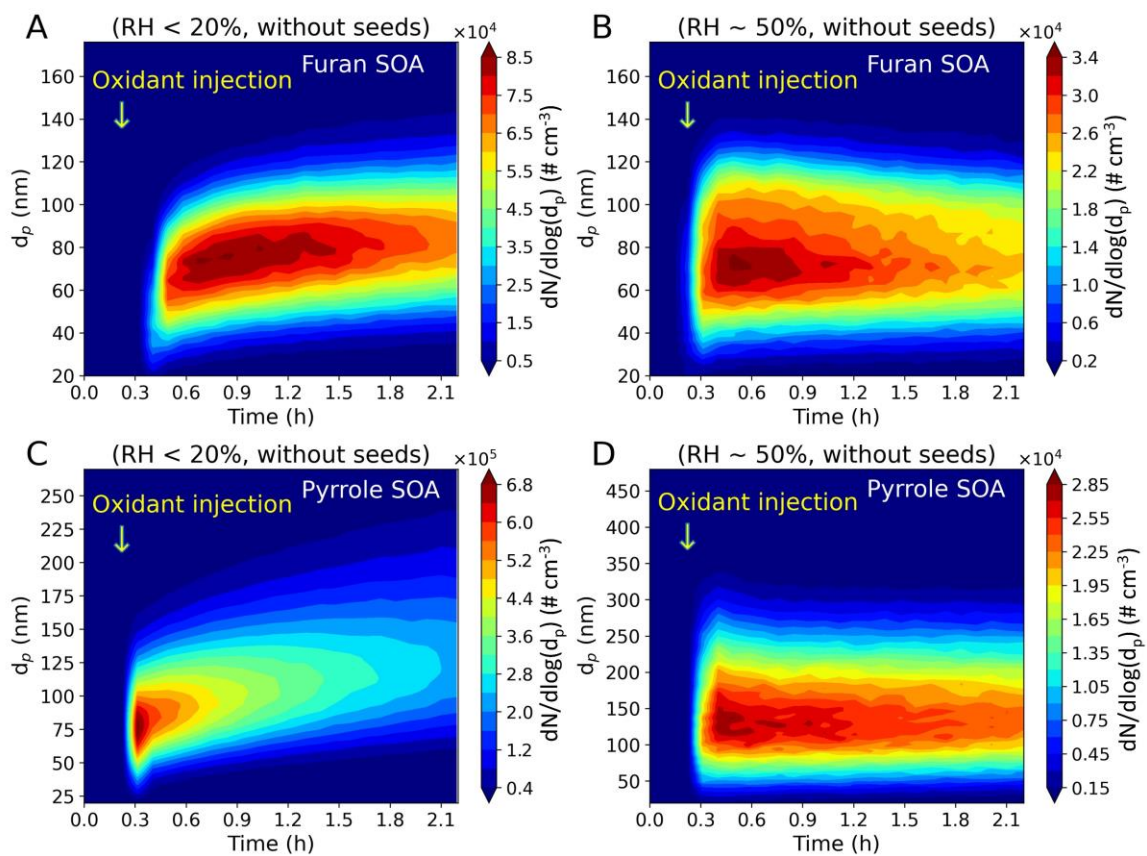
Figure S3.3. Particulate size distribution dynamics without pre-existing particles: (A) furan SOA at RH <20%; (B) furan SOA at RH ~50%; (C) pyrrole SOA at RH <20%; (D) pyrrole SOA at RH ~50%.
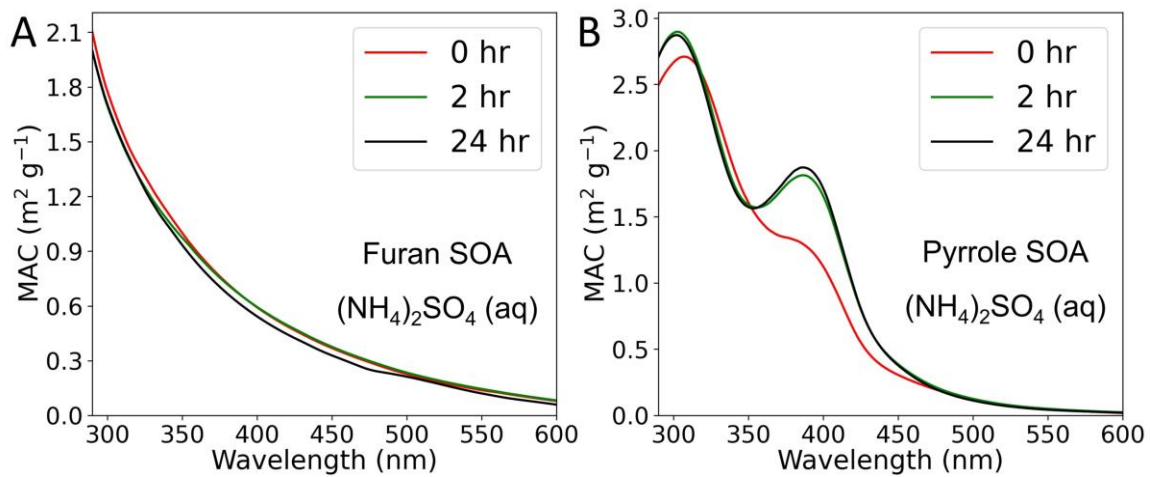
Figure S3.4. MAC profiles of (A) furan SOA and (B) pyrrole SOA in the ammonium sulfate solution experiments.
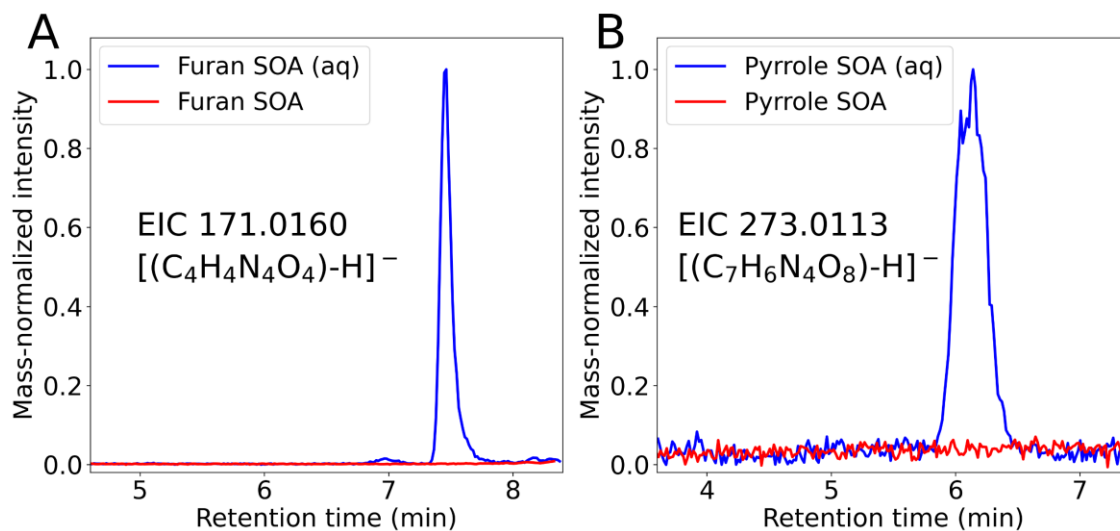
Figure S3.5. Newly formed products from aqueous-phase chemistry characterized by LC-ESI-Q-TOFMS: (A) $C_4H_4N_4O_4$ in furan SOA; (B) $C_7H_6N_4O_8$ in pyrrole SOA.
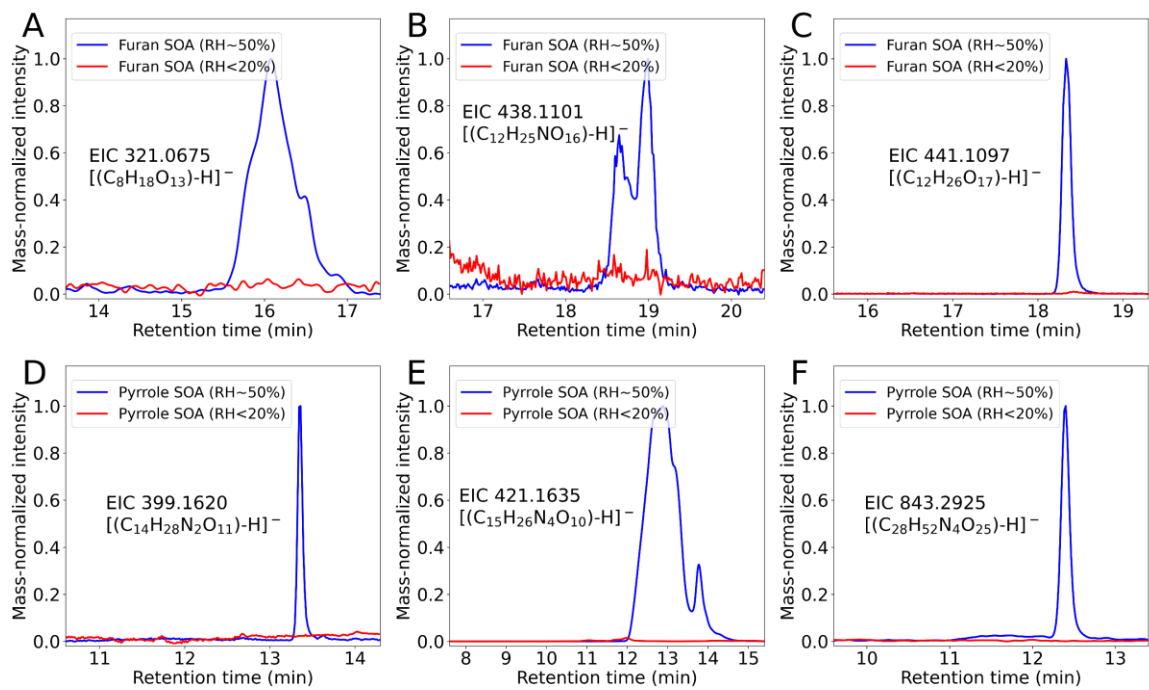
Figure S3.6. Extracted ion chromatograms of characterized non-absorbing oxygenated compounds in furan SOA and pyrrole SOA.
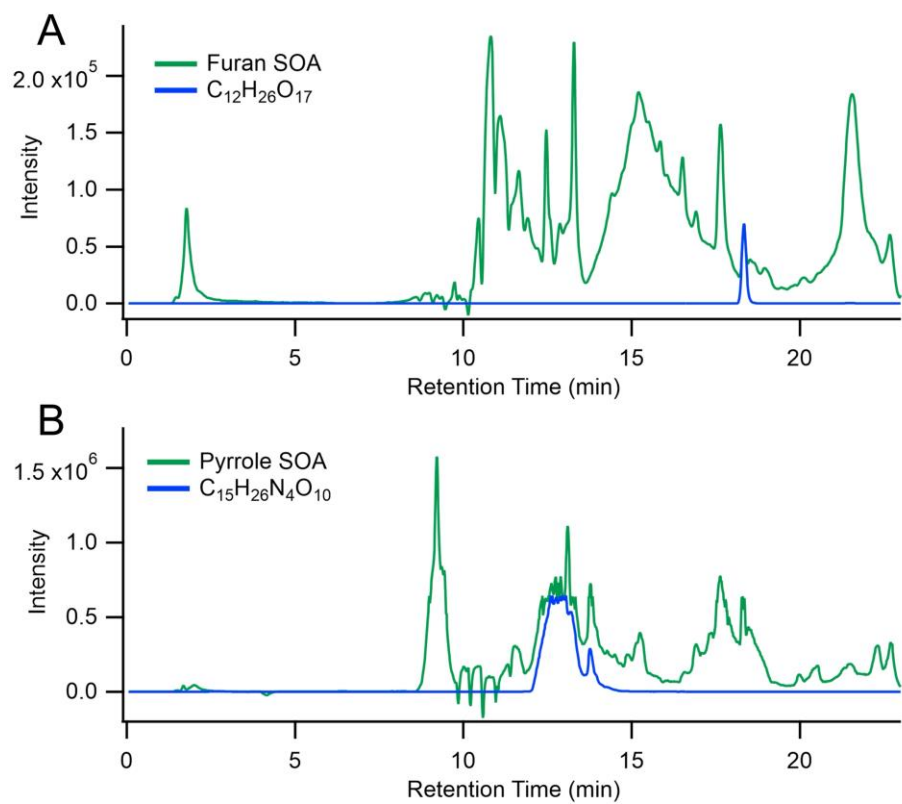
Figure S3.7. Base peak chromatograms of (A) furan SOA and $C_{12}H_{26}O_{17}$, and (B) pyrrole SOA and $C_{15}H_{26}N_4O_{10}$ (RH ~50%).
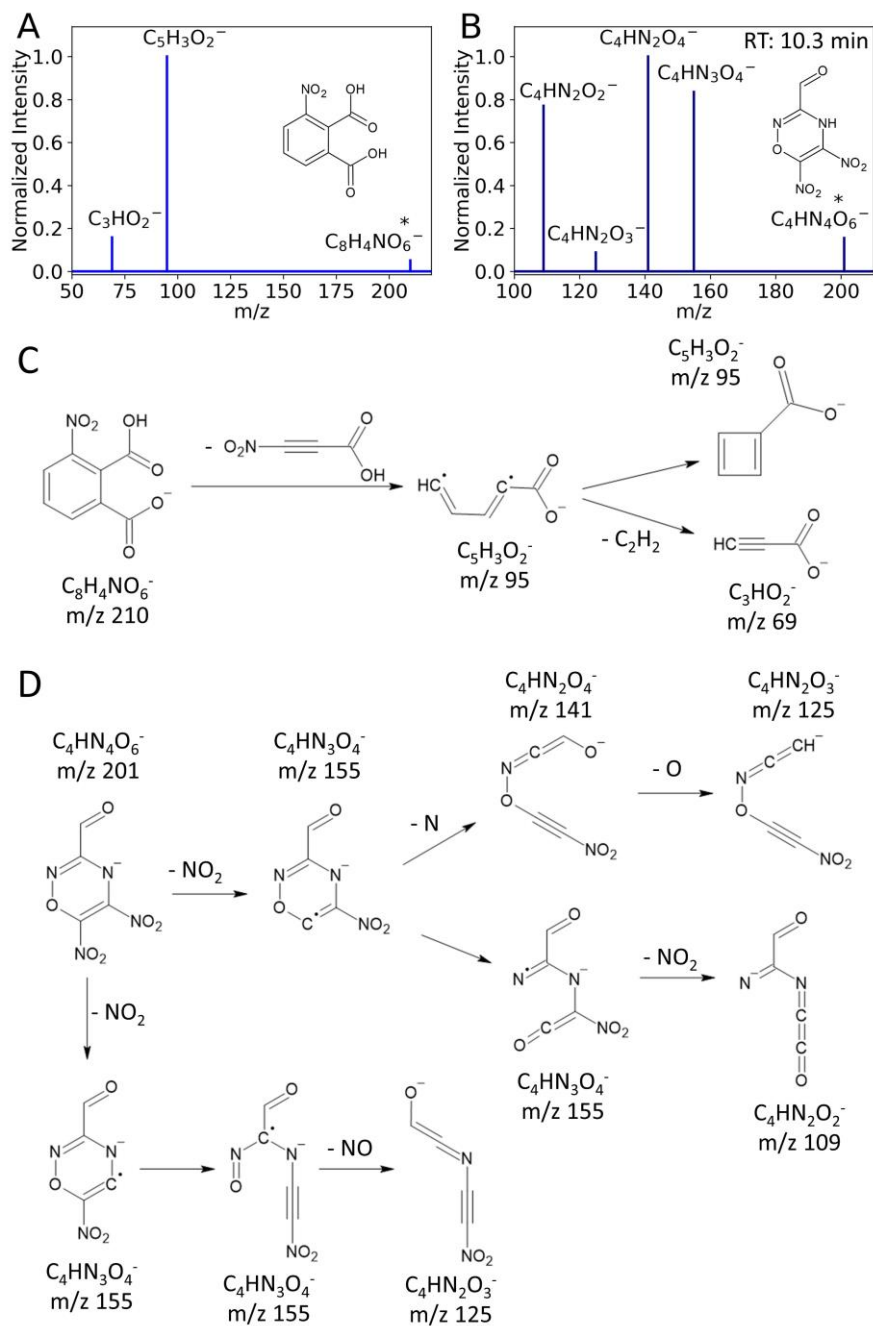
Figure S3.8. Tandem MS spectra and proposed fragmentation schemes of 3-nitrophthalic acid and 5,6-dinitro-4*H*-1,2,4-oxadiazine-3-carbaldehyde in SOA samples by LC-ESI-Q-TOFMS.
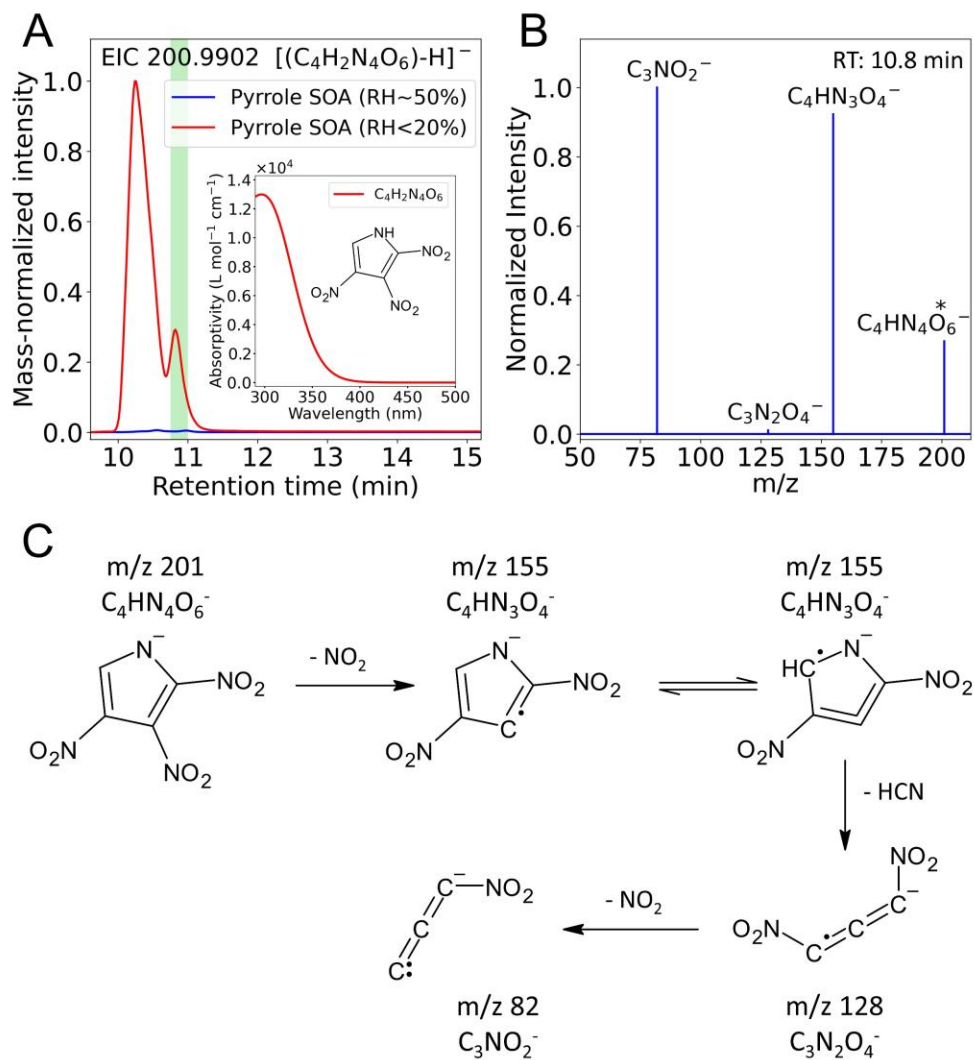
Figure S3.9. Characterization of 2,3,4-trinitro-pyrrole in pyrrole SOA by LC-ESI-Q-TOFMS.

3.6. References

1. Ferrero, L.; Močnik, G.; Cogliati, S.; Gregorič, A.; Colombo, R.; Bolzacchini, E., Heating Rate of Light Absorbing Aerosols: Time-Resolved Measurements, the Role of Clouds, and Source Identification. *Environ. Sci. Technol.* **2018**, 52, (6), 3546-3555.

2. Liu, D.; He, C.; Schwarz, J. P.; Wang, X., Lifecycle of light-absorbing carbonaceous aerosols in the atmosphere. *npj Clim. Atmos. Sci.* **2020**, 3, (1), 40.

3. Ding, K.; Huang, X.; Ding, A.; Wang, M.; Su, H.; Kerminen, V.-M.; Petäjä, T.; Tan, Z.; Wang, Z.; Zhou, D.; Sun, J.; Liao, H.; Wang, H.; Carslaw, K.; Wood, R.; Zuidema, P.; Rosenfeld, D.; Kulmala, M.; Fu, C.; Pöschl, U.; Cheng, Y.; Andreae, M. O., Aerosol-boundary-layer-monsoon interactions amplify semi-direct effect of biomass smoke on low cloud formation in Southeast Asia. *Nat. Commun.* **2021**, 12, (1), 6416.

4. Bowman, D. M. J. S.; Balch, J. K.; Artaxo, P.; Bond, W. J.; Carlson, J. M.; Cochrane, M. A.; D'Antonio, C. M.; DeFries, R. S.; Doyle, J. C.; Harrison, S. P.; Johnston, F. H.; Keeley, J. E.; Krawchuk, M. A.; Kull, C. A.; Marston, J. B.; Moritz, M. A.; Prentice, I. C.; Roos, C. I.; Scott, A. C.; Swetnam, T. W.; van der Werf, G. R.; Pyne, S. J., Fire in the Earth System. *Science* **2009**, 324, (5926), 481-484.

5. Jolly, W. M.; Cochrane, M. A.; Freeborn, P. H.; Holden, Z. A.; Brown, T. J.; Williamson, G. J.; Bowman, D. M. J. S., Climate-induced variations in global wildfire danger from 1979 to 2013. *Nat. Commun.* **2015**, 6, (1), 7537.

6. Goss, M.; Swain, D. L.; Abatzoglou, J. T.; Sarhadi, A.; Kolden, C. A.; Williams, A. P.; Diffenbaugh, N. S., Climate change is increasing the likelihood of extreme autumn wildfire conditions across California. *Environ. Res. Lett.* **2020**, 15, (9), 094016.

7. Andreae, M. O.; Merlet, P., Emission of trace gases and aerosols from biomass burning. *Glob. Biogeochem. Cycles* **2001**, 15, (4), 955-966.

8. Andreae, M. O., Emission of trace gases and aerosols from biomass burning – an updated assessment. *Atmos. Chem. Phys.* **2019**, 19, (13), 8523-8546.

9. Szopa, S., V. Naik, B. Adhikary, P. Artaxo, T. Berntsen, W.D. Collins, S. Fuzzi, L. Gallardo, A. Kiendler-Scharr, Z. Klimont, H. Liao, N. Unger, P. Zanis, Short-Lived Climate Forcers. *In Climate Change 2021: The Physical Science Basis. Contribution of Working Group I to the Sixth Assessment Report of the Intergovernmental Panel on Climate Change* [Masson-Delmotte, V., P. Zhai, A. Pirani, S.L. Connors, C. Péan, S. Berger, N. Caud, Y. Chen, L. Goldfarb, M.I. Gomis, M. Huang, K. Leitzell, E. Lonnoy, J.B.R. Matthews, T.K. Maycock, T. Waterfield, O. Yelekçi, R. Yu, and B. Zhou (eds.)]. Cambridge University Press, Cambridge, United Kingdom and New York, NY, USA: **2021**; p 817–922.

10. Bond, T. C.; Streets, D. G.; Yarber, K. F.; Nelson, S. M.; Woo, J.-H.; Klimont, Z., A technology-based global inventory of black and organic carbon emissions from combustion. *J. Geophys. Res. Atmos.* **2004**, 109, D14203.

11. Yu, P.; Toon, O. B.; Bardeen, C. G.; Zhu, Y.; Rosenlof, K. H.; Portmann, R. W.; Thornberry, T. D.; Gao, R.-S.; Davis, S. M.; Wolf, E. T.; de Gouw, J.; Peterson, D. A.; Fromm, M. D.; Robock, A., Black carbon lofts wildfire smoke high into the stratosphere to form a persistent plume. *Science* **2019**, 365, (6453), 587-590.

12. Chakrabarty, R. K.; Shetty, N. J.; Thind, A. S.; Beeler, P.; Sumlin, B. J.; Zhang, C.; Liu, P.; Idrobo, J. C.; Adachi, K.; Wagner, N. L.; Schwarz, J. P.; Ahern, A.; Sedlacek, A. J.; Lambe, A.; Daube, C.; Lyu, M.; Liu, C.; Herndon, S.; Onasch, T. B.; Mishra, R., Shortwave absorption by wildfire smoke dominated by dark brown carbon. *Nat. Geosci.* **2023**, 16, (8), 683-688.

13. Akherati, A.; He, Y.; Garofalo, L. A.; Hodshire, A. L.; Farmer, D. K.; Kreidenweis, S. M.; Permar, W.; Hu, L.; Fischer, E. V.; Jen, C. N.; Goldstein, A. H.; Levin, E. J. T.; DeMott, P. J.; Campos, T. L.; Flocke, F.; Reeves, J. M.; Toohey, D. W.; Pierce, J. R.; Jathar, S. H., Dilution and photooxidation driven processes explain the evolution of organic aerosol in wildfire plumes. *Environ. Sci. Atmos.* **2022**, 2, (5), 1000-1022.

14. Chen, K.; Mayorga, R.; Raeofy, N.; Lum, M.; Woods, M.; Bahreini, R.; Zhang, H.; Lin, Y.-H., Effects of Nitrate Radical Levels and Pre-Existing Particles on Secondary Brown Carbon Formation from Nighttime Oxidation of Furan. *ACS Earth Space Chem.* **2022**, 6, (11), 2709-2721.

15. Chen, K.; Mayorga, R.; Hamilton, C.; Bahreini, R.; Zhang, H.; Lin, Y.-H., Contribution of Carbonyl Chromophores in Secondary Brown Carbon from Nighttime Oxidation of Unsaturated Heterocyclic Volatile Organic Compounds. *Environ. Sci. Technol.* **2023**, 57, (48), 20085-20096.

16. Seinfeld, J. H.; Erdakos, G. B.; Asher, W. E.; Pankow, J. F., Modeling the Formation of Secondary Organic Aerosol (SOA). 2. The Predicted Effects of Relative Humidity on Aerosol Formation in the α-Pinene-, β-Pinene-, Sabinene-, Δ^3-Carene-, and Cyclohexene-Ozone Systems. *Environ. Sci. Technol.* **2001**, 35, (9), 1806-1817.

17. Jonsson, Å. M.; Hallquist, M.; Ljungström, E., Impact of Humidity on the Ozone Initiated Oxidation of Limonene, Δ^3-Carene, and α-Pinene. *Environ. Sci. Technol.* **2006**, 40, (1), 188-194.

18. Nguyen, T. B.; Roach, P. J.; Laskin, J.; Laskin, A.; Nizkorodov, S. A., Effect of humidity on the composition of isoprene photooxidation secondary organic aerosol. *Atmos. Chem. Phys.* **2011**, 11, (14), 6931-6944.

19. Saukko, E.; Lambe, A. T.; Massoli, P.; Koop, T.; Wright, J. P.; Croasdale, D. R.; Pedernera, D. A.; Onasch, T. B.; Laaksonen, A.; Davidovits, P.; Worsnop, D. R.; Virtanen, A., Humidity-dependent phase state of SOA particles from biogenic and anthropogenic precursors. *Atmos. Chem. Phys.* **2012**, 12, (16), 7517-7529.

20. Boyd, C. M.; Sanchez, J.; Xu, L.; Eugene, A. J.; Nah, T.; Tuet, W. Y.; Guzman, M. I.; Ng, N. L., Secondary organic aerosol formation from the β-pinene+NO3 system: effect of humidity and peroxy radical fate. *Atmos. Chem. Phys.* **2015**, 15, (13), 7497-7522.

21. Boyd, C. M.; Nah, T.; Xu, L.; Berkemeier, T.; Ng, N. L., Secondary Organic Aerosol (SOA) from Nitrate Radical Oxidation of Monoterpenes: Effects of Temperature, Dilution, and Humidity on Aerosol Formation, Mixing, and Evaporation. *Environ. Sci. Technol.* **2017**, 51, (14), 7831-7841.

22. Stirnweis, L.; Marcolli, C.; Dommen, J.; Barmet, P.; Frege, C.; Platt, S. M.; Bruns, E. A.; Krapf, M.; Slowik, J. G.; Wolf, R.; Prévôt, A. S. H.; Baltensperger, U.; El-Haddad, I., Assessing the influence of NOx concentrations and relative humidity on secondary organic aerosol yields from α-pinene photo-oxidation through smog chamber experiments and modelling calculations. *Atmos. Chem. Phys.* **2017**, 17, (8), 5035-5061.

23. Liu, S.; Tsona, N. T.; Zhang, Q.; Jia, L.; Xu, Y.; Du, L., Influence of relative humidity on cyclohexene SOA formation from OH photooxidation. *Chemosphere* **2019**, 231, 478-486.

24. Petters, S. S.; Kreidenweis, S. M.; Grieshop, A. P.; Ziemann, P. J.; Petters, M. D., Temperature- and Humidity-Dependent Phase States of Secondary Organic Aerosols. *Geophys. Res. Lett.* **2019**, 46, (2), 1005-1013.

25. Chen, T.; Chu, B.; Ma, Q.; Zhang, P.; Liu, J.; He, H., Effect of relative humidity on SOA formation from aromatic hydrocarbons: Implications from the evolution of gas- and particle-phase species. *Sci. Total Environ.* **2021**, 773, 145015.

26. Wang, Y.; Voliotis, A.; Shao, Y.; Zong, T.; Meng, X.; Du, M.; Hu, D.; Chen, Y.; Wu, Z.; Alfarra, M. R.; McFiggans, G., Phase state of secondary organic aerosol in chamber photo-oxidation of mixed precursors. *Atmos. Chem. Phys.* **2021**, 21, (14), 11303-11316.

27. Liu, S.; Wang, Y.; Xu, X.; Wang, G., Effects of NO_2 and RH on secondary organic aerosol formation and light absorption from OH oxidation of o-xylene. *Chemosphere* **2022**, 308, 136541.

28. Liu, J.; Lin, P.; Laskin, A.; Laskin, J.; Kathmann, S. M.; Wise, M.; Caylor, R.; Imholt, F.; Selimovic, V.; Shilling, J. E., Optical properties and aging of light-absorbing secondary organic aerosol. *Atmos. Chem. Phys.* **2016**, 16, (19), 12815-12827.

29. Cui, Y.; Frie, A. L.; Dingle, J. H.; Zimmerman, S.; Frausto-Vicencio, I.; Hopkins, F.; Bahreini, R., Influence of Ammonia and Relative Humidity on the Formation and Composition of Secondary Brown Carbon from Oxidation of 1-Methylnaphthalene and Longifolene. *ACS Earth Space Chem.* **2021**, 5, (4), 858-869.

30. Klodt, A. L.; Aiona, P. K.; MacMillan, A. C.; Ji Lee, H.; Zhang, X.; Helgestad, T.; Novak, G. A.; Lin, P.; Laskin, J.; Laskin, A.; Bertram, T. H.; Cappa, C. D.; Nizkorodov, S. A., Effect of relative humidity, NOx, and ammonia on the physical properties of naphthalene secondary organic aerosols. *Environ. Sci. Atmos.* **2023**, 3, (6), 991-1007.

31. Song, C.; Gyawali, M.; Zaveri, R. A.; Shilling, J. E.; Arnott, W. P., Light absorption by secondary organic aerosol from α-pinene: Effects of oxidants, seed aerosol acidity, and relative humidity. *J. Geophys. Res. Atmos.* **2013**, 118, (20), 11,741-11,749.

32. Sullivan, A. P.; Pokhrel, R. P.; Shen, Y.; Murphy, S. M.; Toohey, D. W.; Campos, T.; Lindaas, J.; Fischer, E. V.; Collett Jr, J. L., Examination of brown carbon absorption from wildfires in the western US during the WE-CAN study. *Atmos. Chem. Phys.* **2022**, 22, (20), 13389-13406.

33. Gupta, R. R.; Kumar, M.; Gupta, V., Five-Membered Heterocycles with One Heteroatom. *In Heterocyclic Chemistry: Volume II: Five-Membered Heterocycles*, Gupta, R. R.; Kumar, M.; Gupta, V., Eds. Springer Berlin Heidelberg: Berlin, Heidelberg, **1999**; pp 3-179.

34. Palm, B. B.; Peng, Q.; Fredrickson, C. D.; Lee, B. H.; Garofalo, L. A.; Pothier, M. A.; Kreidenweis, S. M.; Farmer, D. K.; Pokhrel, R. P.; Shen, Y.; Murphy, S. M.; Permar, W.; Hu, L.; Campos, T. L.; Hall, S. R.; Ullmann, K.; Zhang, X.; Flocke, F.; Fischer, E. V.; Thornton, J. A., Quantification of organic aerosol and brown carbon evolution in fresh wildfire plumes. *PNAS* **2020**, 117, (47), 29469.

35. Hatch, L. E.; Luo, W.; Pankow, J. F.; Yokelson, R. J.; Stockwell, C. E.; Barsanti, K. C., Identification and quantification of gaseous organic compounds emitted from biomass burning using two-dimensional gas chromatography–time-of-flight mass spectrometry. *Atmos. Chem. Phys.* **2015**, 15, (4), 1865-1899.

36. Koss, A. R.; Sekimoto, K.; Gilman, J. B.; Selimovic, V.; Coggon, M. M.; Zarzana, K. J.; Yuan, B.; Lerner, B. M.; Brown, S. S.; Jimenez, J. L.; Krechmer, J.; Roberts, J. M.; Warneke, C.; Yokelson, R. J.; de Gouw, J., Non-methane organic gas emissions from biomass burning: identification, quantification, and emission factors from PTR-ToF during the FIREX 2016 laboratory experiment. *Atmos. Chem. Phys.* **2018**, 18, (5), 3299-3319.

37. Permar, W.; Wang, Q.; Selimovic, V.; Wielgasz, C.; Yokelson, R. J.; Hornbrook, R. S.; Hills, A. J.; Apel, E. C.; Ku, I. T.; Zhou, Y.; Sive, B. C.; Sullivan, A. P.; Collett Jr, J. L.; Campos, T. L.; Palm, B. B.; Peng, Q.; Thornton, J. A.; Garofalo, L. A.; Farmer, D. K.; Kreidenweis, S. M.; Levin, E. J. T.; DeMott, P. J.; Flocke, F.; Fischer, E. V.; Hu, L., Emissions of Trace Organic Gases From Western U.S. Wildfires Based on WE-CAN Aircraft Measurements. *J. Geophys. Res. Atmos.* **2021**, 126, (11), e2020JD033838.

38. Decker, Z. C. J.; Zarzana, K. J.; Coggon, M.; Min, K.-E.; Pollack, I.; Ryerson, T. B.; Peischl, J.; Edwards, P.; Dubé, W. P.; Markovic, M. Z.; Roberts, J. M.; Veres, P. R.; Graus, M.; Warneke, C.; de Gouw, J.; Hatch, L. E.; Barsanti, K. C.; Brown, S. S., Nighttime Chemical Transformation in Biomass Burning Plumes: A Box Model Analysis Initialized with Aircraft Observations. *Environ. Sci. Technol.* **2019**, 53, (5), 2529-2538.

39. Jiang, H.; Frie, A. L.; Lavi, A.; Chen, J. Y.; Zhang, H.; Bahreini, R.; Lin, Y.-H., Brown Carbon Formation from Nighttime Chemistry of Unsaturated Heterocyclic Volatile Organic Compounds. *Environ. Sci. Technol. Lett.* **2019**, 6, (3), 184-190.

40. Chen, K.; Raeofy, N.; Lum, M.; Mayorga, R.; Woods, M.; Bahreini, R.; Zhang, H.; Lin, Y.-H., Solvent effects on chemical composition and optical properties of extracted secondary brown carbon constituents. *Aerosol Sci. Tech.* **2022**, 56, (10), 917-930.

41. Mayorga, R.; Chen, K.; Raeofy, N.; Woods, M.; Lum, M.; Zhao, Z.; Zhang, W.; Bahreini, R.; Lin, Y.-H.; Zhang, H., Chemical Structure Regulates the Formation of Secondary Organic Aerosol and Brown Carbon in Nitrate Radical Oxidation of Pyrroles and Methylpyrroles. *Environ. Sci. Technol.* **2022**, 56, (12), 7761-7770.

42. Akagi, S. K.; Craven, J. S.; Taylor, J. W.; McMeeking, G. R.; Yokelson, R. J.; Burling, I. R.; Urbanski, S. P.; Wold, C. E.; Seinfeld, J. H.; Coe, H.; Alvarado, M. J.; Weise, D. R., Evolution of trace gases and particles emitted by a chaparral fire in California. *Atmos. Chem. Phys.* **2012**, 12, (3), 1397-1421.

43. Westerling, A. L.; Gershunov, A.; Brown, T. J.; Cayan, D. R.; Dettinger, M. D., Climate and Wildfire in the Western United States. *Bull. Amer. Meteor. Soc.* **2003**, 84, (5), 595-604.

44. Holden Zachary, A.; Swanson, A.; Luce Charles, H.; Jolly, W. M.; Maneta, M.; Oyler Jared, W.; Warren Dyer, A.; Parsons, R.; Affleck, D., Decreasing fire season precipitation increased recent western US forest wildfire activity. *PNAS* **2018**, 115, (36), E8349-E8357.

45. Jiang, Y.; Zhou, L.; Raghavendra, A., Observed changes in fire patterns and possible drivers over Central Africa. *Environ. Res. Lett.* **2020**, 15, (9), 0940b8.

46. Ramo, R.; Roteta, E.; Bistinas, I.; van Wees, D.; Bastarrika, A.; Chuvieco, E.; van der Werf Guido, R., African burned area and fire carbon emissions are strongly impacted by small fires undetected by coarse resolution satellite data. *PNAS* **2021**, 118, (9), e2011160118.

47. Hobbs, P. V.; Sinha, P.; Yokelson, R. J.; Christian, T. J.; Blake, D. R.; Gao, S.; Kirchstetter, T. W.; Novakov, T.; Pilewskie, P., Evolution of gases and particles from a savanna fire in South Africa. *J. Geophys. Res. Atmos.* **2003**, 108, No. D13, 8485.

48. Junghenn Noyes, K.; Kahn, R.; Sedlacek, A.; Kleinman, L.; Limbacher, J.; Li, Z., Wildfire Smoke Particle Properties and Evolution, from Space-Based Multi-Angle Imaging. *Remote Sens.* **2020**, 12, (22), 3823.

49. Huang, X.; Ding, K.; Liu, J.; Wang, Z.; Tang, R.; Xue, L.; Wang, H.; Zhang, Q.; Tan, Z.-M.; Fu, C.; Davis, S. J.; Andreae, M. O.; Ding, A., Smoke-weather interaction affects extreme wildfires in diverse coastal regions. *Science* **2023**, 379, (6631), 457-461.

50. Baboomian, V. J.; He, Q.; Montoya-Aguilera, J.; Ali, N.; Fleming, L. T.; Lin, P.; Laskin, A.; Laskin, J.; Rudich, Y.; Nizkorodov, S. A., Light absorption and scattering properties of indole secondary organic aerosol prepared under various oxidant and relative humidity conditions. *Aerosol Sci. Tech.* **2023**, 57, (6), 532-545.

51. Dennison, P. E.; Charoensiri, K.; Roberts, D. A.; Peterson, S. H.; Green, R. O., Wildfire temperature and land cover modeling using hyperspectral data. *Remote Sens. Environ.* **2006**, 100, (2), 212-222.

52. Strand, T.; Larkin, N.; Rorig, M.; Krull, C.; Moore, M., PM2.5 measurements in wildfire smoke plumes from fire seasons 2005–2008 in the Northwestern United States. *J. Aerosol Sci.* **2011**, 42, (3), 143-155.

53. Ding, Y.; Cruz, I.; Freedman, F.; Venkatram, A., Improving spatial resolution of PM2.5 measurements during wildfires. *Atmos. Pollut. Res.* **2021**, 12, (5), 101047.

54. Junghenn Noyes, K. T.; Kahn, R. A.; Limbacher, J. A.; Li, Z., Canadian and Alaskan wildfire smoke particle properties, their evolution, and controlling factors, from satellite observations. *Atmos. Chem. Phys.* **2022**, 22, (15), 10267-10290.

55. Bertram, A. K.; Martin, S. T.; Hanna, S. J.; Smith, M. L.; Bodsworth, A.; Chen, Q.; Kuwata, M.; Liu, A.; You, Y.; Zorn, S. R., Predicting the relative humidities of liquid-liquid phase separation, efflorescence, and deliquescence of mixed particles of ammonium sulfate, organic material, and water using the organic-to-sulfate mass ratio of the particle and the oxygen-to-carbon elemental ratio of the organic component. *Atmos. Chem. Phys.* **2011**, 11, (21), 10995-11006.

56. Liu, T.; Huang, D. D.; Li, Z.; Liu, Q.; Chan, M.; Chan, C. K., Comparison of secondary organic aerosol formation from toluene on initially wet and dry ammonium sulfate particles at moderate relative humidity. *Atmos. Chem. Phys.* **2018**, 18, (8), 5677-5689.

57. Atkinson, R.; Aschmann, S. M.; Carter, W. P. L., Kinetics of the reactions of O_3 and OH radicals with furan and thiophene at 298 ± 2 K. *Int. J. Chem. Kinet.* **1983**, 15, (1), 51-61.

58. Atkinson, R.; Aschmann, S. M.; Winer, A. M.; Carter, W. P. L., Rate constants for the gas phase reactions of OH radicals and O_3 with pyrrole at 295 ± 1 K and atmospheric pressure. *Atmos. Environ.* **1984**, 18, (10), 2105-2107.

59. Atkinson, R.; Aschmann, S. M.; Winer, A. M.; Carter, W. P. L., Rate constants for the gas-phase reactions of nitrate radicals with furan, thiophene, and pyrrole at 295 ± 1 K and atmospheric pressure. *Environ. Sci. Technol.* **1985**, 19, (1), 87-90.

60. Bahreini, R.; Keywood, M. D.; Ng, N. L.; Varutbangkul, V.; Gao, S.; Flagan, R. C.; Seinfeld, J. H.; Worsnop, D. R.; Jimenez, J. L., Measurements of Secondary Organic Aerosol from Oxidation of Cycloalkenes, Terpenes, and m-Xylene Using an Aerodyne Aerosol Mass Spectrometer. *Environ. Sci. Technol.* **2005**, 39, (15), 5674-5688.

61. Lopez-Hilfiker, F. D.; Mohr, C.; Ehn, M.; Rubach, F.; Kleist, E.; Wildt, J.; Mentel, T. F.; Lutz, A.; Hallquist, M.; Worsnop, D.; Thornton, J. A., A novel method for online analysis of gas and particle composition: description and evaluation of a Filter Inlet for Gases and AEROsols (FIGAERO). *Atmos. Meas. Tech.* **2014**, 7, (4), 983-1001.

62. Frisch, M. J.; Trucks, G. W.; Schlegel, H. B.; Scuseria, G. E.; Robb, M. A.; Cheeseman, J. R.; Scalmani, G.; Barone, V.; Petersson, G. A.; Nakatsuji, H.; Li, X.; Caricato, M.; Marenich, A. V.; Bloino, J.; Janesko, B. G.; Gomperts, R.; Mennucci, B.; Hratchian, H. P.; Ortiz, J. V.; Izmaylov, A. F.; Sonnenberg, J. L.; Williams; Ding, F.; Lipparini, F.; Egidi, F.; Goings, J.; Peng, B.; Petrone, A.; Henderson, T.; Ranasinghe, D.; Zakrzewski, V. G.; Gao, J.; Rega, N.; Zheng, G.; Liang, W.; Hada, M.; Ehara, M.; Toyota, K.; Fukuda, R.; Hasegawa, J.; Ishida, M.; Nakajima, T.; Honda, Y.; Kitao, O.; Nakai, H.; Vreven, T.; Throssell, K.; Montgomery Jr., J. A.; Peralta, J. E.; Ogliaro, F.; Bearpark, M. J.; Heyd, J. J.; Brothers, E. N.; Kudin, K. N.; Staroverov, V. N.; Keith, T. A.; Kobayashi, R.; Normand, J.; Raghavachari, K.; Rendell, A. P.; Burant, J. C.; Iyengar, S. S.; Tomasi, J.; Cossi, M.; Millam, J. M.; Klene, M.; Adamo, C.; Cammi, R.; Ochterski, J. W.; Martin, R. L.; Morokuma, K.; Farkas, O.; Foresman, J. B.; Fox, D. J. Gaussian 16 Rev. C.01, Wallingford, CT, **2016**.

63. Becke, A. D., Density-functional exchange-energy approximation with correct asymptotic behavior. *Phys. Rev. A* **1988**, 38, (6), 3098-3100.

64. Stephens, P. J.; Devlin, F. J.; Chabalowski, C. F.; Frisch, M. J., *Ab Initio* Calculation of Vibrational Absorption and Circular Dichroism Spectra Using Density Functional Force Fields. *J. Phys. Chem.* **1994**, 98, (45), 11623-11627.

65. Ditchfield, R; Hehre, W. J.; People, J. A., Self-Consistent Molecular-Orbital Methods. IX. An Extended Gaussian-Type Basis for Molecular-Orbital Studies of Organic Molecules. *J. Chem. Phys.* **1971**, 54, (2), 724-728.

66. Jacquemin, D.; Perpète, E. A.; Scuseria, G. E.; Ciofini, I.; Adamo, C., TD-DFT Performance for the Visible Absorption Spectra of Organic Dyes: Conventional versus Long-Range Hybrids. *J. Chem. Theory Comput.* **2008**, 4, (1), 123-135.

67. Chen, J. Y.; Rodriguez, E.; Jiang, H.; Chen, K.; Frie, A.; Zhang, H.; Bahreini, R.; Lin, Y.-H., Time-Dependent Density Functional Theory Investigation of the UV–Vis Spectra of Organonitrogen Chromophores in Brown Carbon. *ACS Earth Space Chem.* **2020**, 4, (2), 311-320.

68. Mennucci, B.; Cammi, R.; Tomasi, J., Excited states and solvatochromic shifts within a nonequilibrium solvation approach: A new formulation of the integral equation formalism method at the self-consistent field, configuration interaction, and multiconfiguration self-consistent field level. *J. Chem. Phys.* **1998**, 109, (7), 2798-2807.

69. Shiraiwa, M.; Yee, L. D.; Schilling, K. A.; Loza, C. L.; Craven, J. S.; Zuend, A.; Ziemann, P. J.; Seinfeld, J. H., Size distribution dynamics reveal particle-phase chemistry in organic aerosol formation. *PNAS* **2013**, 110, (29), 11746-11750.

70. Hamed, A.; Korhonen, H.; Sihto, S.-L.; Joutsensaari, J.; Järvinen, H.; Petäjä, T.; Arnold, F.; Nieminen, T.; Kulmala, M.; Smith, J. N.; Lehtinen, K. E. J.; Laaksonen, A., The role of relative humidity in continental new particle formation. *J. Geophys. Res. Atmos.* **2011**, 116, D03202.

71. Kampf, C. J.; Jakob, R.; Hoffmann, T., Identification and characterization of aging products in the glyoxal/ammonium sulfate system – implications for light-absorbing material in atmospheric aerosols. *Atmos. Chem. Phys.* **2012**, 12, (14), 6323-6333.

72. Aiona, P. K.; Lee, H. J.; Leslie, R.; Lin, P.; Laskin, A.; Laskin, J.; Nizkorodov, S. A., Photochemistry of Products of the Aqueous Reaction of Methylglyoxal with Ammonium Sulfate. *ACS Earth Space Chem.* **2017**, 1, (8), 522-532.

73. Huang, M.; Zhang, J.; Cai, S.; Liao, Y.; Zhao, W.; Hu, C.; Gu, X.; Fang, L.; Zhang, W., Characterization of particulate products for aging of ethylbenzene secondary organic aerosol in the presence of ammonium sulfate seed aerosol. *J. Environ. Sci.* **2017**, 47, 219-229.

74. Grace, D. N.; Sharp, J. R.; Holappa, R. E.; Lugos, E. N.; Sebold, M. B.; Griffith, D. R.; Hendrickson, H. P.; Galloway, M. M., Heterocyclic Product Formation in Aqueous Brown Carbon Systems. *ACS Earth Space Chem.* **2019**, 3, (11), 2472-2481.

75. Lian, X.; Zhang, G.; Yang, Y.; Lin, Q.; Fu, Y.; Jiang, F.; Peng, L.; Hu, X.; Chen, D.; Wang, X.; Peng, P. a.; Sheng, G.; Bi, X., Evidence for the Formation of Imidazole from Carbonyls and Reduced Nitrogen Species at the Individual Particle Level in the Ambient Atmosphere. *Environ. Sci. Technol. Lett.* **2021**, 8, (1), 9-15.

76. Cao, G.; Yan, Y.; Zou, X.; Zhu, R.; Ouyang, F., Applications of Infrared Spectroscopy in Analysis of Organic Aerosols. *Spectr. Anal. Rev.* **2018**, 06, 12-32.

77. Saleh, R., From Measurements to Models: Toward Accurate Representation of Brown Carbon in Climate Calculations. *Curr. Pollut. Rep.* **2020**, 6, (2), 90-104.

78. Joo, T.; Machesky, J. E.; Zeng, L.; Hass-Mitchell, T.; Weber, R. J.; Gentner, D. R.; Ng, N. L., Secondary Brown Carbon Formation From Photooxidation of Furans From Biomass Burning. *Geophys. Res. Lett.* **2024**, 51, (1), e2023GL104900.

79. Nguyen, T. B.; Lee, P. B.; Updyke, K. M.; Bones, D. L.; Laskin, J.; Laskin, A.; Nizkorodov, S. A., Formation of nitrogen- and sulfur-containing light-absorbing compounds accelerated by evaporation of water from secondary organic aerosols. *J. Geophys. Res. Atmos.* **2012**, 117, D01207.

80. Nguyen, T. B.; Laskin, A.; Laskin, J.; Nizkorodov, S. A., Brown carbon formation from ketoaldehydes of biogenic monoterpenes. *Faraday Discuss.* **2013**, 165, (0), 473-494.

81. Lin, P.; Liu, J.; Shilling, J. E.; Kathmann, S. M.; Laskin, J.; Laskin, A., Molecular characterization of brown carbon (BrC) chromophores in secondary organic aerosol generated from photo-oxidation of toluene. *Phys. Chem. Chem. Phys.* **2015**, 17, (36), 23312-23325.

82. Mitra, K.; Mishra, H. R.; Pei, X.; Pathak, R. K., Secondary Organic Aerosol (SOA) from Photo-Oxidation of Toluene: 1 Influence of Reactive Nitrogen, Acidity and Water Vapours on Optical Properties. *Atmosphere* **2022**, 13, (7), 1099.

83. Cho, C.; Kim, S.-W.; Choi, W.; Kim, M.-H., Significant light absorption of brown carbon during the 2020 California wildfires. *Sci. Total Environ.* **2022**, 813, 152453.

84. Kodros, J. K.; Papanastasiou, D. K.; Paglione, M.; Masiol, M.; Squizzato, S.; Florou, K.; Skyllakou, K.; Kaltsonoudis, C.; Nenes, A.; Pandis, S. N., Rapid dark aging of biomass burning as an overlooked source of oxidized organic aerosol. *PNAS* **2020**, 117, (52), 33028.

85. Schnitzler, E. G.; Gerrebos, N. G. A.; Carter, T. S.; Huang, Y.; Heald, C. L.; Bertram, A. K.; Abbatt, J. P. D., Rate of atmospheric brown carbon whitening governed by environmental conditions. *PNAS* **2022**, 119, (38), e2205610119.

86. Wong, J. P. S.; Nenes, A.; Weber, R. J., Changes in Light Absorptivity of Molecular Weight Separated Brown Carbon Due to Photolytic Aging. *Environ. Sci. Technol.* **2017**, 51, (15), 8414-8421.

87. Wong, J. P. S.; Tsagkaraki, M.; Tsiodra, I.; Mihalopoulos, N.; Violaki, K.; Kanakidou, M.; Sciare, J.; Nenes, A.; Weber, R. J., Atmospheric evolution of molecular-weight-separated brown carbon from biomass burning. *Atmos. Chem. Phys.* **2019**, 19, (11), 7319-7334.

88. Shetty, N.; Liu, P.; Liang, Y.; Sumlin, B.; Daube, C.; Herndon, S.; Goldstein, A. H.; Chakrabarty, R. K., Brown carbon absorptivity in fresh wildfire smoke: associations with volatility and chemical compound groups. *Environ. Sci. Atmos.* **2023**, 3, (9), 1262-1271.

Chapter 4. Contribution of carbonyl chromophores to secondary brown carbon from nighttime oxidation of unsaturated heterocyclic volatile organic compounds

4.0. Abstract

The light absorption properties of brown carbon (BrC), which are linked to molecular chromophores, may play a significant role in the Earth's energy budget. While nitroaromatic compounds have been identified as strong chromophores in wildfire-driven BrC, other types of chromophores remain to be investigated. As an electron-withdrawing group ubiquitous in the atmosphere, we characterized carbonyl chromophores in BrC samples from the nighttime oxidation of furan and pyrrole derivatives, which are important but understudied precursors of secondary organic aerosols primarily found in wildfire emissions. Various carbonyl chromophores were identified and quantified in BrC samples, and their ultraviolet−visible spectra were simulated using time-dependent density functional theory. Our findings suggest that chromophores with carbonyls bonded to nitrogen (i.e., imides and amides) derived from N-containing heterocyclic precursors substantially contribute to BrC light absorption. The quantified N-containing carbonyl chromophores contributed to over 40% of the total light absorption at wavelengths below 350 nm and above 430 nm in pyrrole BrC. The contributions of chromophores to total light absorption differed significantly by wavelength, highlighting their divergent importance in different wavelength ranges. Overall, our findings highlight the significance of carbonyl chromophores in secondary BrC and underscore the need for further investigation.

4.1. Introduction

Atmospheric brown carbon (BrC) is an important contributor to global warming, with a +0.10-0.55 W m^{-2} direct radiative effect (1−3) (~20−24% contribution) on the top-of-atmosphere direct radiative forcing. (4, 5) The contribution of BrC absorption is enhanced at higher altitudes (6) and varies by both daily and seasonal cycles, (7) especially due to changes in air pollution and cloud coverage. (7, 8) Conversely, the light absorption of BrC may also indirectly reduce the global coverage of clouds and decrease their cooling effects. (9) The spatial and temporal variations of BrC light absorption, and consequently their impacts, are strongly related to the changes in chemical composition. (8, 10) However, parameterization pertinent to BrC constituents remains underdeveloped in climate models, (11) hindering accurate evaluations of BrC optical properties and climate change prediction. (12, 13)

Accurate representations of BrC's effects on climate change require a comprehensive process-level understanding of the formation and evolution of molecular chromophores, which play a key role in regulating the light absorption properties of BrC. Nitroaromatic chromophores, also known as nitrated aromatic compounds, have been recognized as significant contributors to BrC light absorption. For example, Li et al. and Frka et al. reported that nitroaromatic chromophores may contribute to ~17−31% light absorption of BrC at 365−370 nm, (14, 15) while Bluvshtein et al. and Lin et al. indicated an even higher ratio (i.e., 50−80%) at wavelengths above 350 nm in biomass burning events. (16, 17) Although nitroaromatic chromophores may not account for a large fraction of aerosol mass, their contribution to BrC light absorption at 365 nm can be

~2−10 times that of their mass contribution in BrC samples. (14, 15, 18, 19) Among a variety of nitroaromatic chromophores, nitrophenols and nitrocatechols have been identified as two major groups of nitroaromatic chromophores in ambient aerosols, (19, 20) and they have been widely investigated to characterize the BrC formation and evolution due to photooxidation or photolysis. (21−26)

While nitroaromatic chromophores have been identified as potential tracers of BrC in atmospheric processing due to their significant role in the light absorption of BrC at 365 nm, (27) the contributors to the BrC absorption spectra in the near ultraviolet (UV) range below 365 nm have not been fully deconvoluted. In contrast to the >50% contribution of light absorption above 350 nm, nitroaromatic chromophores only accounted for ~20% of light absorption at 300 nm in biomass burning events, according to studies reported by Bluvshtein et al. and Lin et al. (16, 17) The wavelength-dependent contributions to BrC light absorption suggest the critical role of other types of chromophores in UV absorption. Since the light absorption of BrC chromophores is induced by electronic transitions, similar to nitroaromatics, which have strongly electron-withdrawing nitro groups attached to the aromatic rings, unsaturated organic compounds or conjugated systems coupled with other types of electron-withdrawing groups such as carbonyls could also be chromophore candidates. (13, 28) For instance, the simplest unsaturated carbonyl compound (i.e., acrolein) can absorb sunlight above 290 nm. (29, 30) From field studies, it has been reported that carbonyls may contribute to a large mass fraction of biomass burning aerosols (31, 32) and significant light absorption in the BrC. (10, 33, 34) The molecular absorptivity of numerous carbonyl compounds observed in

ambient aerosols is comparable to the absorptivity of nitroaromatic chromophores at 290−350 nm. (35) Therefore, it is essential to characterize carbonyl chromophores and constrain their roles in BrC light absorption.

In this study, we characterized carbonyl chromophores in secondary organic aerosols (SOAs) from the nighttime oxidation of a series of unsaturated heterocyclic volatile organic compounds (VOCs), including pyrrole, 1-methylpyrrole (1-MP), 2-methylpyrrole (2-MP), furan, and furfural, that have been widely observed in biomass burning events, (36−40) and may account for ~30% of the initial nitrate radical (NO_3) reactivity in wildfire-driven nighttime chemistry. (40) Recently, these VOCs were reported as potentially important precursors for secondary BrC formation during nighttime oxidation, (41−44) in which several carbonyl chromophores were observed. (43) Multi-instrumental characterization along with theoretical calculations of ultraviolet−visible (UV−vis) spectra were employed here to elucidate the structures of carbonyl chromophores and their spectral light absorptivity. This study focuses on the light absorption contribution of carbonyl chromophores in pyrrole SOA and 2-MP SOA; because nitroaromatic chromophores have been identified as critical contributors to BrC light absorption in these systems, they can serve as a benchmark for comparisons. (42)

4.2. Methods

4.2.1. Experimental setup

Experiments were performed in a 10 m^3 Teflon FEP chamber at room temperature (20−25 °C) and low relative humidity (RH< 20%) in the dark. Details of the experimental

114

setup and SOA properties, including number and size distribution, aerosol effective density, and mass fraction of organics, were introduced in our previous studies. (42, 43) In brief, 450 ppb NO_2 and 1500 ppb O_3 (initial $[NO_2]/[O_3] = 0.3$) were first injected into the chamber and allowed to react for one hour, producing nitrate radicals (NO_3). (42) To investigate the effects of NO_3 radical levels on the light absorption contributions of BrC chromophores, additional experiments were carried out with 150 ppb NO_2 and 1500 ppb O_3 (initial $[NO_2]/[O_3] = 0.1$). (42) The concentrations of NO_2 and O_3 were monitored by a NO_x analyzer (Teledyne Instruments) and an O_3 analyzer (Advanced Pollution Instrumentation, Inc.), respectively. Our previous studies indicated that the nighttime oxidation of pyrroles and furans under both conditions was predominantly initiated by NO_3 radicals. (42, 44) After the one-hour reaction between O_3 and NO_2 to produce NO_3 radicals, one of the studied heterocyclic VOCs (~200 ppb) was injected into the chamber. After the mass concentration reached a plateau, the generated SOA particles were collected on polytetrafluoroethylene (PTFE) membrane filters (46.2 mm, 2.0 μm, Tisch Scientific), followed by offline analysis. Although chamber experiments have some limitations in mimicking the real atmosphere, (45) the controlled chamber conditions can systematically facilitate the characterization of carbonyl chromophores and the evaluation of their roles in secondary BrC.

4.2.2. Compositional Analysis

The compositional analysis was conducted using a suite of complementary analytical instruments. A liquid chromatography coupled with a diode array detector, an electrospray ionization source (negative ion mode), and a quadruple-time-of-flight

tandem mass spectrometer (LC-DAD-ESI(−)-Q-TOFMS, Agilent Technologies 1260 Infinity II, and 6545 Q-TOF LC/MS) was used to identify light-absorbing carbonyl products and to characterize their molecular structures. The gradient elution for the changing LC mobile phase composition over time is shown in **Figure S4.1**. A gas chromatography-electron ionization mass spectrometry (GC/EI-MS, Agilent Technologies 6890N GC System, and 5975 inert XL Mass Selective Detector) was also used to complementarily identify carbonyl products. An iodide-adduct time-of-flight chemical ion mass spectrometry coupled with the Filter Inlet for Gases and AEROsols system (FIGAERO-ToF-CIMS, Aerodyne Research Inc.) (46) and an ion mobility spectrometry time-of-flight mass spectrometer (IMS-TOF, Tofwerk Inc.) were used to characterize SOA composition in real time and offline, respectively. Detailed instrumental setups and operational parameters have been described in previous studies. (42, 43, 47−49)

N-containing carbonyl chromophores were identified by LC-DAD-ESI-Q-TOFMS and GC/EI-MS, and their mass contributions were estimated semi-quantitatively using maleimide ($C_4H_3NO_2$) as a surrogate standard. The mass ratio of the identified N-containing carbonyl chromophores ($MR_{carbonyl}$) (eq (4.1)), and the mass ratio of maleimide ($MR_{maleimide}$) in SOA samples from pyrrole and its derivatives had been previously determined by GC/EI-MS using a similar approach. (43)

$$MR_{carbonyl} = MR_{maleimide} \frac{c_{carbonyl}M_{carbonyl}}{c_{maleimide}M_{maleimide}}$$

$$= MR_{maleimide}R_F \frac{A_{carbonyl}M_{carbonyl}}{A_{maleimide}M_{maleimide}} \qquad (4.1)$$

Here, $c_{carbonyl}$ and $c_{maleimide}$ are the molar concentrations of the identified carbonyl chromophores and maleimide in the extracted SOA samples (mol L^{-1}); $M_{carbonyl}$ and $M_{maleimide}$ are the molar masses of the identified carbonyl chromophores and maleimide in the extracted SOA samples (g mol^{-1}); $A_{carbonyl}$ and $A_{maleimide}$ are the peak areas of parent ions of the identified carbonyl chromophores and maleimide in their extracted ion chromatograms (EICs) measured by LC-DAD-ESI-Q-TOFMS. Although response factors (R_F) of the identified N-containing carbonyl chromophores may differ slightly from the surrogate standard (**Figure S4.2**), semi-quantification can provide approximate mass ratios and still support comparisons of the representation of various N-containing carbonyl chromophores in SOA samples.

4.2.3. Light Absorption Measurements

The absorbance of SOA samples (290−700 nm) was measured by a UV−vis spectrophotometer (Beckman DU-640). SOA samples were extracted with acetonitrile (ACN), which has been shown to be a suitable solvent for the analysis of secondary BrC due to its chemical stability (aprotic) and solubility for polar compounds. (43) The contribution of molecular chromophores to the total light absorption of SOA samples (*AbsC*), which can vary greatly with wavelength (λ), is estimated by eq (4.2).

$$AbsC \ (\lambda) = \frac{Abs_{chro}(\lambda)}{Abs_{BrC}(\lambda)} \qquad (4.2)$$

$Abs_{BrC}(\lambda)$ is the total light absorbance of the BrC samples, directly measured by the UV−vis spectrophotometer, while $Abs_{chro}(\lambda)$ is the light absorbance of the investigated BrC chromophores, calculated by the Beer-Lambert law (eq (4.3)).

$$Abs_{chro}(\lambda) = \ \varepsilon_{chro}(\lambda) \times \frac{m_{chro}}{M_{chro}} \times b \qquad (4.3)$$

$\varepsilon_{chro}(\lambda)$ is the molecular absorptivity of the investigated BrC chromophores (L mol^{-1} cm^{-1}), which has been reported in our previous work; (43) m_{chro} is the mass concentration of molecular chromophores in the SOA solution samples (ng μL^{-1}); M_{chro} is the molar mass of the molecular chromophores (g mol^{-1}); and b is the instrumental light path (i.e., 1 cm).

4.2.4. Computational of Theoretical UV−Vis Spectra

The time-dependent density functional theory (TD-DFT) was used to simulate the wavelength-dependent light absorptivity of the identified carbonyl products, for which no authentic standards were available. The Gaussian 16 program (revision C. 01) (50) was used for all computations, with the B3LYP functional (51, 52) and the 6-311++G(d,p) basis set (53) as suggested in previous studies. (54, 55) The ACN environment was simulated by the integral equation formalism extension of the polarizable continuum model (IEFPCM). (56) The GaussView 6 program was used to generate the theoretical UV−vis spectra. All the Cartesian coordinates for geometrical structures were summarized in **Table S4.1**.

4.3. Results and Discussions

4.3.1. Distribution of Chromophores in the LC-DAD Heatmaps

The LC-DAD heatmaps provide a snapshot of BrC chromophore distributions for all the SOA samples (**Figure 4.1, S4.3−S4.5**), where the hotspots illustrate the retention time (RT) and wavelengths of light absorption. **Figure 4.1** shows the LC-DAD heatmap of pyrrole SOA, which is divided into two panels, corresponding to the RT ranges of 0−2 min and 2−21 min, respectively (**Figure 4.1A, B**). The light absorption of chromophores was normalized to the highest value of the whole LC-DAD heatmap, with each panel having its own color scale for a clear representation of chromophore distribution. With LC mobile phase changing (**Figure S4.1**), the separated hotspots in two unique RT zones represent distinct chromophores with different polarities.

Compositional analysis revealed that the major hotspots detected at RT of 1.6−1.7 min may be attributed to mono-nitrogen chromophores (**Figure 4.1C**), while those detected at RT of 8.7−12.3 min may be ascribed to the di-nitrogen and tri-nitrogen chromophores (**Figure 4.1D**). Notably, the analytes at RT of 1.6−1.7 min were comprised of many mono-nitrogen compounds, while only two products were shown at RT of 8.7−12.3 min. The mono-nitrogen chromophores (**Figure 4.1A**) in pyrrole SOA collectively acquired much stronger light absorption compared to di-nitrogen and tri-nitrogen chromophores (**Figure 4.1B**), which indicated the potential importance of the mono-nitrogen chromophores in BrC light absorption. The strong light absorption corresponding to mono-nitrogen chromophores is also observed in 1-MP SOA (**Figure S4.3**) and 2-MP SOA (**Figure S4.4**), wherein the mono-nitrogen chromophores led to

much higher or similar absorption intensities compared to those of the di-nitrogen and tri-nitrogen chromophores. In a recent study, we found di-nitrogen and tri-nitrogen chromophores in pyrrole SOA and 2-MP SOA as nitro- and dinitro-substituted chromophores. (42) As a result, the mono-nitrogen chromophores would lack nitro groups, and their nitrogen may be inherited from the pyrrole backbones, as evidenced by the structural characterization in the following section. However, in contrast to electron-withdrawing groups such as nitro groups, the nitrogen atom on the pyrrole backbone cannot attract electron density toward itself and thus is unlikely to cause a red shift of UV−vis spectral peaks above 290 nm. The light absorption of the mono-nitrogen chromophores is most likely influenced by other types of electron-withdrawing groups. Furthermore, our previous study of furan SOA revealed that nitrogen-free products were the predominant contributors to the major LC-DAD hotspots, (44) whereas the major hotspots in furfural SOA can be attributed to both nitrogen-containing and nitrogen-free products (**Figure S4.5**). Despite this, all the LC-DAD heatmaps indicate the importance of different types of electron-withdrawing groups in BrC light absorption. Analysis of functional groups with attenuated total reflectance Fourier-transform infrared (ATR-FTIR) spectroscopy conducted in our previous study suggested that chromophores with carbonyl groups may account for a significant portion of the light absorption of SOA samples from nighttime oxidation of heterocyclic VOCs. (43)

Even though nitroaromatic chromophores have been identified as important contributors to BrC light absorption in pyrrole SOA and 2-MP SOA, (41, 42) our findings here suggest that mono-nitrogen chromophores could account for the majority of the light

absorption. This is because nitroaromatic chromophores and mono-nitrogen chromophores have absorption peaks at different wavelength ranges and, as a result, have wavelength-dependent light absorption contributions, which will be discussed further in the following sections.
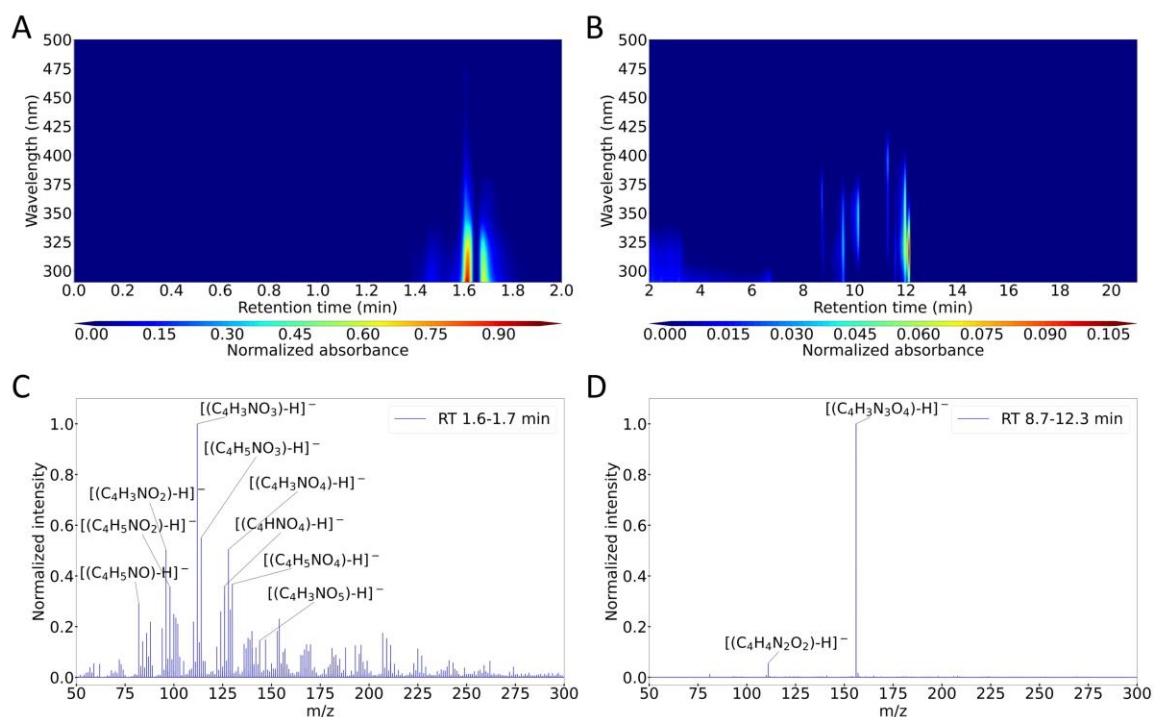
Figure 4.1. LC-DAD heatmaps of pyrrole SOA: (A) 0−2 min, and (B) 2−21 min, followed by the mass spectra corresponding to the major hotspots, respectively (C−D).

4.3.2. Molecular Characterization of Carbonyl Chromophores

In the current study, the molecular composition of carbonyl chromophores was determined by complementary analytical instrumentation, and their UV−vis spectra were simulated using quantum chemical approaches (**Figure 4.2, 4.3**). Following the identification of the molecular formula in **Figure 4.1C**, we performed tandem MS

experiments to elucidate their structures. Here, $C_4H_4NO_4^-$, a deprotonated ion of $C_4H_5NO_4$, is selected as an example. The LC-ESI-Q-ToFMS measurements showed a single peak in the EIC of this ion as well as its fragmentation pattern (**Figure 4.2A**), which can help derive the tentative molecular structures and thus support the theoretical computation of UV−vis spectra. The IMS-TOF measurements also confirmed the presence of $C_4H_4NO_4^-$ in ESI(−) and indicated two major isomers for this ion (**Figure 4.2B**). To rule out the potential interference from solvent and LC electrospray ionization efficiency, (43, 44) the presence of $C_4H_5NO_4$ was supplementally verified by *in situ* characterization with FIGAERO-ToF-CIMS (**Figure 4.2C**). Plausible fragmentation pathways were derived based on the tandem MS data (**Figure S4.6A**), wherein $C_4H_5NO_4$ can be identified as formyl carbonyl amino acetic acid and its imidic acid isomer. Both compounds are chain-structural carbonyl chromophores, as confirmed by the theoretical computation of their UV−vis spectra (**Figure 4.2D**). Using the same approaches, the ring-retained carbonyl chromophores in pyrrole SOA were also identified, including 2-hydroxy-2-pyrroline-4,5-dione ($C_4H_3NO_3$), 5-hydroxy-2,3,4-pyrrolidinetrione ($C_4H_3NO_4$) and 5-hydroxy-2,3-pyrrolidinedione ($C_4H_5NO_3$) (**Figure S4.7−S4.10**). Similar to pyrrole, nighttime oxidation of furan can generate light-absorbing diones. As one of the major products in furan SOA, $C_4H_2O_4$ was identified as 4-hydroxyfuran-2,3-dione and 5-hydroxyfuran-2,3-dione (**Figure 4.2E−G, S4.6B**). (44) These products exhibit distinct UV−vis spectra with different line centers and peak absorptivity (**Figure 4.2H**).
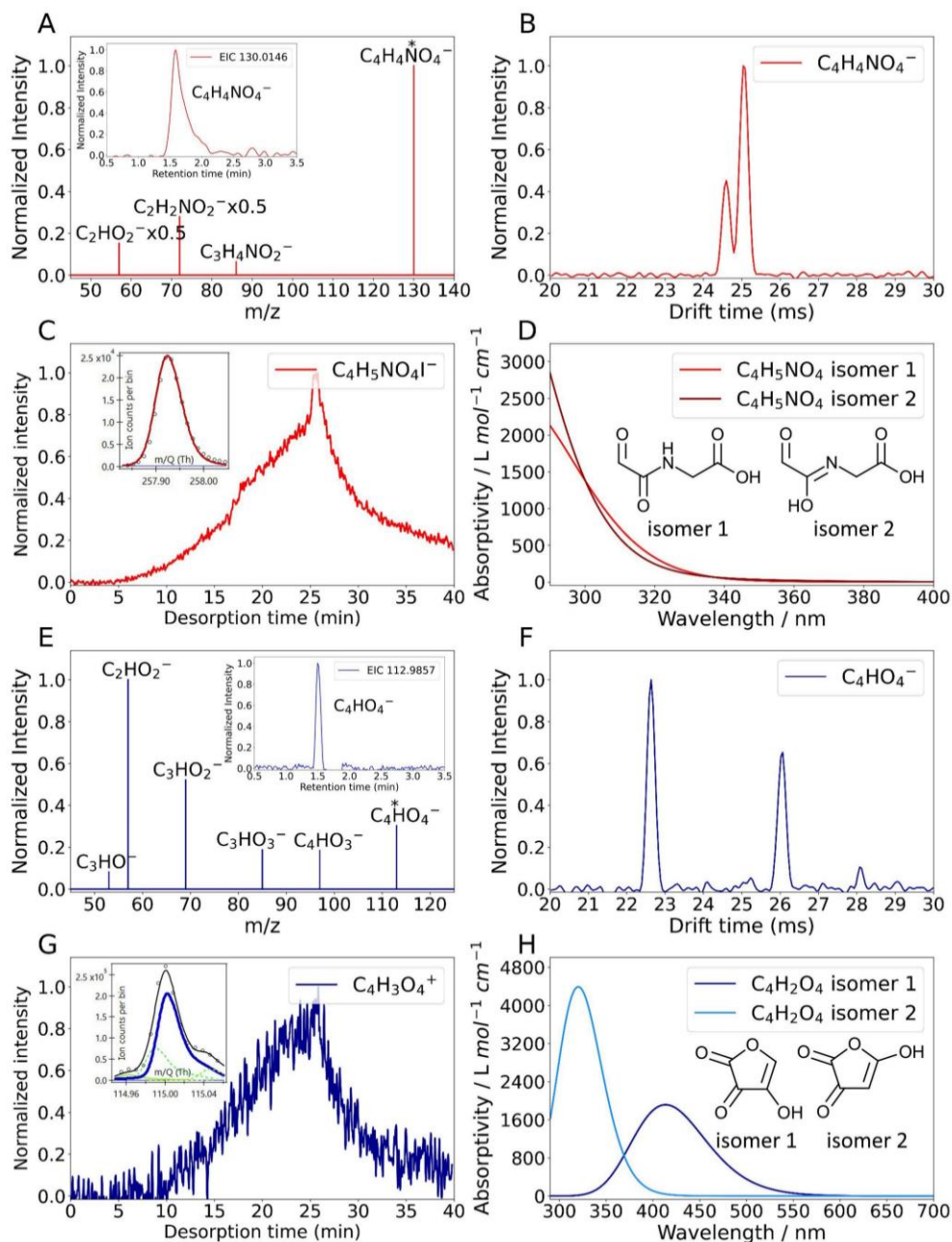
Figure 4.2. Characterization of carbonyl chromophores in pyrrole SOA and furan SOA: (A) EICs and tandem mass spectra of $C_4H_5NO_4$; (B) IMS-TOF drift grams of $C_4H_5NO_4$; (C) FIGAERO-ToF-CIMS peak fitting and thermograms of $C_4H_5NO_4$; (D) theoretical UV−vis spectra of isomers of $C_4H_5NO_4$; (E) EICs and tandem mass spectra of $C_4H_2O_4$; (F) IMS-TOF drift grams of $C_4H_2O_4$; (G) FIGAERO-ToF-CIMS peak fitting and thermograms of $C_4H_2O_4$; (H) theoretical UV−vis spectra of $C_4H_2O_4$ isomers.
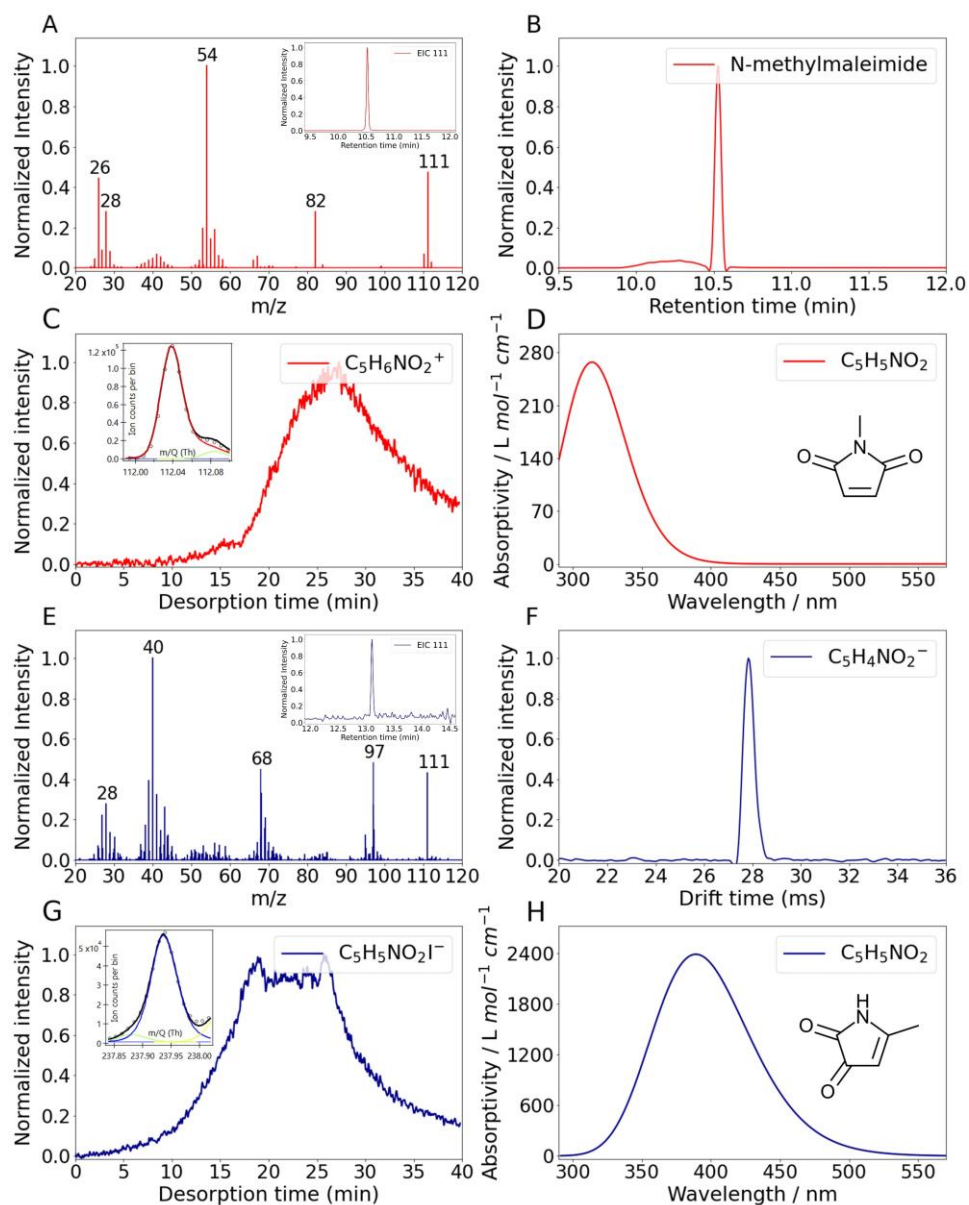
Figure 4.3. Characterization of carbonyl chromophores in 1-MP SOA and 2-MP SOA: (A) GC/EI-MS characterization of $C_5H_5NO_2$ in 1-MP SOA; (B) EIC of *m/z* 111 from the N-methylmaleimide chemical standard; (C) FIGAERO-ToF-CIMS peak fitting and thermograms of $C_5H_5NO_2$ in 1-MP SOA; (D) theoretical UV−vis spectrum of $C_5H_5NO_2$ in 1-MP SOA; (E) GC/EI-MS characterization of $C_5H_5NO_2$ in 2-MP SOA; (F) IMS-TOF drift gram of $C_5H_5NO_2$ in 2-MP SOA; (G) FIGAERO-ToF-CIMS peak fitting and thermograms of $C_5H_5NO_2$ in 2-MP SOA; (H) theoretical UV−vis spectrum of $C_5H_5NO_2$ in 2-MP SOA.

Given that both LC-ESI-Q-ToFMS and IMS-TOF could only detect deprotonated ions (because of the nature and limitations of ESI) and may not characterize all carbonyls generated, GC/EI-MS was used to investigate more diverse carbonyl chromophores. Previous GC/EI-MS analysis of secondary BrC samples revealed a number of light-absorbing heterocyclic diones, including maleimide (from pyrrole and its derivatives), maleic anhydride, and phthalic anhydride (from furan and furfural). (43) In the current study, N-methylmaleimide was discovered by GC/EI-MS (RT =10.5 min) in 1-MP SOA samples (**Figure 4.3A**). The presence of this compound was confirmed by its authentic chemical standard (**Figure 4.3B**) and also supported by the tentative fragmentation pathways (**Figure S4.11A**) as well as the *in situ* FIGAERO-ToF-CIMS measurement (**Figure 4.3C**). Also, the presence of 2-methyl-2-pyrroline-4,5-dione, an isomer of N-methylmaleimide, in 2-MP SOA was confirmed by multi-instrumental measurements (**Figure 4.3E−G**) and the tentative fragmentation pathways (**Figure S4.11B**). The calculated UV−vis spectra showed that both diones can contribute to light absorption above 290 nm (**Figure 4.3D, H**).

Notably, N-containing carbonyl chromophores such as imides and amides, whose nitrogen is retained from the N-containing heterocyclic VOC precursors (e.g., pyrrole and its derivatives in our study), may be important contributors to the light absorption of secondary BrC. The lone pair electrons from the nitrogen atom in imides and amides can conjugate with the unsaturated bonds (e.g., carbonyl groups), which facilitate the n−π* excitation of delocalized electrons and hence support the formation of BrC chromophores. However, different N-containing carbonyl chromophores may lead to

different contributions to BrC light absorption, depending on their mass ratio in SOA samples, spectral wavelengths, and absorptivity. For example, $C_4H_5NO_4$ and $C_4H_3NO_3$ have similar mass ratios in pyrrole SOA (3.37±0.11% and 2.86±0.57%, respectively) based on the semi-quantification, but the UV−vis spectrum of $C_4H_5NO_4$ only covers 290−350 nm (**Figure 4.2D**), while the UV−vis spectrum of $C_4H_3NO_3$ can extend to 500 nm (**Figure S4.7J**). Although the UV−vis spectra of $C_4H_3NO_3$ and $C_4H_3NO_4$ cover a similar range of wavelengths, the latter possesses a higher mass ratio (8.86±1.11%) and a larger absorptivity (**Figure S4.7K**). Nevertheless, the total light absorption of a collection of N-containing carbonyl chromophores may contribute to BrC light absorption within a wide range of wavelengths.

4.3.3. Light Absorption Contribution of Carbonyl and Nitroaromatic Chromophores

The light absorption contributions of identified carbonyl and nitroaromatic chromophores can be estimated by integrating their LC-DAD absorbance within the corresponding RT ranges, which are similar to those described in the literature. (16, 17) Although the estimated light absorption contributions may not be rigorously accurate due to instrumental limitations such as incomplete detection of weak chromophores, (17) this approach has successfully revealed the indispensable role of nitroaromatic chromophores in BrC aerosols from biomass burning events. (16, 17) Similarly, the relative importance of carbonyl chromophores and nitroaromatic chromophores at different wavelengths can thus be evaluated by this approach. Here, C_4 carbonyls and C_4 nitroaromatics in pyrrole SOA, which may predominantly contribute to the major hotspots in the LC-DAD heatmaps (**Figure 4.1**), were categorized as two groups of chromophores, while other

126

chromophores, which may comprise oxidation products with higher molecular weights and high double bond equivalence (DBE) (**Figure S4.5A, B**), were classified as "others." It is noted that the C_4 carbonyls and C_4 nitroaromatics are produced from the C_4 backbone of pyrrole; in other VOC systems, the carbon number of the lower-molecular-weight chromophores can be different and dependent on the VOC precursors. The light absorption contribution of each group of chromophores was visualized along with the wavelengths in both percentages (**Figure S4.12**) and mass absorption coefficient (MAC) profiles (**Figure 4.4**). The latter was estimated by combining **Figure S4.13** and the MAC profiles reported in our prior study. (42)
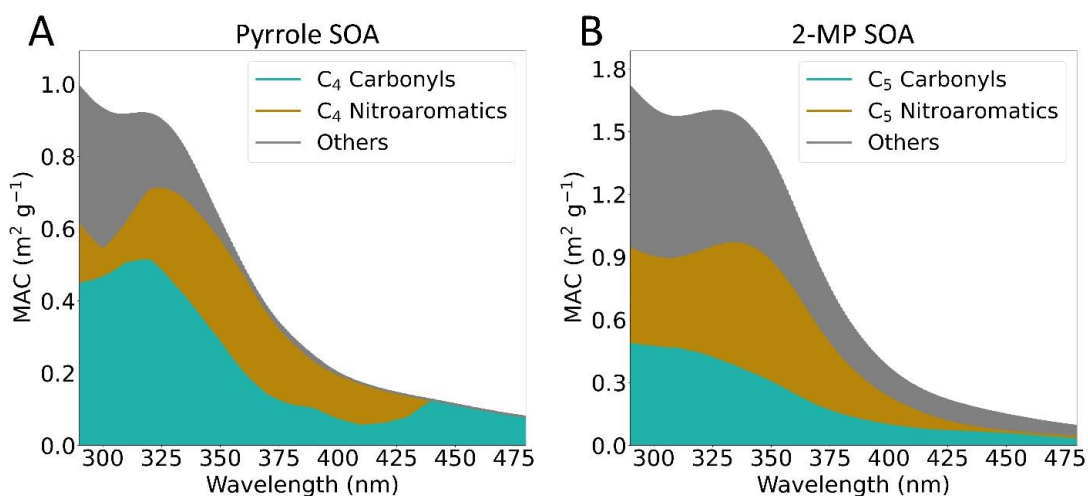
Figure 4.4. Light absorption contribution of chromophores to MAC profiles: (A) C_4 carbonyls, C_4 nitroaromatics and other chromophores in pyrrole SOA; (B) C_5 carbonyls, C_5 nitroaromatics and other chromophores in 2-MP SOA.

Our results showed that, while C_4 nitroaromatics account for the majority of light absorption in the 350−430 nm range, C_4 carbonyls contribute significantly more below 350 nm and above 430 nm, accounting for over 40% of the total light absorption in both

wavelength ranges (**Figure 4.4A, S4.13A**). The C_5 nitroaromatics and C_5 carbonyls in 2-MP SOA revealed comparable tendencies in the wavelength dependence of light absorption contribution (**Figure 4.4B, S4.13B**). However, in the visible range, the contribution of C_4 carbonyls to light absorption was greater than the other two categories in pyrrole SOA (**Figure 4.4A, S4.13A**), whereas the contributions of the three categories in 2-MP SOA were comparable (**Figure 4.4B, S4.13B**). The quantitative differences between **Figure 4.4A** and **Figure 4.4B** (also between **Figure S4.13A** and **Figure S4.13B**) reveal the vital role of VOC structures in regulating the relative contributions of carbonyl chromophores and nitroaromatic chromophores to secondary BrC light absorption, which could be due to the interference of diverse oxidation pathways. (42) In particular, the heteroatoms in heterocyclic VOCs may greatly alter the oxidation pathways and hence the light absorption contribution of carbonyl and nitroaromatic chromophores. For example, nighttime oxidation of furan tends to generate carbonyls via the "addition-elimination mechanism" of NO_3 radicals, (57) which differs from the formation mechanisms of nitroaromatics in nighttime oxidation of pyrrole and 2-MP. (42)

The relative impact of carbonyl chromophores on BrC light absorption is further evaluated by the ratio of their absorption cross-section emission factors (EF_{absC}), which accounts not only for the MACs but also the carbon emission factors of VOC precursors from burning sources and the SOA yields. (41) Details of the EF_{absC} calculations for pyrrole SOA and 2-MP SOA were described previously. (42) Taking biomass burning of ponderosa pine forests, which is relevant to wildfires in the western US and Canada, (58) as an example, C_{4-5} carbonyl chromophores may contribute more to BrC light absorption

128

below 350 nm and above 430 nm than C_{4-5} nitroaromatic chromophores (**Table S4.2**). Our previous research and the current findings suggest that the light absorption of 1-MP SOA, furan SOA, and furfural SOA can be primarily attributed to C_{4-5} carbonyls and the "others" category (**Figure S4.14, S4.15**). (42, 44) Nonaromatic nitro-substituted carbonyl chromophores, such as $C_4H_3NO_7$ in furan SOA, (44) may contribute to BrC light absorption. In addition, the carbonyl chromophores contribute the most to light absorption in furfural SOA, which is likely related to the carbonyl functional group in furfural. Collectively, these findings demonstrate the significance of carbonyl chromophores in the light absorption of secondary BrC.
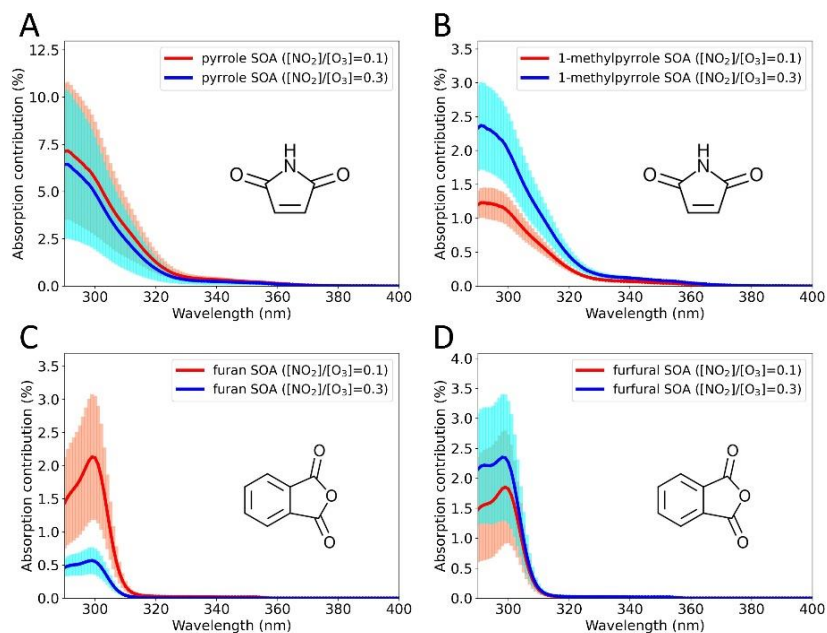
Figure 4.5. Light absorption contributions of maleimide to (A) pyrrole SOA and (B) 1-MP SOA, and phthalic anhydride to (C) furan SOA and (D) furfural SOA under low and high NO₃ levels. The absorption contribution is estimated by the ratio of light absorption of molecular chromophores calculated by the Beer-Lambert law and the total light absorption of BrC samples.

Furthermore, depending on the SOA systems, the light absorption contribution of molecular carbonyl chromophores in secondary BrC may vary under different environmental conditions. The NO_3 radical level has been reported as a critical environmental factor that affects the secondary BrC formation of pyrroles and furans. (42−44) As marker compounds of secondary BrC from the nighttime oxidation of several unsaturated heterocyclic VOC precursors, maleimide and phthalic anhydride were selected to investigate the influence of NO_3 radical levels on their light absorption contribution, and their molecular light absorptivity and mass ratio in various SOA samples have been experimentally measured in prior studies. (43) Our results indicated that the light absorption contribution of maleimide in pyrrole SOA remained essentially constant as the NO_3 radical level increased (**Figure 4.5A**), whereas it increased significantly in 1-MP SOA as the nitrate radical level increased (**Figure 4.5B**). The light absorption contribution of phthalic anhydride exhibited a divergent trend in furan SOA and in furfural SOA as the NO_3 radical level increased; specifically, it reduced in furan SOA and enhanced in furfural SOA (**Figure 4.5C, D**). The dependence of light absorption contribution on the level of NO_3 radicals may be attributed to the alteration of chemical kinetics and, consequently, the branching ratios of carbonyl chromophores production as the NO_3 concentrations change. The effects of VOC types on the contribution of molecular carbonyl chromophores to light absorption should also be noted. Maleimide, for instance, may account for ~7% of light absorption at 290 nm in pyrrole SOA (**Figure 4.5A**), but a much lower value in 1-MP SOA (**Figure 4.5B**). The observed discrepancy could be attributed to the methyl group on 1-MP, which could

hinder the formation of maleimide and alternatively generate other chromophores (e.g., N-methylmaleimide in **Figure 4.3D**). Thus, the role of carbonyl chromophores in secondary BrC is significantly influenced by complex atmospheric conditions and VOC emissions.

Overall, our results indicate the prevalence of carbonyl chromophores in SOA from the nighttime oxidation of heterocyclic VOCs. The UV−vis spectra of the identified carbonyl chromophores cover a wider range of wavelengths (i.e., ~290−500 nm) compared to the nitroaromatic chromophores (i.e., ~290−400 nm) identified in our previous studies, (42, 55) suggesting their distinct contributions to BrC light absorption at different wavelengths. Comparison between isomers also highlights that the spectral light absorptivity of carbonyl chromophores in secondary BrC can be governed by the structure of VOC precursors, which is consistent with our previous research on nitroaromatic chromophores. (42) The structural dependence of UV−vis spectra indicates the importance of structure-related information in the process-level prediction of secondary BrC formation. Moreover, the characterized carbonyl chromophores and their structural analogues, including heterocyclic diones and triones, have been widely observed in SOA systems from other VOCs, for example, those generated by photooxidation of a variety of aromatic hydrocarbons. (59−63) Heterocyclic diones have also been widely observed in field measurements of ambient aerosols from biomass burning plumes. (38, 64, 65) Although triones in ambient aerosols were less reported, (66) they have been suggested as possible contributors to BrC generated from aqueous-phase reactions. (67, 68) The collective evidence demonstrates that carbonyl

131

chromophores are ubiquitous constituents in SOA and may play an active role in secondary BrC formation.

4.4. Atmospheric implications

Molecular chromophores are the key to BrC light absorption, connecting the microscopic physicochemical processes in atmospheric aerosols with the macroscopic radiative budget in the Earth system. The newly identified chromophores enable a more detailed process-level depiction of BrC formation, which is essential for improving the assessment of BrC's impact in the context of climate change. Our study shows that carbonyl chromophores can be important constituents of secondary BrC from nighttime oxidation of heterocyclic VOCs, with wavelengths ranging from UV to visible. While research on ambient aerosols in wildfires has suggested that nitroaromatic chromophores, such as nitrophenols, nitrocatechols, nitroguaiacols, and nitrosyringols, may predominately contribute to BrC light absorption in the visible range, (16, 17) field studies have also provided increasing evidence indicating that carbonyl chromophores could be distinct contributors to BrC light absorption in the UV range. (69) It is further noted that the carbonyl chromophores identified in our studies are not only found in other SOA systems but are also commonly observed in field studies. (38, 59−65) Indeed, carbonyl compounds are ubiquitous in atmospheric aerosols and have long been recognized as the key species in tropospheric chemistry, (70, 71) the active players in the hygroscopicity of atmospheric particles, i.e., cloud condensation nuclei (CCN) activity, (72) and the critical precursors of secondary BrC formation in the aerosol phase via NH_3/amine-driven reactions (73−76) or forming charge transfer complexes with alcohols.

(77, 78) Our study can complementarily provide a new perspective for evaluating the role of carbonyls in atmospheric aerosols based on their intrinsic light absorption.

Furthermore, carbonyl chromophores produced by nighttime oxidation of N-containing VOCs may represent a potentially important component in secondary BrC that was previously unrecognized. Our study reveals that light-absorbing imides and amides can be critical chromophores in the SOA of pyrrole and its derivatives. Given that biomass burning releases a variety of N-containing heterocyclic VOC precursors, (37−39) the formation of N-containing carbonyl chromophores could be a potentially significant contributor to the light absorption of secondary BrC. Furthermore, as widely observed in field studies of wildfire emissions, (33, 38, 79, 80) N-containing carbonyl chromophores offer another pivot in addition to the nitroaromatic chromophores for a more in-depth understanding of secondary BrC formation, particularly the wavelength-dependent change of BrC light absorption as well as the diverse physicochemical processes. Although nitroaromatic chromophores may likely possess stronger absorptivity compared to carbonyl chromophores, the former are largely related to anthropogenic emissions of NO_x, (81, 82) whereas the latter may be generated by more divergent atmospheric oxidation pathways, such as OH-driven oxidation of VOCs. (64) Broader sources of carbonyl chromophores may result in greater ubiquity in the atmosphere under different environmental conditions, implying more extensive effects. Overall, this study expands the current understanding of chromophore formation and provides a foundation for further investigations into the effects of secondary BrC formation on the Earth's energy budget in the context of climate change.

4.5. Supplemental Information

Table S4.1. Cartesian coordinates of molecular structures in the TD-DFT computation.

$C_4H_5NO_4$ isomer 1

N	0.37769600	-0.12037200	0.68470500
C	1.23707100	0.57167700	-0.08335400
C	2.61149600	-0.09192200	-0.24502600
H	3.31496300	0.50038100	-0.85437200
C	-0.96995000	0.32241800	0.95603400
H	-1.26590900	0.00067000	1.95592500
H	-1.00090000	1.41312300	0.94042800
C	-2.04598400	-0.16513400	-0.00838000
O	2.89249600	-1.15821800	0.24180300
O	1.01521200	1.64569100	-0.63181500
O	-3.20645000	0.15201900	0.10647000
O	-1.58296400	-0.97035600	-0.97302800
H	-2.32696000	-1.23328000	-1.53928700
H	0.69278800	-1.01361800	1.04128600

$C_4H_5NO_4$ isomer 2

N	0.35641700	-0.31358700	0.72965800
C	1.17729900	0.39631200	0.07841300
C	2.58004700	-0.11613300	-0.19164500
H	3.24519700	0.59569900	-0.71806200
C	-0.97117200	0.21097800	0.99604900
H	-1.31299500	-0.17357700	1.95843500
H	-1.00179600	1.30565900	1.04716400
C	-2.03697300	-0.18737300	-0.01626800
O	2.96419200	-1.20920800	0.13192400

O	0.88729200	1.62431600	-0.41257800
O	-3.22033800	-0.04988500	0.19294400
O	-1.54157100	-0.67804700	-1.16113800
H	-2.28422700	-0.88387200	-1.75206800
H	1.64709500	2.03109500	-0.85157900

$C_4H_2O_4$ isomer 1

C	-1.25766000	-0.08632000	-0.00004900
C	0.03152200	0.78743900	0.00006200
C	1.10963700	-0.18974300	0.00001800
C	0.54040800	-1.41120900	-0.00001100
O	-0.85888200	-1.39798300	0.00009800
O	-2.39784900	0.25429600	0.00019900
O	0.04021400	1.99554900	-0.00037700
O	2.40181300	0.19378500	0.00006100
H	0.97994400	-2.39648100	0.00001200
H	2.99423900	-0.56969900	0.00002600

$C_4H_2O_4$ isomer 2

C	0.80281600	-0.75963300	-0.00032200
C	0.88511100	0.79902800	-0.00035400
C	-0.47806400	1.22248600	0.00000200
C	-1.24224900	0.09227300	-0.00010100
O	-0.55745900	-1.08949400	-0.00011500
O	1.65172000	-1.58694600	0.00019000
O	1.94598500	1.39443300	0.00030000
O	-2.53285200	-0.10488200	0.00012500
H	-3.01737100	0.73537500	0.00033400
H	-0.84746300	2.23481400	0.00032800

C₄H₃NO₃

C	1.26509500	0.07750900	0.00023000
C	0.50609000	1.22077200	0.00029600
C	-0.86509700	0.81374200	-0.00021900
C	-0.83298600	-0.76560900	0.00033900
N	0.51222800	-1.08522300	-0.00006700
H	0.88438500	2.23017500	0.00043000
O	-1.76578900	-1.52790400	-0.00033600
O	2.57096100	-0.09600800	0.00014900
O	-1.91085100	1.44292500	-0.00029200
H	0.90152900	-2.01842900	-0.00037900
H	3.03531600	0.75423100	0.00037900

C₄H₃NO₄

C	0.82258900	0.79892200	-0.04010400
C	-0.70412200	0.84962000	0.16468700
C	-1.18831900	-0.59740900	0.37162200
O	-1.38984500	1.83170000	0.12907900
H	-1.63678600	-0.70901800	1.36166600
O	-2.09484800	-0.95215100	-0.64049900
H	-2.86938600	-1.37128900	-0.24891600
O	1.55938600	1.73002400	-0.20109100
O	2.32794600	-1.14061500	-0.10920000
C	1.20945900	-0.68552200	0.02346200
N	0.05582100	-1.35726000	0.27821000
H	0.05666300	-2.36420300	0.39546900

Table S4.2. Wavelength-dependent absorption cross-section emission factors (EF_{absC}) of C_{4-5} carbonyls and C_{4-5} nitroaromatics in pyrrole SOA and 2-MP SOA.

Wavelength (nm)	EF_{absC} (C_{4-5} Carbonyls)		EF_{absC} (C_{4-5} Nitroaromatics)		EF_{absC} Ratio
	Pyrrole SOA	2-MP SOA	Pyrrole SOA	2-MP SOA	
290	0.0268	0.0047	0.0099	0.0045	2.19
300	0.0279	0.0046	0.0045	0.0042	3.72
310	0.0302	0.0045	0.0066	0.0042	3.20
320	0.0307	0.0043	0.0116	0.0048	2.13
330	0.0266	0.0039	0.0152	0.0055	1.47
340	0.0220	0.0034	0.0165	0.0059	1.14
350	0.0170	0.0029	0.0167	0.0056	0.90
360	0.0119	0.0024	0.0160	0.0048	0.68
370	0.0083	0.0018	0.0133	0.0037	0.60
380	0.0066	0.0014	0.0104	0.0026	0.61
390	0.0060	0.0011	0.0076	0.0018	0.76
400	0.0043	0.0009	0.0071	0.0013	0.62
410	0.0032	0.0008	0.0069	0.0009	0.51
420	0.0035	0.0007	0.0056	0.0006	0.68
430	0.0045	0.0006	0.0038	0.0003	1.25
440	0.0072	0.0006	0.0003	0.0002	15.04
450	0.0068	0.0005	0.0000	0.0001	57.58
460	0.0061	0.0004	0.0000	0.0001	65.53
470	0.0053	0.0004	0.0000	0.0001	67.13
480	0.0047	0.0003	0.0000	0.0001	64.43

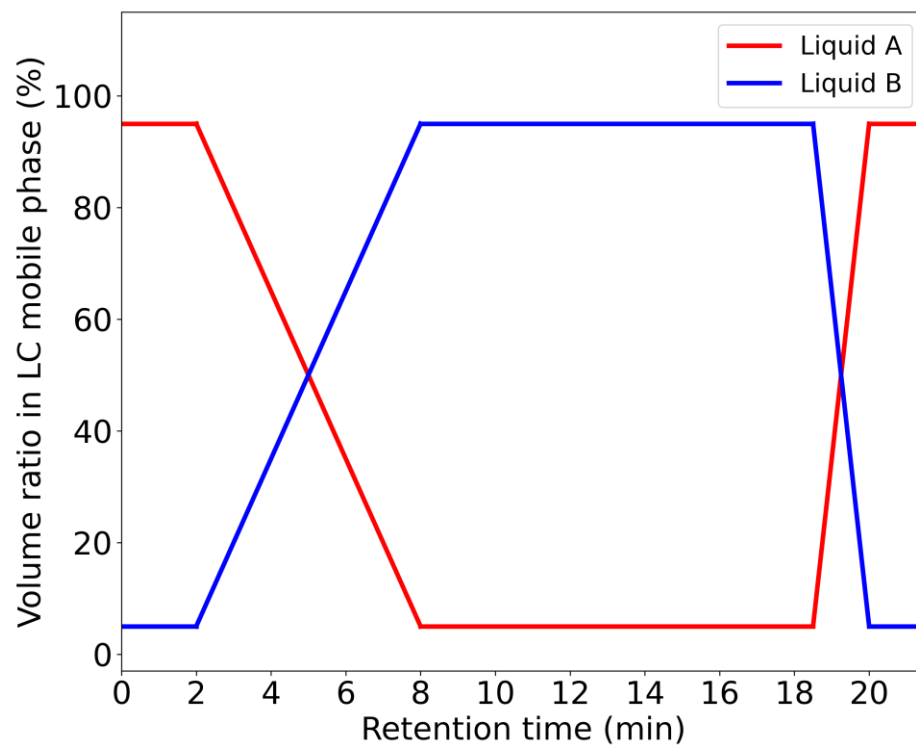**Figure S4.1.** Volume ratio of liquid A (water + 0.1% formic acid) and liquid B (acetonitrile + 0.1% formic acid) in the LC mobile phase along with the retention time for gradient elution.
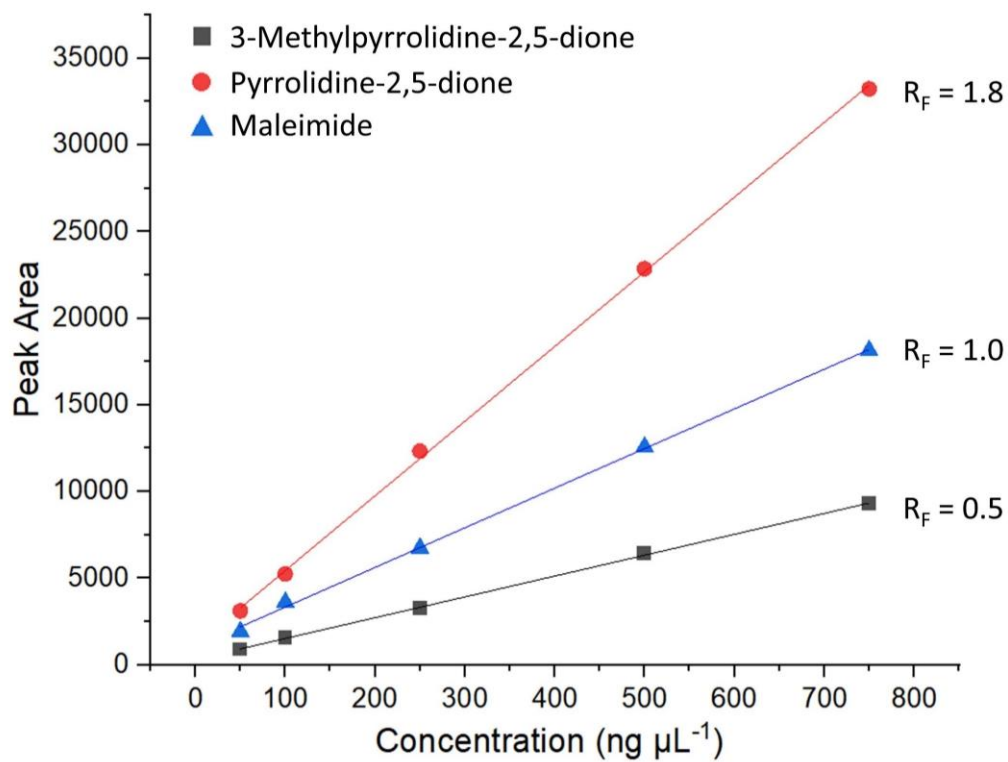
Figure S4.2. Response factors (R_F) of three N-containing carbonyls (maleimide, pyrrolidine-2,5-dione and 3-methypyrrolidine-2,5-dione) estimated by LC-DAD-ESI-Q-TOFMS with their commercially available standards.
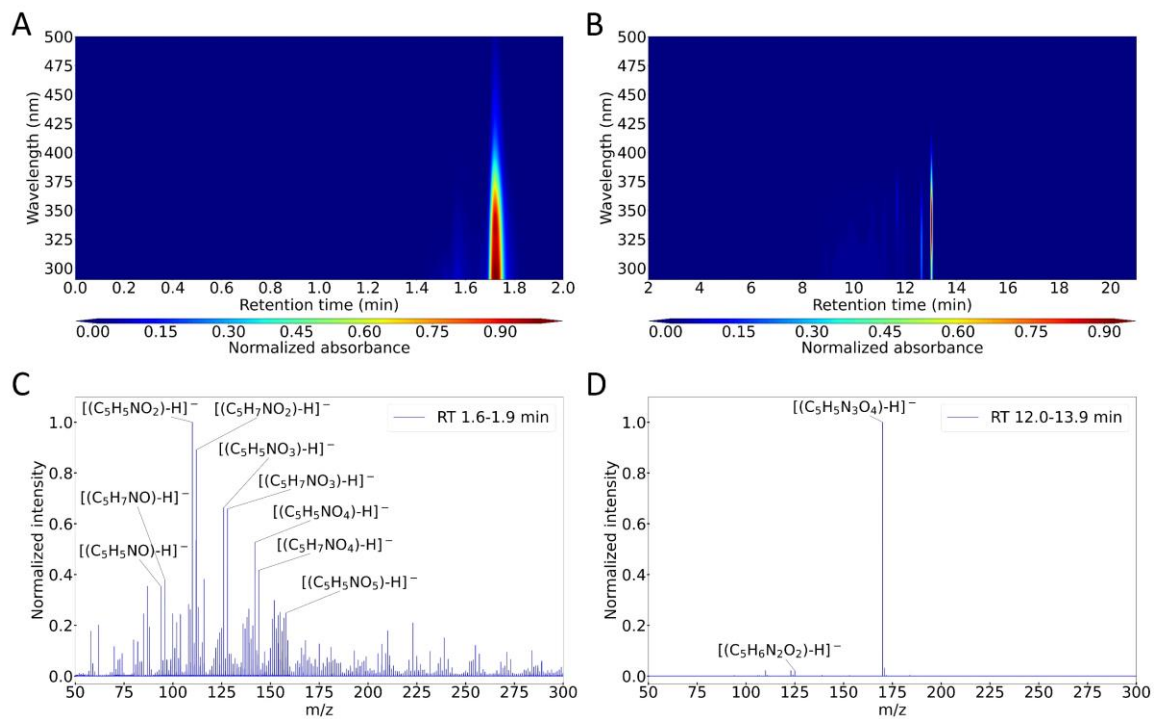
Figure S4.3. LC-DAD heatmaps at retention times of (A) 0−2 min, (B) 2−21 min, and (C−D) the mass spectra of corresponding hotspots of 2-MP SOA.
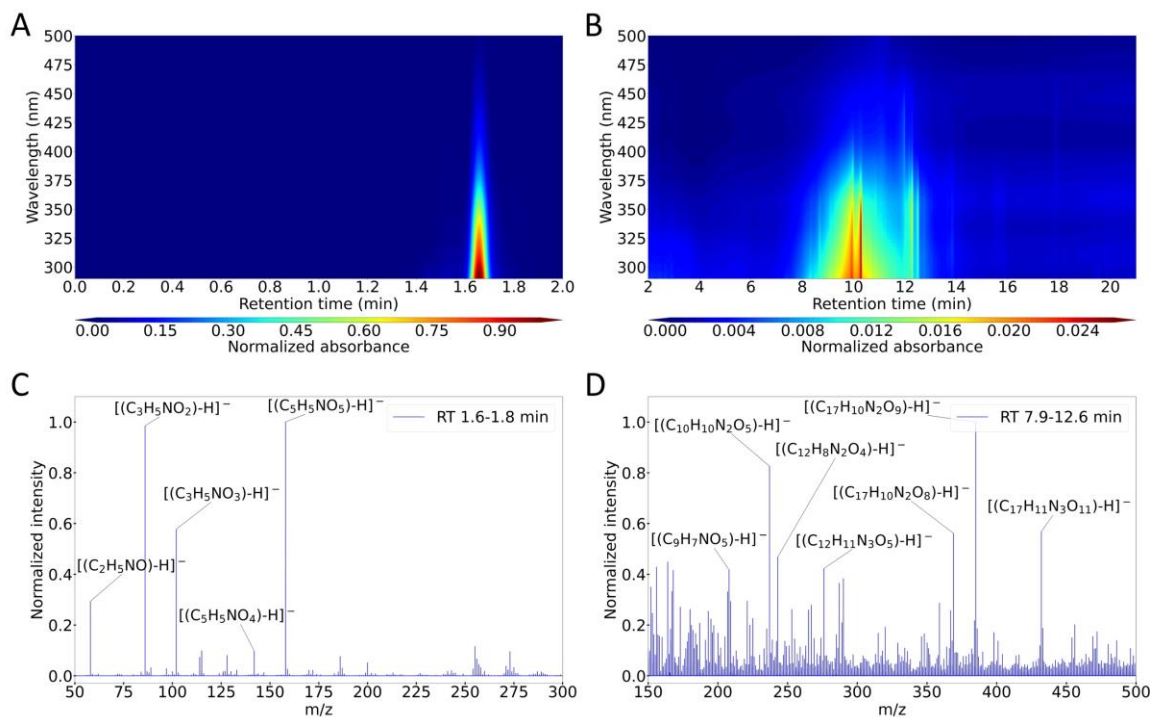
Figure S4.4. LC-DAD heatmaps at retention times of (A) 0−2 min, (B) 2−21 min, and (C−D) the mass spectra of corresponding hotspots of 1-MP SOA.
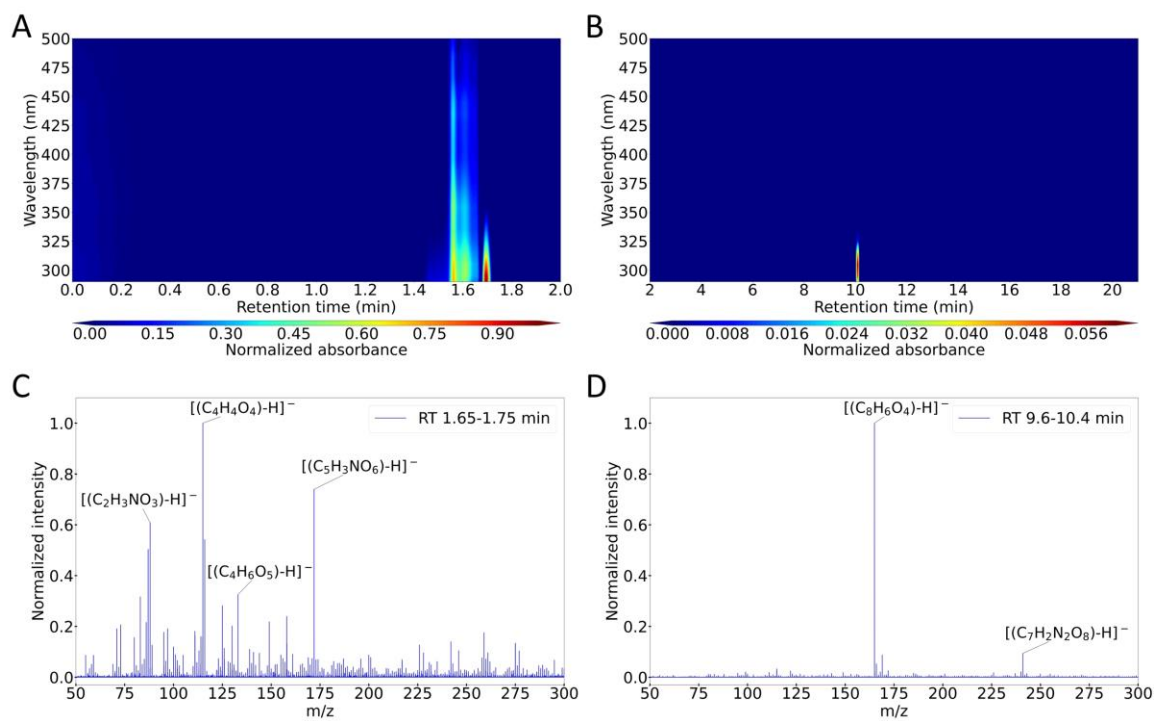
Figure S4.5. LC-DAD heatmaps at retention times of (A) 0−2 min, (B) 2−21 min, and (C−D) the mass spectra of corresponding hotspots of furfural SOA.

**Figure S4.6.** Tentative fragmentation pathways of (A) $C_4H_4NO_4^-$ and (B) $C_4HO_4^-$ based on the tandem MS data.
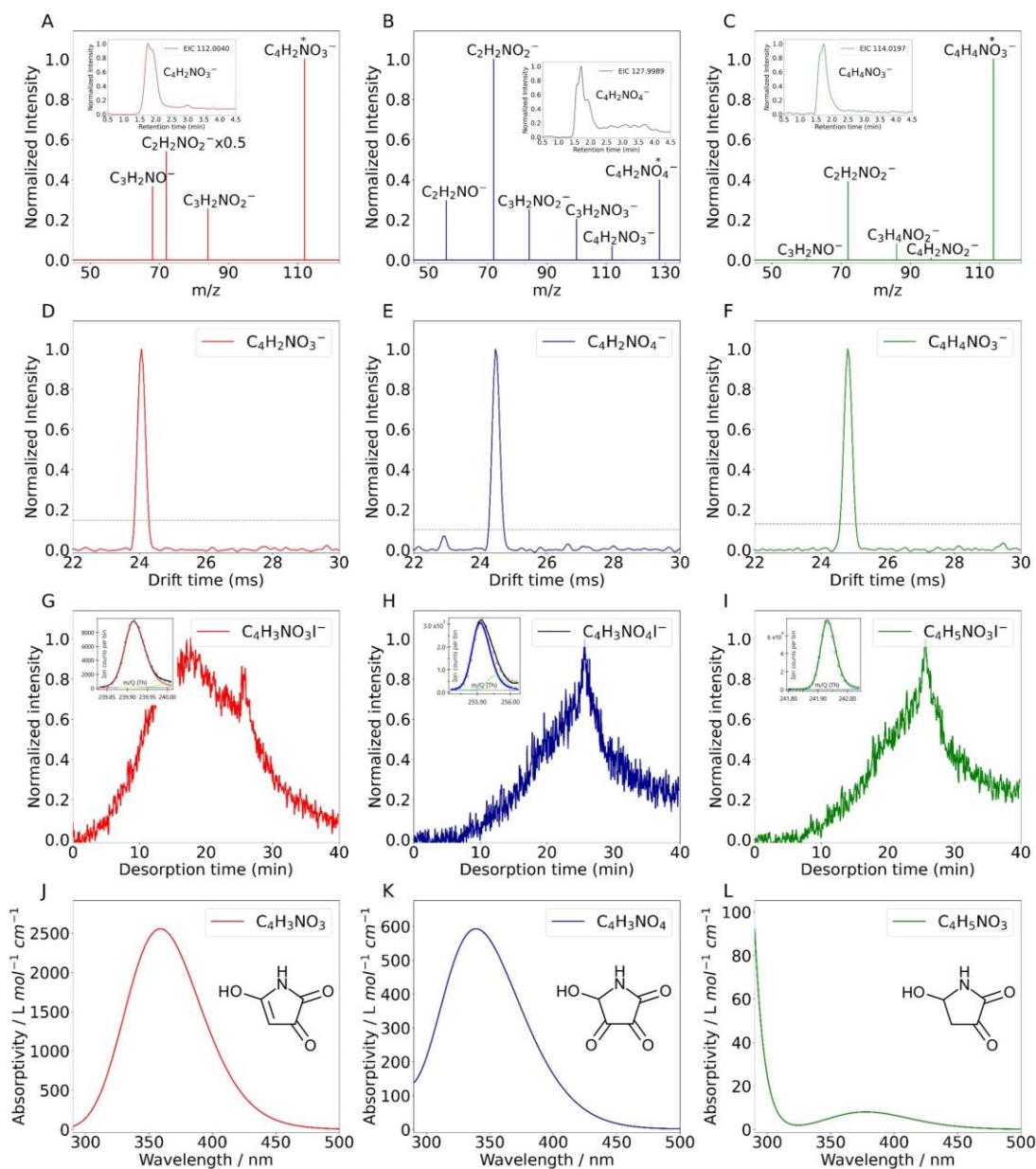
Figure S4.7. Characterization of heterocyclic carbonyl chromophores identified in pyrrole SOA, involving (A−C) EICs and tandem mass spectra, (D−F) IMS-TOF drift grams; (G−I) FIGAERO-ToF-CIMS peak fitting and thermograms and (J−L) theoretical UV−vis spectra.
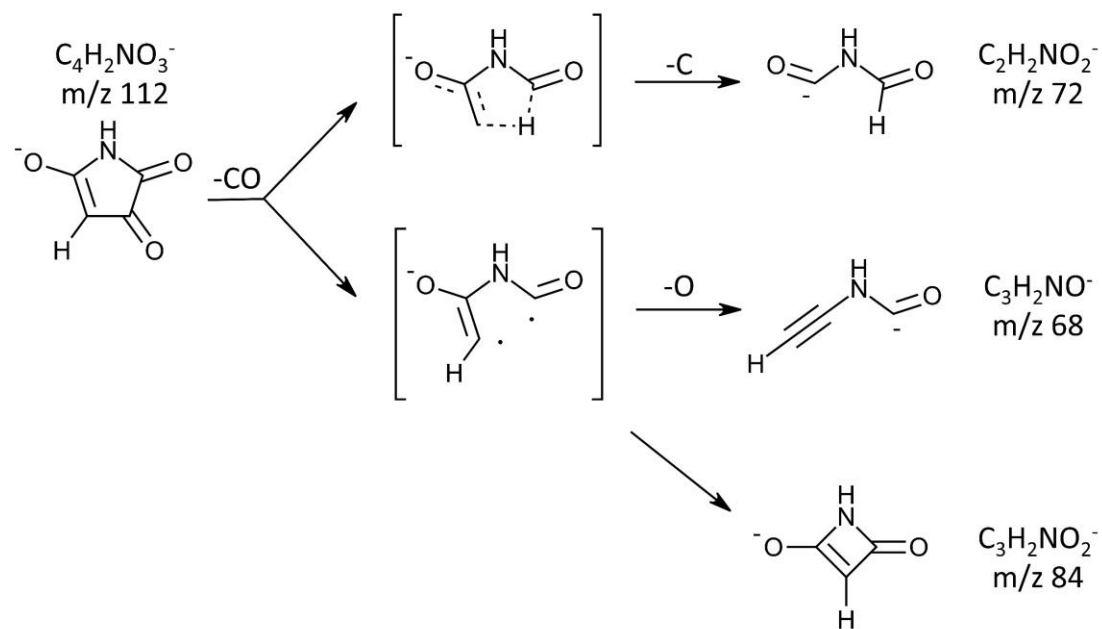
Figure S4.8. Tentative fragmentation pathways of the $C_4H_2NO_3^-$ ion based on the tandem MS data.
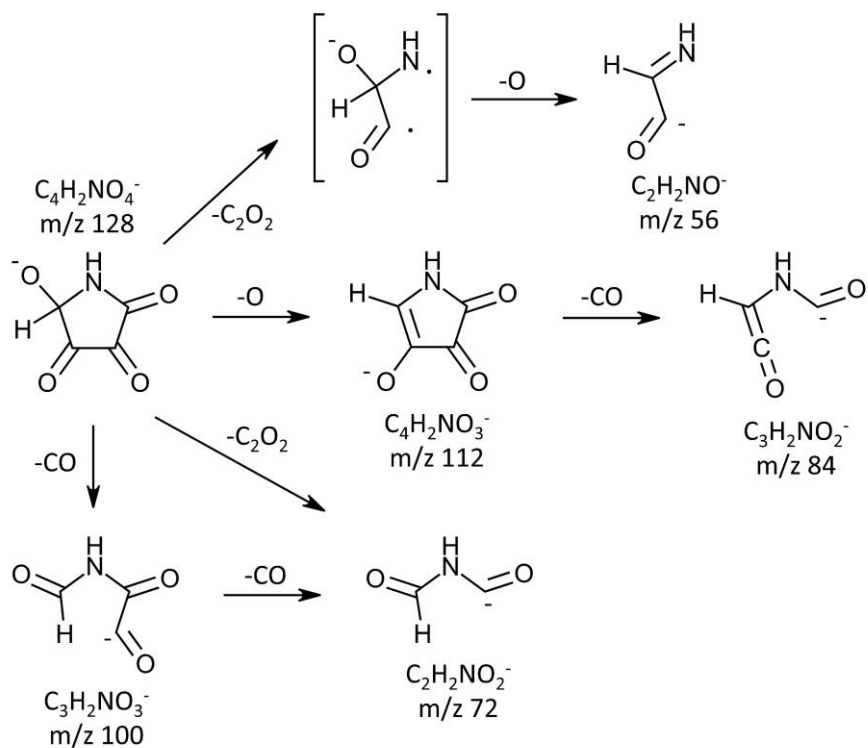
Figure S4.9. Tentative fragmentation pathways of the $C_4H_2NO_4^-$ ion based on the tandem MS data.
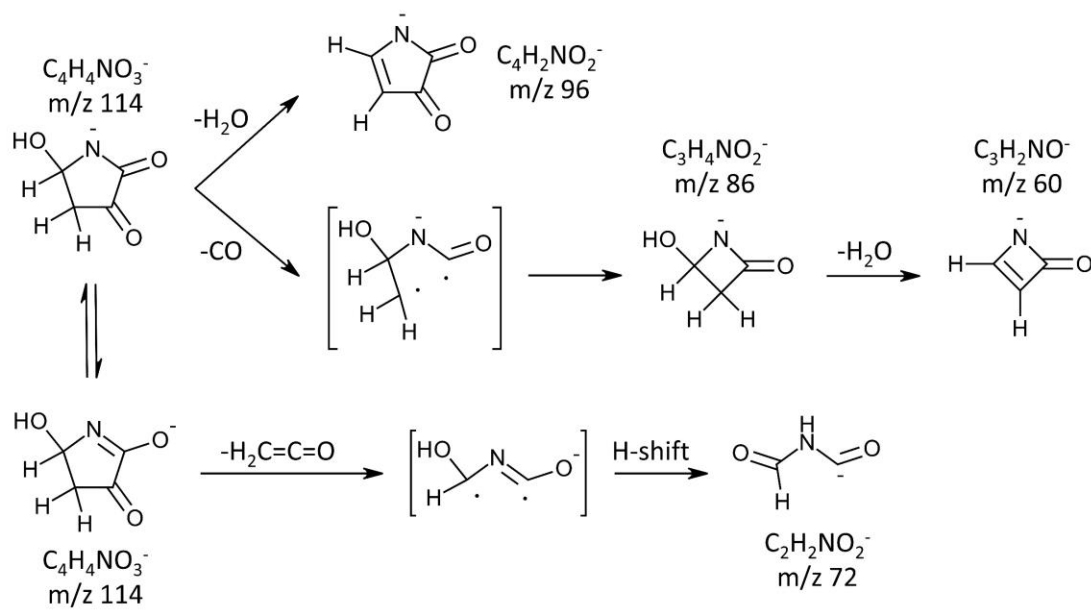
Figure S4.10. Tentative fragmentation pathways of the $C_4H_4NO_3^-$ ion based on the tandem MS data.
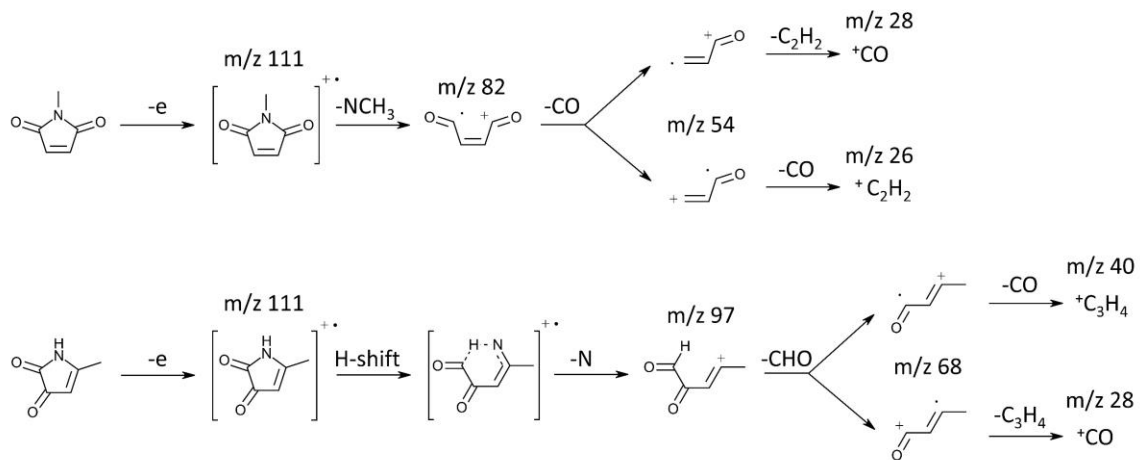
Figure S4.11. Tentative fragmentation pathways of $C_5H_5NO_2$ in 1-MP SOA and 2-MP SOA based on the GC/EI-MS data.
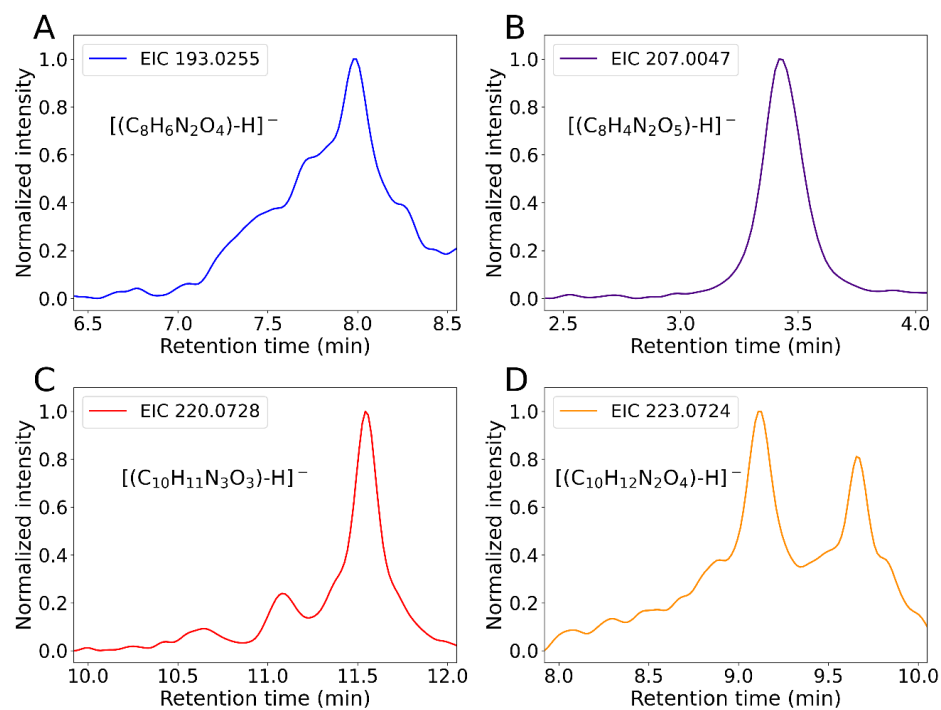
Figure S4.12. Examples of oxidation products with higher molecular weights and high double bond equivalence identified in (A−B) pyrrole SOA and (C−D) 2-MP SOA.
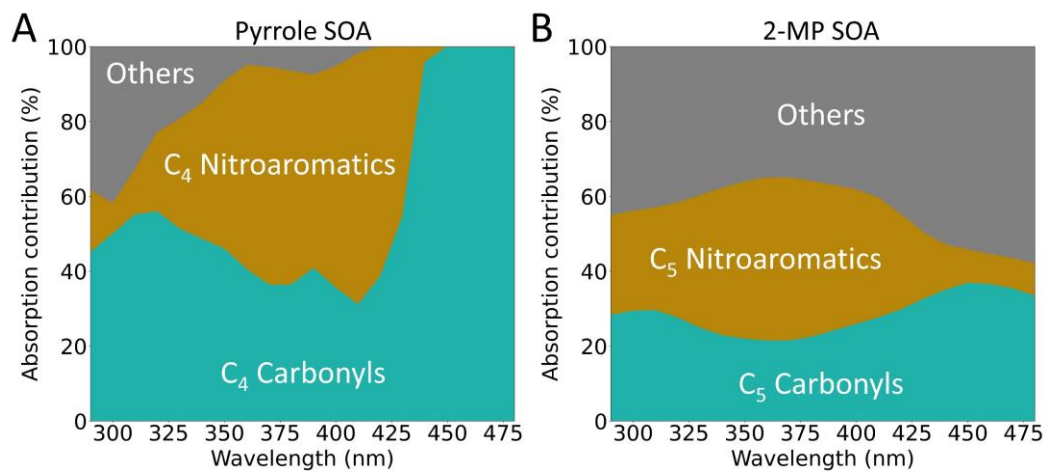
Figure S4.13. Light absorption contributions of chromophores in percentages: (A) C_4 nitroaromatics, C_4 carbonyls and other chromophores in pyrrole SOA; (B) C_5 nitroaromatics, C_5 carbonyls and other chromophores in 2-MP SOA.
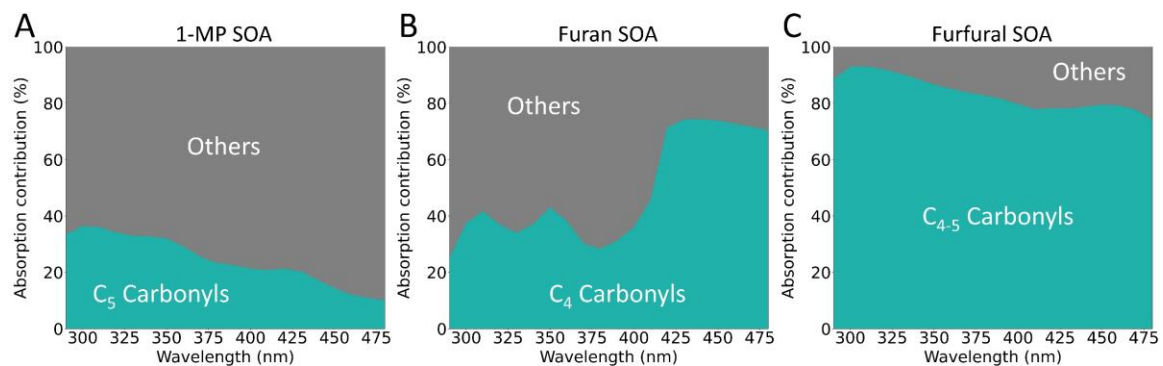
Figure S4.14. Light absorption contributions of chromophores in percentages: (A) C_5 carbonyls and other chromophores in 1-MP SOA; (B) C_4 carbonyls and other chromophores in furan SOA; (C) $C_{4–5}$ carbonyls and other chromophores in furfural SOA.
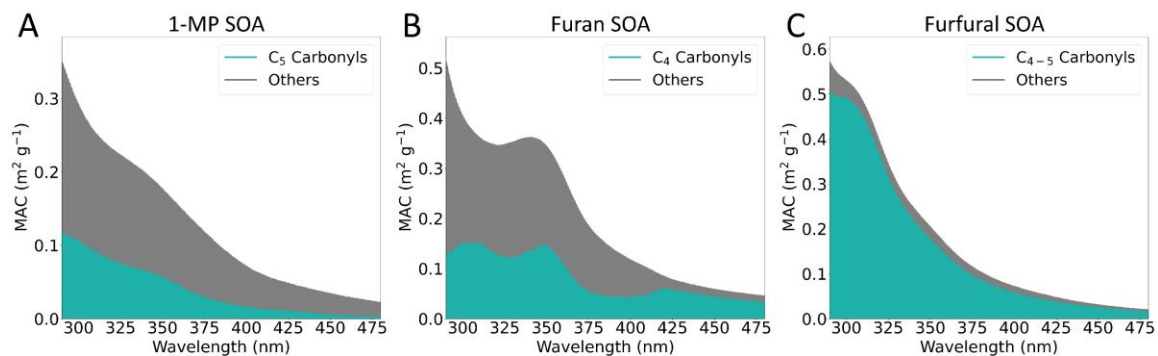
Figure S4.15. Light absorption contributions of chromophores to MAC profiles: (42−44) (A) C_5 carbonyls and other chromophores in 1-MP SOA; (B) C_4 carbonyls and other chromophores in furan SOA; (C) C_{4-5} carbonyls and other chromophores in furfural SOA.

4.6. References

1. Lin, G.; Penner, J. E.; Flanner, M. G.; Sillman, S.; Xu, L.; Zhou, C., Radiative forcing of organic aerosol in the atmosphere and on snow: Effects of SOA and brown carbon. *J. Geophys. Res. Atmos.* **2014**, 119, (12), 7453-7476.

2. Feng, Y.; Ramanathan, V.; Kotamarthi, V. R., Brown carbon: a significant atmospheric absorber of solar radiation? *Atmos. Chem. Phys.* **2013**, 13, (17), 8607-8621.

3. Zhang, A.; Wang, Y.; Zhang, Y.; Weber, R. J.; Song, Y.; Ke, Z.; Zou, Y., Modeling the global radiative effect of brown carbon: a potentially larger heating source in the tropical free troposphere than black carbon. *Atmos. Chem. Phys.* **2020**, 20, (4), 1901-1920.

4. Liu, J.; Scheuer, E.; Dibb, J.; Ziemba, L. D.; Thornhill, K. L.; Anderson, B. E.; Wisthaler, A.; Mikoviny, T.; Devi, J. J.; Bergin, M.; Weber, R. J., Brown carbon in the continental troposphere. *Geophys. Res. Lett.* **2014**, 41, (6), 2191-2195.

5. Zhang, Y.; Forrister, H.; Liu, J.; Dibb, J.; Anderson, B.; Schwarz, J. P.; Perring, A. E.; Jimenez, J. L.; Campuzano-Jost, P.; Wang, Y.; Nenes, A.; Weber, R. J., Top-of-atmosphere radiative forcing affected by brown carbon in the upper troposphere. *Nat. Geosci.* **2017**, 10, (7), 486-489.

6. Zhao, S.; Qi, S.; Yu, Y.; Kang, S.; Dong, L.; Chen, J.; Yin, D., Measurement report: Contrasting elevation-dependent light absorption by black and brown carbon: lessons from in situ measurements from the highly polluted Sichuan Basin to the pristine Tibetan Plateau. *Atmos. Chem. Phys.* **2022**, 22, (22), 14693-14708.

7. Ferrero, L.; Močnik, G.; Cogliati, S.; Gregorič, A.; Colombo, R.; Bolzacchini, E., Heating Rate of Light Absorbing Aerosols: Time-Resolved Measurements, the Role of Clouds, and Source Identification. *Environ. Sci. Technol.* **2018**, 52, (6), 3546-3555.

8. Tian, P.; Liu, D.; Zhao, D.; Yu, C.; Liu, Q.; Huang, M.; Deng, Z.; Ran, L.; Wu, Y.; Ding, S.; Hu, K.; Zhao, G.; Zhao, C.; Ding, D., In situ vertical characteristics of optical properties and heating rates of aerosol over Beijing. *Atmos. Chem. Phys.* **2020**, 20, (4), 2603-2622.

9. Brown, H.; Liu, X.; Feng, Y.; Jiang, Y.; Wu, M.; Lu, Z.; Wu, C.; Murphy, S.; Pokhrel, R., Radiative effect and climate impacts of brown carbon with the Community Atmosphere Model (CAM5). *Atmos. Chem. Phys.* **2018**, 18, (24), 17745-17768.

10. Xu, J.; Hettiyadura, A. P. S.; Liu, Y.; Zhang, X.; Kang, S.; Laskin, A., Atmospheric Brown Carbon on the Tibetan Plateau: Regional Differences in Chemical Composition and Light Absorption Properties. *Environ. Sci. Technol. Lett.* **2022**, 9, (3), 219-225.

11. Liu, D.; He, C.; Schwarz, J. P.; Wang, X., Lifecycle of light-absorbing carbonaceous aerosols in the atmosphere. *npj Clim. Atmos. Sci.* **2020**, 3, (1), 40.

12. Laskin, A.; Laskin, J.; Nizkorodov, S. A., Chemistry of Atmospheric Brown Carbon.

Chem. Rev. **2015**, 115, (10), 4335-4382.

13. Moise, T.; Flores, J. M.; Rudich, Y., Optical Properties of Secondary Organic Aerosols and Their Changes by Chemical Processes. *Chem. Rev.* **2015**, 115, (10), 4400-4439.

14. Li, X.; Wang, Y.; Hu, M.; Tan, T.; Li, M.; Wu, Z.; Chen, S.; Tang, X., Characterizing chemical composition and light absorption of nitroaromatic compounds in the winter of Beijing. *Atmos. Environ.* **2020**, 237, 117712.

15. Frka, S.; Šala, M.; Brodnik, H.; Štefane, B.; Kroflič, A.; Grgić, I., Seasonal variability of nitroaromatic compounds in ambient aerosols: Mass size distribution, possible sources and contribution to water-soluble brown carbon light absorption. *Chemosphere* **2022**, 299, 134381.

16. Bluvshtein, N.; Lin, P.; Flores, J. M.; Segev, L.; Mazar, Y.; Tas, E.; Snider, G.; Weagle, C.; Brown, S. S.; Laskin, A.; Rudich, Y., Broadband optical properties of biomass-burning aerosol and identification of brown carbon chromophores. *J. Geophys. Res. Atmos.* **2017**, 122, (10), 5441-5456.

17. Lin, P.; Bluvshtein, N.; Rudich, Y.; Nizkorodov, S. A.; Laskin, J.; Laskin, A., Molecular Chemistry of Atmospheric Brown Carbon Inferred from a Nationwide Biomass Burning Event. *Environ. Sci. Technol.* **2017**, 51, (20), 11561-11570.

18. Xie, M.; Hays, M. D.; Holder, A. L., Light-absorbing organic carbon from prescribed and laboratory biomass burning and gasoline vehicle emissions. *Sci. Rep.* **2017**, 7, (1), 7318.

19. Li, X.; Hu, M.; Wang, Y.; Xu, N.; Fan, H.; Zong, T.; Wu, Z.; Guo, S.; Zhu, W.; Chen, S.; Dong, H.; Zeng, L.; Yu, X.; Tang, X., Links between the optical properties and chemical compositions of brown carbon chromophores in different environments: Contributions and formation of functionalized aromatic compounds. *Sci. Total Environ.* **2021**, 786, 147418.

20. Wang, Z.; Zhang, J.; Zhang, L.; Liang, Y.; Shi, Q., Characterization of nitroaromatic compounds in atmospheric particulate matter from Beijing. *Atmos. Environ.* **2020**, 118046.

21. Zhao, R.; Lee, A. K. Y.; Huang, L.; Li, X.; Yang, F.; Abbatt, J. P. D., Photochemical processing of aqueous atmospheric brown carbon. *Atmos. Chem. Phys.* **2015**, 15, (11), 6087-6100.

22. Hems, R. F.; Abbatt, J. P. D., Aqueous Phase Photo-oxidation of Brown Carbon Nitrophenols: Reaction Kinetics, Mechanism, and Evolution of Light Absorption. *ACS Earth Space Chem.* **2018**, 2, (3), 225-234.

23. Braman, T.; Dolvin, L.; Thrasher, C.; Yu, H.; Walhout, E. Q.; O'Brien, R. E., Fresh versus Photo-recalcitrant Secondary Organic Aerosol: Effects of Organic Mixtures on

Aqueous Photodegradation of 4-Nitrophenol. *Environ. Sci. Technol. Lett.* **2020**, 7, (4), 248-253.

24. Wang, Y.; Huang, W.; Tian, L.; Wang, Y.; Li, F.; Huang, D. D.; Zhang, R.; Go Mabato, B. R.; Huang, R.-J.; Chen, Q.; Ge, X.; Du, L.; Ma, Y. G.; Gen, M.; Hoi, K. I.; Mok, K. M.; Yu, J. Z.; Chan, C. K.; Li, X.; Li, Y. J., Decay Kinetics and Absorption Changes of Methoxyphenols and Nitrophenols during Nitrate-Mediated Aqueous Photochemical Oxidation at 254 and 313 nm. *ACS Earth Space Chem.* **2022**, 6, (4), 1115-1125.

25. Yang, J.; Au, W. C.; Law, H.; Leung, C. H.; Lam, C. H.; Nah, T., pH affects the aqueous-phase nitrate-mediated photooxidation of phenolic compounds: implications for brown carbon formation and evolution. *Environ. Sci. Process Impacts* **2022**, 25, 176-189.

26. Witkowski, B.; Jain, P.; Gierczak, T., Aqueous chemical bleaching of 4-nitrophenol brown carbon by hydroxyl radicals; products, mechanism, and light absorption. *Atmos. Chem. Phys.* **2022**, 22, (8), 5651-5663.

27. Xie, M.; Chen, X.; Hays, M. D.; Lewandowski, M.; Offenberg, J.; Kleindienst, T. E.; Holder, A. L., Light Absorption of Secondary Organic Aerosol: Composition and Contribution of Nitroaromatic Compounds. *Environ. Sci. Technol.* **2017**, 51, (20), 11607-11616.

28. McNeill, V. F., Atmospheric Aerosols: Clouds, Chemistry, and Climate. *Annu. Rev. Chem. Biomol. Eng.* **2017**, 8, (1), 427-444.

29. Gardner, E. P.; Sperry, P. D.; Calvert, J. G., Photodecomposition of acrolein in oxygen-nitrogen mixtures. *J. Phys. Chem.* **1987**, 91, (7), 1922-1930.

30. Magneron, I.; Thévenet, R.; Mellouki, A.; Le Bras, G.; Moortgat, G. K.; Wirtz, K., A Study of the Photolysis and OH-initiated Oxidation of Acrolein and trans-Crotonaldehyde. *J. Phys. Chem. A* **2002**, 106, (11), 2526-2537.

31. Mayol-Bracero, O. L.; Guyon, P.; Graham, B.; Roberts, G.; Andreae, M. O.; Decesari, S.; Facchini, M. C.; Fuzzi, S.; Artaxo, P., Water-soluble organic compounds in biomass burning aerosols over Amazonia 2. Apportionment of the chemical composition and importance of the polyacidic fraction. *J. Geophys. Res. Atmos.*, 107, (D20), LBA 59-1-LBA 59-15.

32. Garcia-Hurtado, E.; Pey, J.; Borrás, E.; Sánchez, P.; Vera, T.; Carratalá, A.; Alastuey, A.; Querol, X.; Vallejo, V. R., Atmospheric PM and volatile organic compounds released from Mediterranean shrubland wildfires. *Atmos. Environ.* **2014**, 89, 85-92.

33. Zhou, Y.; West, C. P.; Hettiyadura, A. P. S.; Pu, W.; Shi, T.; Niu, X.; Wen, H.; Cui, J.; Wang, X.; Laskin, A., Molecular Characterization of Water-Soluble Brown Carbon Chromophores in Snowpack from Northern Xinjiang, China. *Environ. Sci. Technol.* **2022**, 56, (7), 4173-4186.

34. Desyaterik, Y.; Sun, Y.; Shen, X.; Lee, T.; Wang, X.; Wang, T.; Collett Jr, J. L.,

Speciation of "brown" carbon in cloud water impacted by agricultural biomass burning in eastern China. *J. Geophys. Res. Atmos.* **2013**, 118, (13), 7389-7399.

35. Jacobson, M. Z., Isolating nitrated and aromatic aerosols and nitrated aromatic gases as sources of ultraviolet light absorption. *J. Geophys. Res. Atmos.* **1999**, 104, (D3), 3527-3542.

36. Karl, T. G.; Christian, T. J.; Yokelson, R. J.; Artaxo, P.; Hao, W. M.; Guenther, A., The Tropical Forest and Fire Emissions Experiment: method evaluation of volatile organic compound emissions measured by PTR-MS, FTIR, and GC from tropical biomass burning. *Atmos. Chem. Phys.* **2007**, 7, (22), 5883-5897.

37. Hatch, L. E.; Luo, W.; Pankow, J. F.; Yokelson, R. J.; Stockwell, C. E.; Barsanti, K. C., Identification and quantification of gaseous organic compounds emitted from biomass burning using two-dimensional gas chromatography–time-of-flight mass spectrometry. *Atmos. Chem. Phys.* **2015**, 15, (4), 1865-1899.

38. Koss, A. R.; Sekimoto, K.; Gilman, J. B.; Selimovic, V.; Coggon, M. M.; Zarzana, K. J.; Yuan, B.; Lerner, B. M.; Brown, S. S.; Jimenez, J. L.; Krechmer, J.; Roberts, J. M.; Warneke, C.; Yokelson, R. J.; de Gouw, J., Non-methane organic gas emissions from biomass burning: identification, quantification, and emission factors from PTR-ToF during the FIREX 2016 laboratory experiment. *Atmos. Chem. Phys.* **2018**, 18, (5), 3299-3319.

39. Andreae, M. O., Emission of trace gases and aerosols from biomass burning – an updated assessment. *Atmos. Chem. Phys.* **2019**, 19, (13), 8523-8546.

40. Decker, Z. C. J.; Zarzana, K. J.; Coggon, M.; Min, K.-E.; Pollack, I.; Ryerson, T. B.; Peischl, J.; Edwards, P.; Dubé, W. P.; Markovic, M. Z.; Roberts, J. M.; Veres, P. R.; Graus, M.; Warneke, C.; de Gouw, J.; Hatch, L. E.; Barsanti, K. C.; Brown, S. S., Nighttime Chemical Transformation in Biomass Burning Plumes: A Box Model Analysis Initialized with Aircraft Observations. *Environ. Sci. Technol.* **2019**, 53, (5), 2529-2538.

41. Jiang, H.; Frie, A. L.; Lavi, A.; Chen, J. Y.; Zhang, H.; Bahreini, R.; Lin, Y.-H., Brown Carbon Formation from Nighttime Chemistry of Unsaturated Heterocyclic Volatile Organic Compounds. *Environ. Sci. Technol. Lett.* **2019**, 6, (3), 184-190.

42. Mayorga, R.; Chen, K.; Raeofy, N.; Woods, M.; Lum, M.; Zhao, Z.; Zhang, W.; Bahreini, R.; Lin, Y.-H.; Zhang, H., Chemical Structure Regulates the Formation of Secondary Organic Aerosol and Brown Carbon in Nitrate Radical Oxidation of Pyrroles and Methylpyrroles. *Environ. Sci. Technol.* **2022**, 56, (12), 7761-7770.

43. Chen, K.; Raeofy, N.; Lum, M.; Mayorga, R.; Woods, M.; Bahreini, R.; Zhang, H.; Lin, Y.-H., Solvent effects on chemical composition and optical properties of extracted secondary brown carbon constituents. *Aerosol Sci. Tech.* **2022**, 56, (10), 917-930.

44. Chen, K.; Mayorga, R.; Raeofy, N.; Lum, M.; Woods, M.; Bahreini, R.; Zhang, H.; Lin, Y.-H., Effects of Nitrate Radical Levels and Pre-Existing Particles on Secondary Brown Carbon Formation from Nighttime Oxidation of Furan. *ACS Earth Space Chem.* **2022**, 6, (11), 2709-2721.

45. Ziemann, P. J.; Atkinson, R., Kinetics, products, and mechanisms of secondary organic aerosol formation. *Chem. Soc. Rev.* **2012**, 41, (19), 6582-6605.

46. Lopez-Hilfiker, F. D.; Mohr, C.; Ehn, M.; Rubach, F.; Kleist, E.; Wildt, J.; Mentel, T. F.; Lutz, A.; Hallquist, M.; Worsnop, D.; Thornton, J. A., A novel method for online analysis of gas and particle composition: description and evaluation of a Filter Inlet for Gases and AEROsols (FIGAERO). *Atmos. Meas. Tech.* **2014**, 7, (4), 983-1001.

47. Zhang, X.; Zhang, H.; Xu, W.; Wu, X.; Tyndall, G. S.; Orlando, J. J.; Jayne, J. T.; Worsnop, D. R.; Canagaratna, M. R., Molecular characterization of alkyl nitrates in atmospheric aerosols by ion mobility mass spectrometry. *Atmos. Meas. Tech.* **2019**, 12, (10), 5535-5545.

48. Zhao, Z.; Yang, X.; Lee, J.; Tolentino, R.; Mayorga, R.; Zhang, W.; Zhang, H., Diverse Reactions in Highly Functionalized Organic Aerosols during Thermal Desorption. *ACS Earth Space Chem.* **2020**, 4, (2), 283-296.

49. Mayorga, R. J.; Zhao, Z.; Zhang, H., Formation of secondary organic aerosol from nitrate radical oxidation of phenolic VOCs: Implications for nitration mechanisms and brown carbon formation. *Atmos. Environ.* **2021**, 244, 117910.

50. Frisch, M. J.; Trucks, G. W.; Schlegel, H. B.; Scuseria, G. E.; Robb, M. A.; Cheeseman, J. R.; Scalmani, G.; Barone, V.; Petersson, G. A.; Nakatsuji, H.; Li, X.; Caricato, M.; Marenich, A. V.; Bloino, J.; Janesko, B. G.; Gomperts, R.; Mennucci, B.; Hratchian, H. P.; Ortiz, J. V.; Izmaylov, A. F.; Sonnenberg, J. L.; Williams; Ding, F.; Lipparini, F.; Egidi, F.; Goings, J.; Peng, B.; Petrone, A.; Henderson, T.; Ranasinghe, D.; Zakrzewski, V. G.; Gao, J.; Rega, N.; Zheng, G.; Liang, W.; Hada, M.; Ehara, M.; Toyota, K.; Fukuda, R.; Hasegawa, J.; Ishida, M.; Nakajima, T.; Honda, Y.; Kitao, O.; Nakai, H.; Vreven, T.; Throssell, K.; Montgomery Jr., J. A.; Peralta, J. E.; Ogliaro, F.; Bearpark, M. J.; Heyd, J. J.; Brothers, E. N.; Kudin, K. N.; Staroverov, V. N.; Keith, T. A.; Kobayashi, R.; Normand, J.; Raghavachari, K.; Rendell, A. P.; Burant, J. C.; Iyengar, S. S.; Tomasi, J.; Cossi, M.; Millam, J. M.; Klene, M.; Adamo, C.; Cammi, R.; Ochterski, J. W.; Martin, R. L.; Morokuma, K.; Farkas, O.; Foresman, J. B.; Fox, D. J. Gaussian 16 Rev. C.01, Wallingford, CT, **2016**.

51. Becke, A. D., Density-functional exchange-energy approximation with correct asymptotic behavior. *Phys. Rev. A* **1988**, 38, (6), 3098-3100.

52. Stephens, P. J.; Devlin, F. J.; Chabalowski, C. F.; Frisch, M. J., *Ab Initio* Calculation of Vibrational Absorption and Circular Dichroism Spectra Using Density Functional Force Fields. *J. Phys. Chem.* **1994**, 98, (45), 11623-11627.

53. Ditchfield, R; Hehre, W. J.; People, J. A., Self-Consistent Molecular-Orbital Methods. IX. An Extended Gaussian-Type Basis for Molecular-Orbital Studies of Organic Molecules. *J. Chem. Phys.* **1971**, 54, (2), 724-728.

54. Jacquemin, D.; Perpète, E. A.; Scuseria, G. E.; Ciofini, I.; Adamo, C., TD-DFT Performance for the Visible Absorption Spectra of Organic Dyes: Conventional versus Long-Range Hybrids. *J. Chem. Theory Comput.* **2008**, 4, (1), 123-135.

55. Chen, J. Y.; Rodriguez, E.; Jiang, H.; Chen, K.; Frie, A.; Zhang, H.; Bahreini, R.; Lin, Y.-H., Time-Dependent Density Functional Theory Investigation of the UV–Vis Spectra of Organonitrogen Chromophores in Brown Carbon. *ACS Earth Space Chem.* **2020**, 4, (2), 311-320.

56. Mennucci, B.; Cammi, R.; Tomasi, J., Excited states and solvatochromic shifts within a nonequilibrium solvation approach: A new formulation of the integral equation formalism method at the self-consistent field, configuration interaction, and multiconfiguration self-consistent field level. *J. Chem. Phys.* **1998**, 109, (7), 2798-2807.

57. Zhang, W.; Wang, T.; Du, B.; Mu, L.; Feng, C., Mechanism for the gas-phase reaction between NO3 and furan: A theoretical study. *Chem. Phys. Lett.* **2008**, 455, (4), 164-168.

58. Veblen, T. T.; Kitzberger, T.; Donnegan, J., Climatic and Human Influences on Fire Regimes in Ponderosa Pine Forests in the Colorado Front Range. *Ecol Appl.* **2000**, 10, (4), 1178-1195.

59. Forstner, H. J. L.; Flagan, R. C.; Seinfeld, J. H., Secondary Organic Aerosol from the Photooxidation of Aromatic Hydrocarbons: Molecular Composition. *Environ. Sci. Technol.* **1997**, 31, (5), 1345-1358.

60. Yu, J.; Jeffries, H. E.; Sexton, K. G., Atmospheric photooxidation of alkylbenzenes—I. Carbonyl product analyses. *Atmos. Environ.* **1997**, 31, (15), 2261-2280.

61. Edney, E. O.; Driscoll, D. J.; Weathers, W. S.; Kleindienst, T. E.; Conver, T. S.; McIver, C. D.; Li, W., Formation of Polyketones in Irradiated Toluene/Propylene/NO x /Air Mixtures. *Aerosol Sci. Tech.* **2001**, 35, (6), 998-1008.

62. Hamilton, J. F.; Lewis, A. C.; Bloss, C.; Wagner, V.; Henderson, A. P.; Golding, B. T.; Wirtz, K.; Martin-Reviejo, M.; Pilling, M. J., Measurements of photo-oxidation products from the reaction of a series of alkyl-benzenes with hydroxyl radicals during EXACT using comprehensive gas chromatography. *Atmos. Chem. Phys.* **2003**, 3, (6), 1999-2014.

63. Lee, J. Y.; Lane, D. A., Unique products from the reaction of naphthalene with the hydroxyl radical. *Atmos. Environ.* **2009**, 43, (32), 4886-4893.

64. Coggon, M. M.; Lim, C. Y.; Koss, A. R.; Sekimoto, K.; Yuan, B.; Gilman, J. B.; Hagan, D. H.; Selimovic, V.; Zarzana, K. J.; Brown, S. S.; Roberts, J. M.; Müller, M.; Yokelson, R.; Wisthaler, A.; Krechmer, J. E.; Jimenez, J. L.; Cappa, C.; Kroll, J. H.; de Gouw, J.; Warneke, C., OH chemistry of non-methane organic gases (NMOGs) emitted

from laboratory and ambient biomass burning smoke: evaluating the influence of furans and oxygenated aromatics on ozone and secondary NMOG formation. *Atmos. Chem. Phys.* **2019**, 19, (23), 14875-14899.

65. Liang, Y.; Weber, R. J.; Misztal, P. K.; Jen, C. N.; Goldstein, A. H., Aging of Volatile Organic Compounds in October 2017 Northern California Wildfire Plumes. *Environ. Sci. Technol.* **2022**, 56, (3), 1557-1567.

66. Edney, E. O.; Kleindienst, T. E.; Conver, T. S.; McIver, C. D.; Corse, E. W.; Weathers, W. S., Polar organic oxygenates in PM2.5 at a southeastern site in the United States. *Atmos. Environ.* **2003**, 37, (28), 3947-3965.

67. De Haan, D. O.; Jansen, K.; Rynaski, A. D.; Sueme, W. R. P.; Torkelson, A. K.; Czer, E. T.; Kim, A. K.; Rafla, M. A.; De Haan, A. C.; Tolbert, M. A., Brown Carbon Production by Aqueous-Phase Interactions of Glyoxal and SO_2. *Environ. Sci. Technol.* **2020**, 54, (8), 4781-4789.

68. Al-Abadleh, H. A.; Rana, M. S.; Mohammed, W.; Guzman, M. I., Dark Iron-Catalyzed Reactions in Acidic and Viscous Aerosol Systems Efficiently Form Secondary Brown Carbon. *Environ. Sci. Technol.* **2021**, 55, (1), 209-219.

69. Lin, P.; Aiona, P. K.; Li, Y.; Shiraiwa, M.; Laskin, J.; Nizkorodov, S. A.; Laskin, A., Molecular Characterization of Brown Carbon in Biomass Burning Aerosol Particles. *Environ. Sci. Technol.* **2016**, 50, (21), 11815-11824.

70. Carlier, P.; Hannachi, H.; Mouvier, G., The chemistry of carbonyl compounds in the atmosphere—A review. *Atmos. Environ.* **1986**, 20, (11), 2079-2099.

71. Lary, D. J.; Shallcross, D. E., Central role of carbonyl compounds in atmospheric chemistry. *J. Geophys. Res. Atmos.* **2000**, 105, (D15), 19771-19778.

72. Petters, S. S.; Pagonis, D.; Claflin, M. S.; Levin, E. J. T.; Petters, M. D.; Ziemann, P. J.; Kreidenweis, S. M., Hygroscopicity of Organic Compounds as a Function of Carbon Chain Length and Carboxyl, Hydroperoxy, and Carbonyl Functional Groups. *J. Phys. Chem. A* **2017**, 121, (27), 5164-5174.

73. Updyke, K. M.; Nguyen, T. B.; Nizkorodov, S. A., Formation of brown carbon via reactions of ammonia with secondary organic aerosols from biogenic and anthropogenic precursors. *Atmos. Environ.* **2012**, 63, 22-31.

74. Kampf, C. J.; Jakob, R.; Hoffmann, T., Identification and characterization of aging products in the glyoxal/ammonium sulfate system - implications for light-absorbing material in atmospheric aerosols. *Atmos. Chem. Phys.* **2012**, 12, (14), 6323-6333.

75. Kampf, C. J.; Filippi, A.; Zuth, C.; Hoffmann, T.; Opatz, T., Secondary brown carbon formation via the dicarbonyl imine pathway: nitrogen heterocycle formation and synergistic effects. *Phys. Chem. Chem. Phys.* **2016**, 18, (27), 18353-18364.

76. Marrero-Ortiz, W.; Hu, M.; Du, Z.; Ji, Y.; Wang, Y.; Guo, S.; Lin, Y.; Gomez-

Hermandez, M.; Peng, J.; Li, Y.; Secrest, J.; Zamora, M. L.; Wang, Y.; An, T.; Zhang, R., Formation and Optical Properties of Brown Carbon from Small α-Dicarbonyls and Amines. *Environ. Sci. Technol.* **2019**, 53, (1), 117-126.

77. Phillips, S. M.; Smith, G. D., Light Absorption by Charge Transfer Complexes in Brown Carbon Aerosols. *Environ. Sci. Technol. Lett.* **2014**, 1, (10), 382-386.

78. Phillips, S. M.; Smith, G. D., Further Evidence for Charge Transfer Complexes in Brown Carbon Aerosols from Excitation–Emission Matrix Fluorescence Spectroscopy. *J. Phys. Chem. A* **2015**, 119, (19), 4545-4551.

79. Permar, W.; Wang, Q.; Selimovic, V.; Wielgasz, C.; Yokelson, R. J.; Hornbrook, R. S.; Hills, A. J.; Apel, E. C.; Ku, I. T.; Zhou, Y.; Sive, B. C.; Sullivan, A. P.; Collett Jr, J. L.; Campos, T. L.; Palm, B. B.; Peng, Q.; Thornton, J. A.; Garofalo, L. A.; Farmer, D. K.; Kreidenweis, S. M.; Levin, E. J. T.; DeMott, P. J.; Flocke, F.; Fischer, E. V.; Hu, L., Emissions of Trace Organic Gases From Western U.S. Wildfires Based on WE-CAN Aircraft Measurements. *J. Geophys. Res. Atmos.* **2021**, 126, (11), e2020JD033838.

80. Hayden, K. L.; Li, S. M.; Liggio, J.; Wheeler, M. J.; Wentzell, J. J. B.; Leithead, A.; Brickell, P.; Mittermeier, R. L.; Oldham, Z.; Mihele, C. M.; Staebler, R. M.; Moussa, S. G.; Darlington, A.; Wolde, M.; Thompson, D.; Chen, J.; Griffin, D.; Eckert, E.; Ditto, J. C.; He, M.; Gentner, D. R., Reconciling the total carbon budget for boreal forest wildfire emissions using airborne observations. *Atmos. Chem. Phys.* **2022**, 22, (18), 12493-12523.

81. Wang, Y.; Hu, M.; Wang, Y.; Zheng, J.; Shang, D.; Yang, Y.; Liu, Y.; Li, X.; Tang, R.; Zhu, W.; Du, Z.; Wu, Y.; Guo, S.; Wu, Z.; Lou, S.; Hallquist, M.; Yu, J. Z., The formation of nitro-aromatic compounds under high NO_x and anthropogenic VOC conditions in urban Beijing, China. *Atmos. Chem. Phys.* **2019**, 19, (11), 7649-7665.

82. Siemens, K.; Morales, A.; He, Q.; Li, C.; Hettiyadura, A. P. S.; Rudich, Y.; Laskin, A., Molecular Analysis of Secondary Brown Carbon Produced from the Photooxidation of Naphthalene. *Environ. Sci. Technol.* **2022**, 56, (6), 3340-3353.

Chapter 5. Conclusions and Implications

Overall, this dissertation investigates secondary brown carbon (BrC) formation from the nighttime oxidation of heterocyclic volatile organic compounds (VOCs) under different environmental conditions. Environmental factors discussed in this dissertation include nitrate radical (NO_3) levels, pre-existing particles, and relative humidity (RH). The NO_3 level represents the nighttime oxidant level, while the pre-existing particles refer to the background particles in the atmosphere; both are key factors in determining the secodnary organic aerosol (SOA) burden in the future atmosphere. (1) RH is an essential factor that can regulate the physicochemical processing of SOA formation and secondary BrC light absorption. The crucial role of carbonyl chromophores in secondary BrC light absorption is particularly emphasized. The findings in this dissertation reveal that different combinations of environmental factors can remarkably modulate the optical properties and chemical composition of secondary BrC.

The effects of NO_3 levels and pre-existing particles on secondary BrC formation were explored by using the nighttime oxidation of furan as the studied system. A change in NO_3 levels exhibited an insignificant impact on the overall composition of furan-derived SOA, while the presence of pre-existing particles exerted influence on the SOA composition. The mass absorption coefficient (MAC) profiles showed that furan-derived BrC light absorption increased with higher NO_3 levels but decreased in the presence of pre-existing particles. Such a divergent trend suggsets that NO_3-initiated oxidation of furan can facilitate the generation of light-absorbing compounds, while pre-existing

particles may facilitate the gas-to-particle partitioning of non-absorbing products. Chemical characterization revealed consistent patterns of molecular chromophores across the studied environmental conditions, with highly oxygenated monomers, dimers, and oligomers identified as contributors to BrC light absorption. All these findings can provide process-level insights on how the key factors of future SOA burden can affect secondary BrC formation.

The effects of RH on secondary BrC formation were explored by using the nighttime oxidation of furan and pyrrole as the studied systems. The increase in RH notably influenced the size distribution dynamics of both SOAs, with pyrrole-derived SOA showing a stronger potential to generate ultrafine particles through nucleation. Higher RH was associated with the increased mass fractions of oxygenated compounds in both SOAs, which may suggest enhanced gas-phase and/or multiphase oxidation in humid environments. Moreover, higher RH resulted in decreased MAC of both BrC, diverging from those originating from homocyclic precursors. This divergence can be attributed to the formation of non-absorbing high-molecular-weight oxygenated compounds and the declining mass fractions of molecular chromophores. All these findings highlight that RH can be a pivotal factor that modulates the size distribution dynamics, chemical composition, and optical properties of secondary BrC in wildfire smoke.

Moreover, this dissertation further sheds light on the role of carbonyl chromophores in secondary BrC light absorption. A variety of carbonyl chromophores were charaterized in the secondary BrC derived from the nighttime oxidation of furan,

163

pyrrole, 1-methylpyrrole, 2-methylpyrrole, and furfural. Chromophores with carbonyl groups bonded to nitrogen, such as imides and amides, may substantially contribute to BrC light absorption. These N-containing carbonyl chromophores can contribute to more than 40% of the total light absorption in pyrrole-derived BrC at wavelengths below 350 nm and above 430 nm. Such a wavelength dependency indicates that BrC light absorption may not be solely attributed to a certain type of chromophore but instead account for a combination of different types of chromophores with their dominant light absorption contribution in certain wavelength ranges.

Taken together, this dissertation contributes to a better understanding of the role of NO_3 levels, pre-existing particles, and RH in regulating the optical properties and chemical compositions of secondary BrC from the nighttime oxidation of heterocyclic VOCs. This dissertation also provides a new perspective on the role of atmospheric carbonyls by highlighting their substantial contribution to secondary BrC light absorption. At present, the uncertainty of BrC radiative forcing is still large due to the variation of chromophore composition, exacerbated by the intricate influence of atmospheric processing under different environmental conditions. This dissertation underscores the necessity for continued research on how the interplay of different environmental factors can affect the formation and evolution of secondary BrC chromophores.

Further, this dissertation also demonstrates that secondary BrC is a potential key to better constraining the interconnection between atmospheric chemistry and climate change. As highlighted in the sixth assessment report from the Intergovernmental Panel

on Climate Change (IPCC), the role of the fire-climate feedback in the Earth's energy budget is inconclusive since the radiative effects of wildfire smoke are highly uncertain. (2) This dissertation establishes the foundation for understanding how wildfire smoke environments influence secondary BrC formation. The findings in this dissertation can be incorporated into climate models for more accurate parameterization of BrC's radiative forcing. Future studies should delve into a more in-depth understanding of how the chemical complexity of atmospheric BrC aerosols can modulate the radiative forcing of wildfire smoke and, consequently, future climate change.

References

1. Tsigaridis, K.; Kanakidou, M., Secondary organic aerosol importance in the future atmosphere. *Atmos. Environ.* **2007**, 41, (22), 4682-4692.

2. Szopa, S., V. Naik, B. Adhikary, P. Artaxo, T. Berntsen, W.D. Collins, S. Fuzzi, L. Gallardo, A. Kiendler-Scharr, Z. Klimont, H. Liao, N. Unger, P. Zanis, Short-Lived Climate Forcers. *In Climate Change 2021: The Physical Science Basis. Contribution of Working Group I to the Sixth Assessment Report of the Intergovernmental Panel on Climate Change* [Masson-Delmotte, V., P. Zhai, A. Pirani, S.L. Connors, C. Péan, S. Berger, N. Caud, Y. Chen, L. Goldfarb, M.I. Gomis, M. Huang, K. Leitzell, E. Lonnoy, J.B.R. Matthews, T.K. Maycock, T. Waterfield, O. Yelekçi, R. Yu, and B. Zhou (eds.)]. Cambridge University Press, Cambridge, United Kingdom and New York, NY, USA: **2021**; p 817–922.